

Tampereen teknillinen korkeakoulu
Julkaisu 375

Tampere University of Technology
Publications 375



Ridha Hamila

Synchronization and Multipath Delay Estimation Algorithms for Digital Receivers

Tampere 2002

**Tampereen teknillinen korkeakoulu
Julkaisuja 375**

**Tampere University of Technology
Publications 375**



Ridha Hamila

Synchronization and Multipath Delay Estimation Algorithms for Digital Receivers

Thesis for the degree of Doctor of Technology to be presented with due permission for public examination and criticism in Tietotalo Building, Auditorium TB109, at Tampere University of Technology, on the 19th of June 2002, at 12 o'clock noon.

Tampere 2002

ABSTRACT

This thesis considers the development of synchronization and signal processing techniques for digital communication receivers, which is greatly influenced by the digital revolution of electronic systems. Even though synchronization concepts are well studied and established in the literature, there is always a need for new algorithms depending on new system requirements and new trends in receiver architecture design. The new trend of using digital receivers where the sampling of the baseband signal is performed by a free running oscillator reduces the analog components by performing most of the functions digitally, which increases the flexibility, configurability, and integrability of the receiver. Also, this new design approach contributes greatly to the software radio (SWR) concept which is the natural progression of digital radio receivers towards multimode, multistandard terminals where the radio functionalities are defined by software.

The first part of this research work introduces a new technique for jointly estimating the symbol timing and carrier phase of digital receivers with non-synchronized sampling clock for both data-aided and non-data-aided systems using a block-based feed-forward architecture. This technique is a practical, rapidly converging, fully digitally implemented synchronization concept based on a low-order polynomial approximation of the likelihood functions using the Farrow-based interpolator. A review of maximum likelihood theory, which is the basis for coherent theory of synchronization, defines first the criteria and general framework for developing near-optimum synchronization schemes for digital communication systems. Then, efficient Farrow-based polynomial approximations of the typical likelihood functions are derived for systematic symbol timing, carrier phase and fine acquisition frequency synchronization algorithms.

Another important receiver functionality closely related to synchronization is propagation delay estimation which is the basis of positioning technologies. Mobile phone positioning is becoming unavoidable after the mandate imposed by communications regulatory bodies on emergency call positioning. The second part of this thesis reviews and develops new techniques with subchip resolution capabilities for estimating closely-spaced multipath delays in spread-spectrum CDMA systems. Generally, multipath delays caused by distant reflectors have relatively large delay spread, with more than one chip interval between different paths, that can be resolved using conventional delay-locked-loop techniques. However, shorter excess path delays result in overlapped fading multipath components that introduce significant errors to the line-of-sight path delay and gain estimation. Overlapping fading multipath components are considered as one of the major sources of error that have strong impact on high precision mobile positioning solutions, as well as, on mobile applications of dedicated systems like the Global Positioning System (GPS). An overview of the most promising geolocation positioning techniques for wireless systems that are being standardized is first provided with a survey of fundamental concepts and major problems in positioning. Then, the characteristics of different channel models and conventional multipath delay estimation techniques based on maximum likelihood theory are also discussed. Two new techniques with subchip resolution capabilities are proposed for estimating closely-spaced overlapped multipath components. These techniques are intended to improve the accuracy of location estimates by estimating correctly the delay of the line-of-sight path.

Preface

Research work for this thesis has been carried out during the years 1997-2002 in the research project "Advanced Transceiver Architectures and Implementations for Wireless Communications" at the Institute of Communications Engineering (formerly Telecommunications Laboratory) of Tampere University of Technology, Finland. This thesis was financially supported by the Academy of Finland and Tampere Graduate School of Information Science and Engineering (TISE), which are gratefully acknowledged.

First, I would like to express my sincere and deep gratitude to my supervisor Professor Markku Renfors for his invaluable guidance, continuous support, and infinite tolerance during the course of this work.

I would like to thank Associate Professor Peter Händel from the Department of Signals, Sensors and Systems, Royal Institute of Technology, Stockholm, and Professor Timo Laakso from the Signal Processing Laboratory, Helsinki University of Technology, for reviewing my thesis, and for their constructive feedback and comments on the manuscript.

Special thanks are due to Professor Jaakko Astola my former M.Sc. advisor, to Professor Moncef Gabbouj for his encouragement as well as for his kind advice, to Professor Tapio Saramäki for creating an enthusiastic work atmosphere, to professor Jarmo Harju, Dr. Pertti Koivisto coordinator of TISE, to Dr. Jari Syrjärinne, to Professor Fred Harris for giving me the opportunity to visit San Diego State University, California, and to Professor James F. Kaiser for sharing with me Teager energy concept and scientific experience.

I am indebted to all my colleagues and friends at the Institute of Communications Engineering for the pleasant work environment and for the help I have received during my work. I owe special thanks to Dr. Jussi Vesma and M.Sc. Simona Lohan for their cooperation, suggestions, and for the fruitful technical discussions, as well as, to Dr. Juha Yli-Kaakinen for the \LaTeX help. In particular special thanks are due to Tarja Erälaukko, Sari Kinnari and Elina Orava.

Special thanks to all my friends in Finland for their support and care. I'm very obliged to Mohamed Maala, family Gabbouj, Faouzi Alaya Cheick, Saara Maala, Vesma family, Paula Linna, Ali Hazmi, family Hammouda, Monaem Lakhzouri, Mejdi Trimeche, Mika Nieminen, Sari Luhtala, Asheesh family, Abdo family, and to the small Tunisian community in Tampere.

iv *PREFACE*

Most of all I wish to express my deepest gratitude to Satu Lassila, my mother Fatma, my brothers and sisters for their love, endless support, encouragement, and understanding all these years.

Finally, I would like to dedicate this thesis to the memory of my father Salem who did not have the chance to see the outcome of this work, God bless him.

RIDHA HAMILA

Tampere, May 31, 2002

Contents

Preface	iii
List of Publications	ix
List of Supplementary Publications	xi
List of Symbols and Acronyms	xiii
1 Introduction	1
2 Polynomial-Based ML Technique for Synchronization in Digital Receivers	5
2.1 Introduction	5
2.2 Synchronization and Timing Recovery Techniques	6
2.3 Maximum Likelihood Estimation	6
2.3.1 ML Principle for Optimum Receivers	6
2.3.2 Likelihood Function for Systematic Synchronization Algorithms	9
2.3.3 Data-Aided Estimation	11
2.3.4 Non-Data-Aided Estimation	12
2.4 Timing Adjustment Using Polynomial Interpolation	13
2.4.1 Receiver with Non-Synchronized Sampling	13
2.4.2 The Farrow Structure	13
2.5 Polynomial Approximation for the Log-Likelihood Function	15
2.5.1 Data-Aided Estimator	15
2.5.2 Non-Data-Aided Estimator	17
2.6 Summary of Simulation Results	18
3 Multipath Delay Estimation for Accurate Positioning	21
3.1 Introduction	21
3.2 Techniques for Personal Positioning: Principles and Problems	21

3.3	Fundamentals of GPS	24
3.3.1	Satellite Signals	25
3.3.2	Signal Characteristics	26
3.4	Multipath Delay Estimation Techniques	27
3.4.1	Channel Models	27
3.4.2	Conventional ML Based Approaches	29
3.4.3	Multipath Delay Estimation Using Peak Tracking with Pulse Subtraction	31
3.4.4	Multipath Delay Estimation Based on Teager-Kaiser Operator	33
4	Summary of Publications	37
4.1	Receiver Synchronization Studies	37
4.2	Multipath Delay Estimation Studies	38
4.3	Author's Contribution to the Publications	39
5	Conclusions	41
	References	43
	Publications	47

List of Figures

2.1	Timing recovery methods.	7
2.2	Degradation of symbol error probability due to different timing errors, $\Delta\tau$, using QPSK modulation.	8
2.3	Degradation of symbol error probability due to different phase errors, $\Delta\phi$, using QPSK modulation.	8
2.4	Digital receiver with non-synchronized sampling.	11
2.5	Illustrative example of a typical log-likelihood function for $\tau_0 = 0.52T$ and $\theta_0 = 0$, as well as its first order derivative.	11
2.6	The Farrow structure for polynomial-based interpolation filter.	14
2.7	Example of the input and output samples for the Farrow structure. Here the over-sampling ratio is $\beta = T/T_s = 2$	14
2.8	DA symbol timing and carrier phase synchronization scheme.	17
2.9	NDA symbol timing recovery scheme.	18
2.10	NDA carrier phase estimation scheme for M-PSK modulations.	19
3.1	Principles of E-OTD and A-GPS methods in cellular network.	23
3.2	GPS signal structure.	25
3.3	GPS signal spectrum (positive side).	26
3.4	User received minimum power levels with respect to the user elevation angle and signal structure.	27
3.5	Non-coherent DLL S-curve for a multipath channel.	31
3.6	Effect of multipath propagation on the S-curve of a non-coherent DLL using different discriminator values Δ and two paths channel.	32

List of Publications

- [P1] R. Hamila, J. Vesma, T. Saramäki and M. Renfors, "Discrete-Time Simulation of Continuous-Time Systems Using Generalized Interpolation Techniques," in *Proc. 1997 the Summer Computer Simulation Conference, SCSC'97*, Arlington, Virginia, USA, July 1997, pp. 914–919.
- [P2] R. Hamila, J. Vesma, H. Vuolle, and M. Renfors, "Joint Estimation of Carrier Phase and Symbol Timing Using Polynomial-Based Maximum Likelihood Technique," in *Proc IEEE 1998 International Conference on Universal Personal Communications, ICUPC'98*, Florence, Italy, October 1998, pp. 369–373.
- [P3] R. Hamila, J. Vesma, H. Vuolle, and M. Renfors, "NDA Maximum Likelihood Approach for Timing and Phase Adjustment by Polynomial-Based Interpolation," in *Proc. 6th IEEE International Workshop on Intelligent Signal Processing and Communication Systems, ISPACS'98*, Melbourne, Australia, Nov. 1998, pp. 248–252.
- [P4] R. Hamila, J. Vesma, H. Vuolle, and M. Renfors, "Effect of Frequency Offset on Carrier Phase and Symbol Timing Recovery in Digital Receivers," in *Proc. 1998 URSI International Symposium on Signals, Systems, and Electronics, ISSSE'98*, Pisa, Italy, September 1998, pp. 247–252.
- [P5] R. Hamila, M. Renfors, "New Maximum Likelihood Based Frequency Estimator for Digital Receivers," in *Proc. IEEE Wireless Communications and Networking Conference, WCNC'99*, New Orleans, USA, Sept. 1999, pp. 206–210.
- [P6] R. Hamila, S. Lohan, and M. Renfors, "Effect of Correlation Estimation on Multipath Delay Estimation Techniques in DS-CDMA Systems," in *Proc. of 4th International Symposium on Wireless Personal Multimedia Communications, WPMC'01*, Aalborg, Denmark, September 2001, pp. 331–335.
- [P7] R. Hamila, S. Lohan, and M. Renfors, "Novel Technique for Closely-Spaced Multipath Delay Estimation in DS-CDMA Systems," *Submitted to Signal Processing, (EURASIP)*.
- [P8] S. Lohan, R. Hamila, and M. Renfors, "Performance Analysis of an Efficient Multipath Delay Estimation Approach in a CDMA Multiuser Environment," in *Proc. of 12th IEEE International Symposium on Personal, Indoor and Mobile Radio Communications, PIMRC'01*, San Diego, California, USA, Sept. 2001, pp. 6–10.

List of Supplementary Publications

- [S1] R. Hamila, J. Vesma and M. Renfors, "Polynomial-Based Maximum Likelihood Technique for Synchronization in Digital Receivers," *to be published in the IEEE Transactions on Circuit and Systems II: Analog and Digital Signal Processing*.
- [S2] J. Vesma , R. Hamila, T. Saramäki and M. Renfors, "Design of Polynomial Interpolation Filters Based on Taylor Series," *in the European Signal Processing Conference*, Rhodes, Greece, September 1998, pp. 283–286.
- [S3] R. Hamila, J. Astola, F. Alaya Cheikh, M. Gabbouj, and M. Renfors, "Teager Energy and the Ambiguity Function," *IEEE Transactions on Signal Processing*, Vol. 47, No. 1, pp. 260–262, January 1999.
- [S4] R. Hamila, F. Alaya Cheikh, J. Vesma, J. Astola, and M. Gabbouj, "Relationship between Wigner-Distribution and the Teager Energy," *in Proc. European Signal Processing Conference*, Rhodes, Greece, September 1998, pp. 1857–1860
- [S5] R. Hamila, M. Renfors, G. Gunnarsson, M. Alanen, "Data Processing for Mobile Phone Positioning," *in Proc. Vehicular Technology Conference*, Amsterdam, Netherlands, Sept. 1999, pp. 446–449.
- [S6] R. Hamila, S. Lohan, and M. Renfors, "Novel Technique for Multipath Delay Estimation in GPS receivers," *in Proc. IEEE International Conference on Third Generation Wireless and Beyond*, San Francisco, USA, May 2001, pp. 993–998.
- [S7] S. Lohan, R. Hamila, and M. Renfors, "Cramer Rao Bound for Multipath Time Delays in a DS-CDMA System," *in Proc. of 4th International Symposium on Wireless Personal Multimedia Communications*, Aalborg, Denmark, September 2001, pp. 1043–1046.
- [S8] R. Hamila, S. Lohan and M. Renfors, "Subchip Multipath Delay Estimation for Downlink WCDMA System Based on Teager Operator," *Submitted to IEEE Communications Letters*.

List of Symbols and Acronyms

SYMBOLS

$a(n)$	data symbols
$\delta(\cdot)$	Dirac delta function
Δt	time spacing
$(\Delta t)_c$	coherence time
B_c	coherence bandwidth
B_d	Doppler spread
$C(t)$	spreading code
$c_l(\cdot)$	FIR filter coefficient
E_b	energy of a bit
E_s	energy of a symbol
$E\{\cdot\}$	statistical expectation
F_s	sampling frequency
$g_T(\cdot)$	transmitter filter
$g_{MF}(\cdot)$	receiver matched filter
j	imaginary unit ($j = \sqrt{-1}$)
N	block length
N_0	single sided noise PSD
$P(\cdot)$	apriori probability
$p(\cdot \cdot)$	conditional probability density function
$\text{Re}\{\cdot\}$	real part
$r(t)$	received signal
$s(t, \Phi)$	baseband transmitted signal

T	symbol interval
T_0	observation interval
T_m	delay spread
T_s	sample interval
Φ	synchronization parameter vector
$\tilde{\Phi}$	synchronization parameter trial vector
$\hat{\Phi}$	estimated synchronization parameter vector
τ	time delay
$\hat{\tau}$	estimated time delay
θ	phase error
$\hat{\theta}$	estimated phase error
$\mu \in [0, 1)$	fractional interval
$\Lambda(\cdot)$	likelihood function
$\Gamma(\cdot)$	log-likelihood function
$\Pi(\cdot)$	rectangular function
$\nabla(\cdot)$	triangle function
$(\cdot)^*$	complex conjugation
$ \cdot $	absolute value
$\lfloor \cdot \rfloor$	integer part

ACRONYMS

3G	Third Generation Wireless System
3GPP	3rd Generation Partnership Project
ADC	Analog to Digital Converter
AF	Ambiguity Function
AFLT	Advanced Forward Link Trilateration
A-GPS	Assisted Global Positioning System
ANSI	American National Standards Institute
ARIB	Association of Radio Industries and Businesses
BPSK	Binary Phase Shift Keying
BS	Base Station
C/A-Code	Coarse Acquisition Code
CDMA	Code Division Multiple Access

CI	Cell Identity
DA	Data Aided
DD	Decision Directed
DLL	Delay Locked Loop
DoD	Department of Defense
DSP	Digital Signal Processing
DS-SS	Direct Sequence - Spread Spectrum
E-OTD	Enhanced Observed Time Difference
ETSI	European Telecommunications Standards Institute
FCC	Federal Communications Commission
FIR	Finite Impulse Response
GPS	Global Positioning System
IPDL	Idle Period Down Link
GSM	Global System for Mobile Communication
LLF	Log Likelihood Function
LOS	Line Of Sight
MAP	Maximum A Posteriori Probability
ML	Maximum Likelihood
MLE	Maximum Likelihood Estimation
MS	Mobile Station
NCDLL	Non-Coherent Delay Lock Loop
NDA	Non-Data Aided
NLOS	Non-Line Of Sight
OTDOA	Observed Time Difference of Arrival
PAM	Pulse Amplitude Modulation
PLL	Phase Locked Loop
PPS	Precise Position Service
PRN	Pseudo Random Noise
QAM	Quadrature Amplitude Modulation
QPSK	Quadrature Phase Shift Keying
RF	Radio Frequency
sec	Second
SMG	Standard Mobile Group
SNR	Signal-to-Noise Ratio
SPS	Standard Position Service

SWR	Software Radio
SVs	Space Vehicles
TDMA	Time Division Multiple Access
TDOA	Time Difference Of Arrival
TOA	Time Of Arrival
TOT	Time Of Transmission
US	United States
VLSI	Very Large Scale Integration

Chapter 1

Introduction

The high competition between Americans, Asians, and Europeans has led to the coexistence of several radio communication systems and promises a very difficult path towards the convergence to a unique standard wireless mobile system, despite of the benefits of common worldwide standard. This competition introduces new challenges in receiver architecture design to accommodate the different air interfaces. The natural progression of digital radios towards multimode, multistandard terminals is a potential pragmatic solution which is known as the Software Radio (SWR) concept. The main idea is that the radio functionalities of user terminals are defined by software which allows them to dynamically adapt to different radio environments. Even though, the software radio was first introduced for military applications, the digital revolution of electronic systems has enabled software radio to gradually enter also commercial communication systems. The popularity of digital solutions over their analog counterparts resides mainly on their greater flexibility, high integration efficiency, and configurability, as well as on the fast speed at which semiconductor technologies, digital signal processors, and VLSI circuits are developing.

The rapid evolution of communication systems and the new requirements imposed by the standardization authorities have brought various consumer electronics device types and a high demand on new communication services, such as mobile phone positioning with high accuracy. Even if safety was the primary motivation for mobile positioning, a lot of commercial applications have already emerged in the market. For the public interest, mobile phone positioning in a cellular network with reliable and rather accurate position information has become unavoidable after the Federal Communications Commission mandate, FCC-E911 docket on emergency call positioning in USA, and the coming E112 in the European Union [1]. The basic rule of emergency services requires mobile operators to automatically transfer caller location details to the emergency authorities without regard to validation procedures intended to automatic caller identification and localization.

International analysts have also predicted that mobile location services are commercially potential and the most compelling value-added services to the forthcoming third generation mobile systems, taking into consideration the huge range of services that can be provided to the mobile users. Recently, several potential technologies enabling the development of mobile location techniques have emerged and are already competing in the market [2]. A

large number of commercial location-based services are being provided, such as fleet and resource management, vehicle tracking and person to person location and messaging applications [3], [4], location specific traffic information, yacht position, map-based guidance, and navigation [5]. Location based services will allow mobile users to receive personalized and lifestyle-oriented services relative to their geographic location, and provide enormous opportunities for companies and organizations to effectively reach their target groups of strong purchasing power. However, the successful evolution of the mobile location services to a massmarket industry relies mainly on its accuracy, interoperability, end user privacy and availability of attractive services. In view of the sensitivity of location data to the end user privacy and security, appropriate technical solutions that satisfy requirements for security issues must be established to ensure compliance with regulatory rules in this area.

Since the introduction of the software radio concept, several architectures for designing SWR radio platforms have been recently developed through the efforts of commercial and noncommercial organizations [6], [7], [8], [9], [10], [11]. The ultimate goal of designing a single-chip, flexible wireless transceiver supporting multimode and multistandard compatibility introduced new architectures more suitable for integration. The current trend is to push the analog/digital interface towards the antenna to simplify the analog parts and allow the implementation of most receiver functions digitally, increasing therefore the flexibility, configurability, and integrability. As one important functionality, these new receivers require flexible and efficient synchronization algorithms which depend on the system requirements and receiver architecture design.

In digital communication systems, the continuous-time received signal is sampled and these samples are used to make the decisions on the transmitted symbols. The sampling of the received signal must be synchronized to the incoming data symbols. In conventional receivers, the synchronization is performed using a feedback or feed-forward loop to control the phase of the sampling clock which generally requires complicated phase-locked-loop circuits [12]. The new trend of using digital receivers where the sampling of the baseband signal is not synchronized to the incoming data symbols, reduces the analog components since most of the functions are performed digitally [13], [14], [15]. In this receiver architecture, the sampling of the baseband signal is clocked by a free running oscillator, and thus the sampling is not synchronized to the incoming symbols. Therefore, timing adjustment, and in practice also the carrier phase estimation must be done by digital methods after sampling. One way to perform this is to calculate the value of the signal at the desired time instants using interpolation. Maximum likelihood (ML) estimation theory is the basis for coherent theory of synchronization [13]. It provides a general framework for developing near-optimum synchronization schemes for digital communication systems. Joint estimation of signal parameters using the ML approach yields usually to better estimates with respect to the lower bound on the variance, known as the Cramer Rao bound, compared to estimates obtained from separate optimization of the likelihood functions [16].

Another essential receiver functionality closely related to synchronization is the propagation delay estimation which is the basis for positioning technologies. Multipath effects of the mobile channel could degrade the location estimate substantially, and they are regarded as a killer issue in location estimation, and still a challenging topic for research work.

The main goal of the first part of this thesis work is to develop flexible and efficient all-digital synchronization algorithms with good performance and fast convergence. The work focuses on new algorithms for jointly estimating the symbol timing and carrier phase of

digital receivers with non-synchronized sampling clock for both data-aided and non-data-aided systems. To achieve efficient implementation, modest oversampling is used and yet good timing accuracy is achieved by developing low-order polynomial approximations of the likelihood functions. The main emphasis is on the derivation of efficient Farrow-based polynomial approximations of the likelihood function for systematic and practical symbol timing, carrier phase, and fine acquisition frequency synchronization algorithms.

The second main topic is to develop new techniques with subchip resolution capabilities for estimating closely-spaced multipath delays in spread-spectrum CDMA systems in order to estimate correctly the delay of the LOS path. Overlapped closely-spaced multipath components are considered as one of the major sources of error for accurate mobile terminal positioning solutions.

This thesis is organized as follows: In Chapter 2, the polynomial-based maximum likelihood technique for parameter synchronization in digital receivers with non-synchronized sampling clock is established for both DA and NDA systems. Chapter 3 provides an overview of the most promising geolocation solutions, and introduces new techniques for estimating overlapped closely-spaced multipath components. A summary of the main results of this thesis and the author's contribution to the publications are clarified in Chapter 4. The results of this work are given in the publications included in the appendices. Finally, conclusions are drawn in Chapter 5.

Chapter 2

Polynomial-Based ML Technique for Synchronization in Digital Receivers

2.1 INTRODUCTION

In this chapter, new symbol timing and carrier phase estimators are introduced based on ML theory for both data-aided (DA) and non-data-aided (NDA) systems, using a block-based feed-forward architecture. This new technique is a practical, fully digitally implemented synchronization concept using interpolation for jointly estimating the symbol timing and the carrier phase. The interpolation method used in this context is efficiently implemented using the so-called Farrow structure [17] which is characterized by its simple and flexible realization. The likelihood function is expressed in terms of the polynomial coefficients obtained from the Farrow-based interpolator. The feed-forward architecture we are considering provides rapid acquisition characteristics, which are very important especially in the mobile communication systems where the channel characteristics are rapidly changing, and in the case of TDMA system, also the transmission is bursty. Furthermore, the used interpolation approach allows to use modest oversampling (typically twice the symbol rate) while providing the temporal resolution of a highly oversampled system in a computationally efficient manner. In [18], [19], a somewhat similar idea was developed for symbol timing estimation through polynomial approximation of the log-likelihood function. Our approach differs from this earlier idea in that the polynomial approximation of the log-likelihood function is here derived from the piecewise polynomial approximation of the signal in an efficient way. This allows the use of lower sampling rate (oversampling factor of 2 instead of 4). For other approaches to all-digital symbol timing recovery we refer to [14], [15], [20].

This chapter is organized as follows. Section 2.2 discusses briefly the importance of synchronization function and different timing recovery techniques. Section 2.3 gives a brief overview of the maximum likelihood principle for optimum receivers, and presents the typ-

ical likelihood functions required for deriving systematic symbol timing and carrier phase synchronization algorithms. Timing adjustment using polynomial interpolation concept for digital receiver with non-synchronized sampling is reviewed in Section 2.4. The polynomial approximation of the likelihood functions for both DA and NDA systems is derived in Section 2.5. Finally, a summary of the simulation results which are provided in the Publications [P1]-[P5] is presented in Section 2.6.

2.2 SYNCHRONIZATION AND TIMING RECOVERY TECHNIQUES

Synchronization is one of the fundamental functions in communication systems. Its task is to lock the synchronization parameters of the receiver with the received signal. Estimation of synchronization parameters, such as symbol timing, carrier phase and frequency is very essential for performing demodulation and detection of the data from the transmitted signal with high reliability. In conventional receivers, the synchronization is performed using a feedback or feed-forward loop to control the phase of the sampling clock as shown in Fig. 2.1 (a) and (b). These analog and hybrid methods of synchronization are well established in the literature and studied thoroughly [13], [21]. However, their major drawbacks are the large amounts of board space, power consumption, and circuit complexity of phase-locked-loops (PLLs) which are used to control the sampling of incoming signals [12]. Another synchronization method suitable for digital receiver implementation has been introduced during the last decade as shown in Fig. 2.1 (c). In this architecture, the received signal is sampled by a free running clock and thus sampling is not synchronized to the incoming data symbols. Consequently, the synchronization parameters are estimated by digital methods after sampling. This new type of receiver architecture with non-synchronized sampling clock is very relevant to the context of software radio. In fact, existing communication standards are using different data rates, and consequently they employ different master clock rates. In order to reduce the receiver complexity, we can use a single master clock with this receiver architecture and generate the different clock rates virtually by means of sampling rate conversion [10].

The synchronization function is generally very critical to the error performance. Typical examples shown in Figs. 2.2 and 2.3 illustrate the effect of timing offset and phase error on theoretical symbol error probability using QPSK modulation [15], [16].

2.3 MAXIMUM LIKELIHOOD ESTIMATION

In this section, the maximum a posteriori (MAP) and maximum likelihood (ML) estimation criteria are shortly reviewed. Then, the ML criterion is used to devise the symbol timing and carrier phase estimators for both DA and NDA systems.

2.3.1 ML Principle for Optimum Receivers

The optimum decision rule to detect the symbol sequence \mathbf{a} in a received signal corrupted by noise is based on the *maximum a posteriori probability* (MAP) estimation criterion, also known as Bayesian estimation [16]. This decision criterion is trying to select the values of

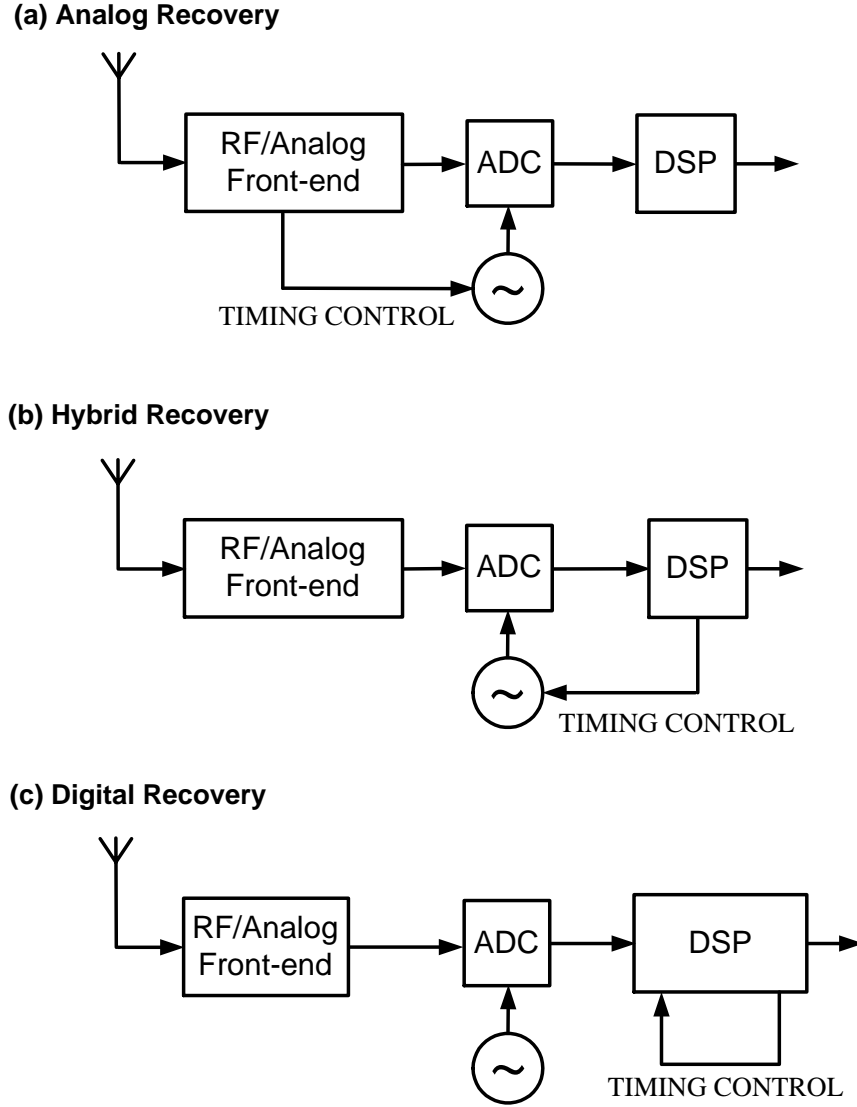


Fig. 2.1 Timing recovery methods.

\mathbf{a} in each transmitted signal interval based on the observation vector \mathbf{r} , such that the set of posteriori probabilities is maximized. Under the condition that the prior probabilities are all equal (symbols are uniformly distributed), a detector based on the MAP criterion reduces to the decision criterion based on the maximum of the conditional probability density functions, known as maximum-likelihood (ML) criterion [15].

An optimal ML receiver would perform joint estimation of data \mathbf{a} and synchronization parameters $\Phi = \{\tau, \theta\}$ simultaneously [20]. Here, τ and θ denote the time delay and carrier phase, respectively. The ML criterion for both data detection and synchronization parameter estimation is trying to select the set of values $\{\hat{\mathbf{a}}, \hat{\Phi}\}$ which maximizes the likelihood function $p(\mathbf{r}|\mathbf{a}, \Phi)$ as follows

$$(\hat{\mathbf{a}}, \hat{\Phi}) = \arg \max_{\mathbf{a}, \Phi} p(\mathbf{r}|\mathbf{a}, \Phi). \quad (2.1)$$

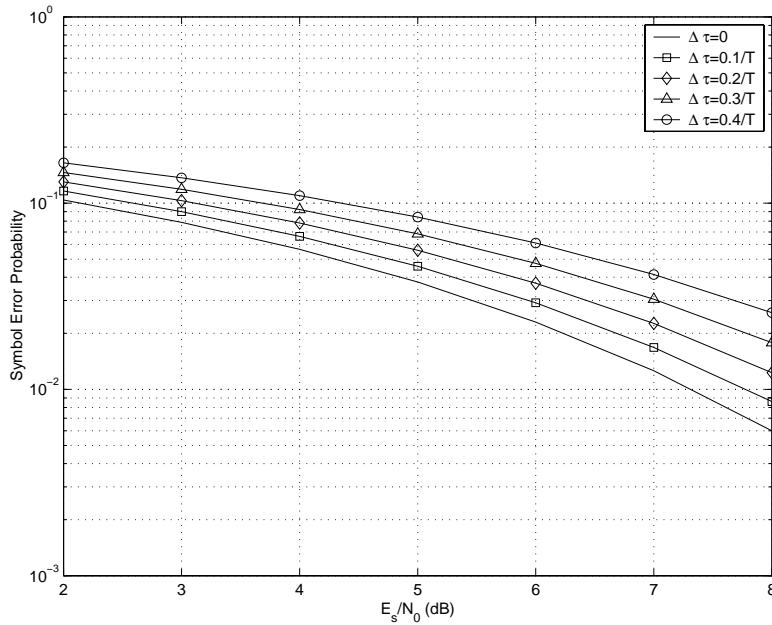


Fig. 2.2 Degradation of symbol error probability due to different timing errors, $\Delta\tau$, using QPSK modulation.

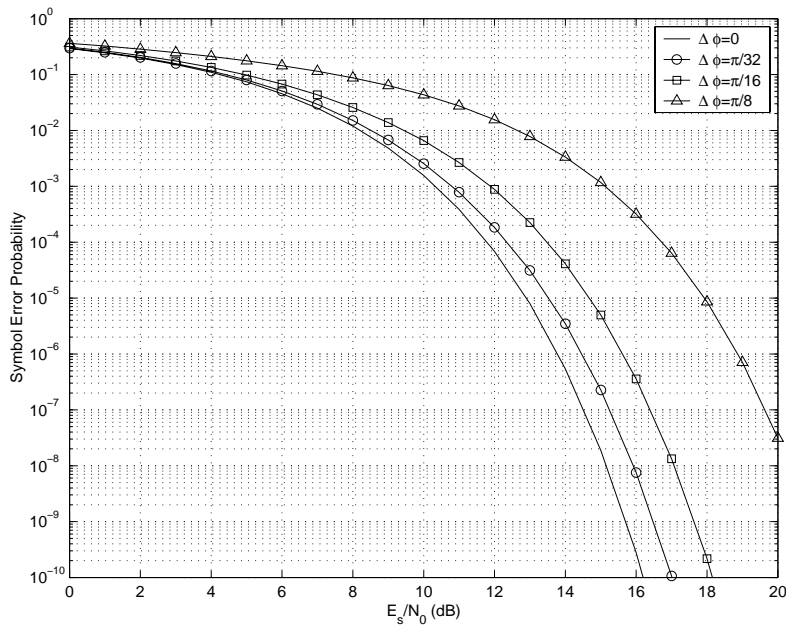


Fig. 2.3 Degradation of symbol error probability due to different phase errors, $\Delta\phi$, using QPSK modulation.

Unfortunately, the optimal joint detection/estimation approach is rather complicated for practical receiver implementation [15], [20]. Therefore, separate data detection algorithms, and independent estimates of each synchronization parameter are commonly derived for re-

alizable receiver structures. Depending on the data dependency, there are three main classes of ML synchronizers:

- The ML data-aided (DA) synchronization algorithms use known data sequence \mathbf{a}_0 (preamble, training sequence) at the receiver for the estimation as follows

$$(\hat{\Phi})^{DA} = \arg \max_{\Phi} p(\mathbf{r} | \mathbf{a} = \mathbf{a}_0, \Phi). \quad (2.2)$$

- The ML decision-directed (DD) synchronization algorithms use detected data sequence $\hat{\mathbf{a}}$ instead of the true symbol values for the estimation,

$$(\hat{\Phi})^{DD} = \arg \max_{\Phi} p(\mathbf{r} | \mathbf{a} = \hat{\mathbf{a}}, \Phi). \quad (2.3)$$

- The third class is the ML non-data-aided (NDA) synchronization algorithms. They are using neither the data symbol values nor their estimates. However, they remove the data dependency by averaging over all prior probabilities as follows

$$p(\mathbf{r} | \Phi) = \sum_{\mathbf{a}} p(\mathbf{r} | \mathbf{a}, \Phi) P(\mathbf{a}). \quad (2.4)$$

Then, by maximizing the above likelihood function (2.4) with respect to each/all synchronization parameter, the ML NDA algorithms are given by

$$(\hat{\Phi})^{NDA} = \arg \max_{\Phi} p(\mathbf{r} | \Phi). \quad (2.5)$$

2.3.2 Likelihood Function for Systematic Synchronization Algorithms

A linearly modulated transmitted signal in baseband is given by

$$s(t, \Phi) = e^{j\theta_0} \sum_n a(n) g_T(t - nT - \tau_0), \quad (2.6)$$

where the couple (τ_0, θ_0) are the true values of the unknown clock timing and carrier phase offsets, respectively, $\{a(n)\}$ is the sequence of independent equiprobable data symbols, $g_T(t)$ is the transmitter filter pulse shape, and $1/T$ is the symbol rate.

We assume that $s(t, \Phi)$ is completely known at the receiver except for the synchronization parameter vector Φ which consists of the time delay τ and carrier phase θ , and possibly the data symbols. The parameter vector Φ is also assumed to remain unchanged over an observation interval T_0 (or sufficiently large number $N = T_0/T$ of transmitted symbols).

The linearly modulated received signal is given by

$$r(t) = s(t, \Phi) + \eta(t), \quad (2.7)$$

where $\eta(t)$ is an independent white stationary Gaussian noise with flat power spectral density N_0 . Recalling the Gaussian nature of the random process, the likelihood function that is to be maximized is given by [15], [16]

$$p(\mathbf{r} | \mathbf{a}, \Phi) = \xi \exp \left[-\frac{1}{\sigma^2} \int_{T_0} \left| r(t) - \tilde{s}(t, \Phi) \right|^2 dt \right], \quad (2.8)$$

where ξ is a positive constant, independent of the synchronization parameters which can be neglected, and $\tilde{s}(t, \tilde{\Phi})$ is the trial local replica generated at the receiver defined by

$$\tilde{s}(t, \tilde{\Phi}) = e^{j\hat{\theta}} \sum_n a(n) g_T(t - nT - \tilde{\tau}). \quad (2.9)$$

Maximum likelihood estimation (MLE) is simply trying to minimize the distance between the corrupted received signal $r(t)$ and the trial local replica $\tilde{s}(t, \tilde{\Phi})$. Equivalently, MLE is trying to estimate one or both values from the parameter set $\hat{\Phi} = \{\hat{\tau}, \hat{\theta}\}$ using the trial vector $\tilde{\Phi} = \{\tilde{\tau}, \tilde{\theta}\}$ in order to maximize the likelihood function $p(\mathbf{r}|\mathbf{a}, \Phi)$.

As mentioned earlier, consistent approximations of the above likelihood function are needed to derive systematic ML synchronization algorithms. By expanding the integral in Eq. (2.8), and observing that the energy quantities resulting from the received noisy signal and the local trial signal can be ignored since they are independent of the synchronization parameters, it follows [16]

$$p(\mathbf{r}|\mathbf{a}, \Phi) \approx \xi \exp \left[\frac{2}{\sigma^2} \int_0^{T_0} \text{Re} \left\{ r(t) \tilde{s}^*(t, \tilde{\Phi}) \right\} dt \right]. \quad (2.10)$$

The above approximation is accurate for constant envelope signals (equal symbol energies), e.g., M-PSK, but it is commonly used also for QAM signals.

In the basic system model of Fig. 2.4, after down-conversion to the baseband through mixing and filtering, the received signal is first applied to a receiver matched filter $g_{MF}(t)$, then sampled with a fixed sampling rate $1/T_s$. In practice, the order of sampling and matched filter can be reversed. Under the assumptions that the transmitter and receiver matched filters satisfy the Nyquist properties and the channel is ideal, there is no inter-symbol interference provided that the samples are taken at the correct time instant, i.e., $\tau_0 = \hat{\tau}$. By replacing the local trial signal replica (2.9) in Eq. (2.10), after some manipulations, the likelihood function or objective function becomes [20]

$$\Lambda(\mathbf{a}, \Phi) = \xi \exp \left[\frac{2}{\sigma^2} \text{Re} \left\{ e^{-j\hat{\theta}} \sum_n a^*(n) m(n, \tau) \right\} \right], \quad (2.11)$$

where $m(n, \tau)$ denotes samples from the output of the matched filter given by

$$m(n, \tau) = \int_0^{T_0} r(t) g_{MF}(nT + \tau - t) dt. \quad (2.12)$$

Taking the logarithm of (2.11) and dropping the resulting constants, we obtain the log-likelihood function (LLF)

$$\Gamma(\mathbf{a}, \Phi) = \text{Re} \left\{ e^{-j\hat{\theta}} \sum_n a^*(n) m(n, \tau) \right\}. \quad (2.13)$$

An illustrative example of the likelihood function and its first order derivative is depicted in Fig. 2.5 using QPSK constellation signal and an oversampling factor equal to 50. Several techniques for searching the maximum location of the likelihood function have been devised with a complexity mostly related to the data sample rate and used technology. The

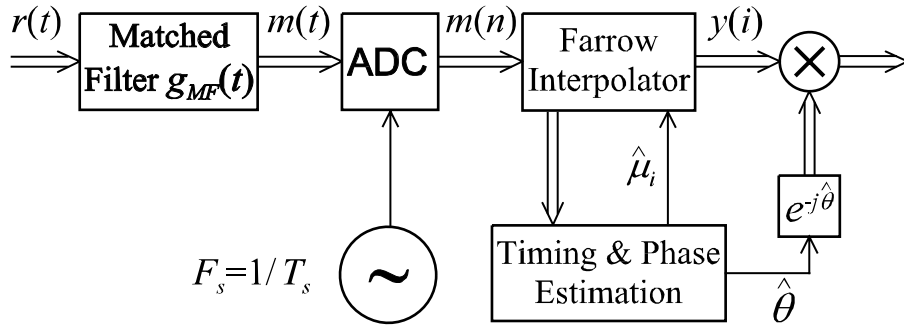


Fig. 2.4 Digital receiver with non-synchronized sampling.

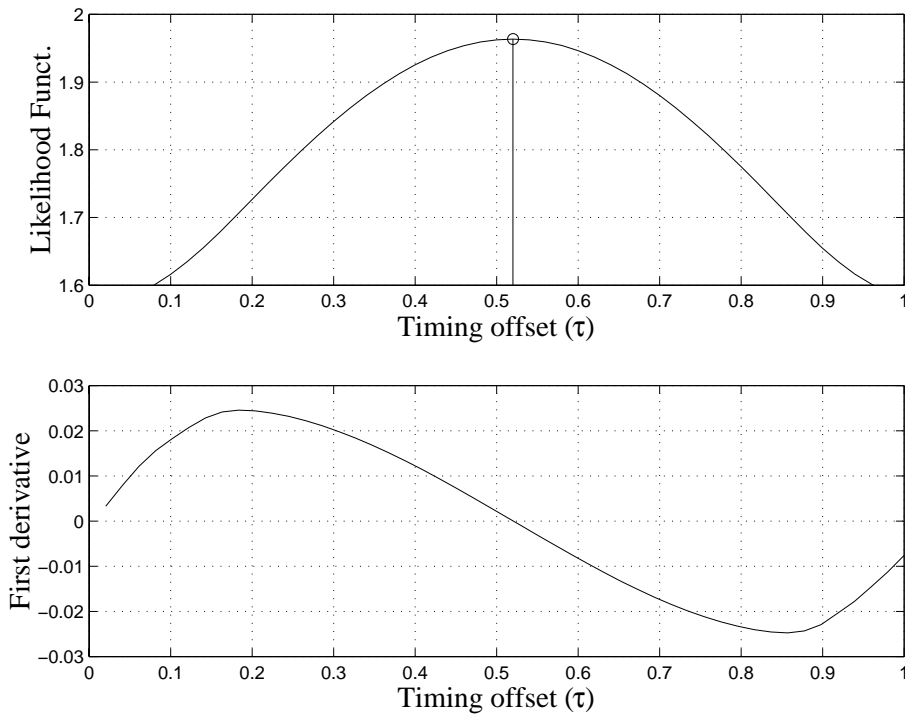


Fig. 2.5 Illustrative example of a typical log-likelihood function for $\tau_0 = 0.52T$ and $\theta_0 = 0$, as well as its first order derivative.

straightforward approach of calculating the log-likelihood function from the discrete-time matched filter output samples would require excessive oversampling factor to achieve sufficient temporal resolution, especially with high-order modulations. Generally, the most straightforward approaches are based on the partial derivatives of the LLF. Namely, the iterative search procedure or the error tracking feedback method [20]. However, the maximum search can be facilitated and optimized using the proposed idea of polynomial-based approximation of the maximum likelihood function.

2.3.3 Data-Aided Estimation

In this case, the symbols $\{a(n)\}$ used for synchronization (preamble, training sequence) are known at the receiver. Similarly, the decision-directed synchronization algorithms use

detected data sequence instead of the true symbol values. For jointly estimating the symbol timing and carrier phase $(\hat{\tau}, \hat{\theta})$, the log-likelihood function has to be maximized with respect to the two parameters τ and θ as follows [15]

$$(\hat{\tau}, \hat{\theta}) = \arg \max_{\tau, \theta} \Gamma(\tau, \theta) \quad (2.14)$$

where the LLF (2.13) can be expressed as

$$\Gamma(\tau, \theta) = \left| \sum_n a^*(n) m(n, \tau) \right| \operatorname{Re} \left\{ e^{-j(\theta - \arg \sum_n a^*(n) m(n, \tau))} \right\}. \quad (2.15)$$

By observing that the magnitude term in Eq. (2.15) is independent of θ , the joint estimation of $(\hat{\tau}, \hat{\theta})$ can be performed by first estimating $\hat{\tau}$ by finding the maximum of the magnitude term

$$\hat{\tau} = \arg \max_{\tau} \left| \sum_n a^*(n) m(n, \tau) \right| \quad (2.16)$$

and then, the carrier phase estimate $\hat{\theta}$ is easily deduced as

$$\hat{\theta} = \arg \sum_n a^*(n) m(n, \hat{\tau}). \quad (2.17)$$

2.3.4 Non-Data-Aided Estimation

Under the assumptions of low SNR and independent equiprobable transmitted data symbols, using quadratic Taylor series expansion of the exponential term in the objective function in Eq. (2.11) and then removing of the data dependency by averaging, the desired approximation of the marginal likelihood function is given by [20]

$$\Lambda(\tau, \theta) = \sum_n E[|a(n)|^2] |m(n, \tau)|^2 + \operatorname{Re} \left\{ \sum_n E[a^2(n)] (m^*(n, \tau))^2 e^{-2j\theta} \right\}. \quad (2.18)$$

Detailed mathematical derivations of the above marginal likelihood function are provided in [20], Chapter 5.

Consequently, for a uniformly distributed phase, the likelihood function of Eq. (2.18) is reduced to

$$\Lambda(\tau) = \sum_n |m(n, \tau)|^2. \quad (2.19)$$

Hence, the NDA timing estimate for any linear digital modulation is given by [15]

$$\hat{\tau} = \arg \max_{\tau} \sum_n |m(n, \tau)|^2. \quad (2.20)$$

For M-PSK signalling, joint symbol timing and carrier phase estimate is feasible and carrier phase estimate is given by

$$\hat{\theta} = \frac{1}{M} \arg \sum_n (m(n, \hat{\tau}))^M. \quad (2.21)$$

2.4 TIMING ADJUSTMENT USING POLYNOMIAL INTERPOLATION

This section reviews and demonstrates how the symbol timing adjustment can be done digitally using an interpolator if the sampling of the receiver signal is not synchronized to the symbol timing instants. It is also discussed how the polynomial-based interpolation methods can be efficiently implemented using the so-called Farrow structure. In the next section, the polynomial-based interpolation and the Farrow structure are utilized to derive the proposed ML based symbol timing and carrier phase estimation algorithm.

2.4.1 Receiver with Non-Synchronized Sampling

In this work we consider the receiver structure where the sampling is done using a free-running oscillator and the symbol timing and carrier phase estimation and correction are done completely in the digital part of the receiver, as shown in Fig. 2.4. Here the received baseband signal after the matched filter, denoted by $m(t)$, is sampled using the over-sampling ratio of $\beta = T/T_s$, where T and T_s are the symbol and sampling intervals, respectively. In the digital part of the receiver, the timing error ($\hat{\tau}_i$) and phase error ($\hat{\theta}$) are estimated (to be discussed in the next section) and the symbol timing adjustment is done first using interpolator and, after that, the phase error is corrected using a phase rotator.

For convenience, it is assumed that the ADC sampling rate is an integer multiple of the symbol rate, and the interpolator output sampling rate is equal to the symbol rate. In this case, the fractional interval is constant, $\mu_i = \mu$, in stationary conditions. The fractional interval and timing offset are related as follows:

$$\mu = \frac{\tau}{T_s} - \left\lfloor \frac{\tau}{T_s} \right\rfloor \quad \text{where } \mu \in [0, 1). \quad (2.22)$$

Here, $\lfloor x \rfloor$ stands for the integer part of x .

2.4.2 The Farrow Structure

It has turned out that the polynomial-based interpolation methods are the most widely used solution for performing the symbol timing adjustment in digital receivers. The reason for the popularity of these methods lies in the fact that interpolator can then be efficiently implemented using the Farrow structure [17]. This filter structure, shown in Fig. 2.6, consists of $L + 1$ parallel FIR filters having the transfer functions $C_l(z)$ for $l = 0, 1, \dots, L$. Here L denotes the degree of the polynomial interpolation. The impulse response of the interpolator in each T_s -segment with basepoints $k = I_1$ to I_2 :

$$h(t) = h(iT) = h[(k + \hat{\mu}_i)T_s] = \sum_{l=0}^L c_l(k) \hat{\mu}_i^l \quad (2.23)$$

with $c_l(k)$'s being the fixed coefficients of the FIR filters of length $I_2 - I_1 + 1$.

The synchronized output samples of this structure are be given by

$$y(i) = \sum_{k=I_1}^{I_2} m(n_i - k) h[(k + \hat{\mu}_i)T_s] = \sum_{l=0}^L v_l(n_i) \hat{\mu}_i^l, \quad (2.24)$$

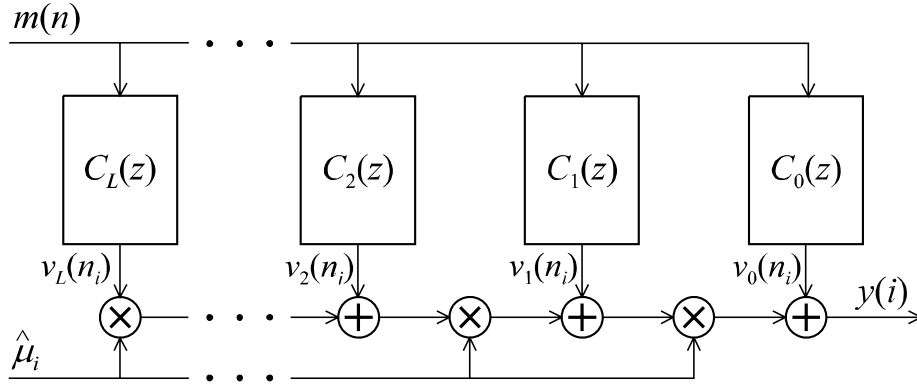


Fig. 2.6 The Farrow structure for polynomial-based interpolation filter.

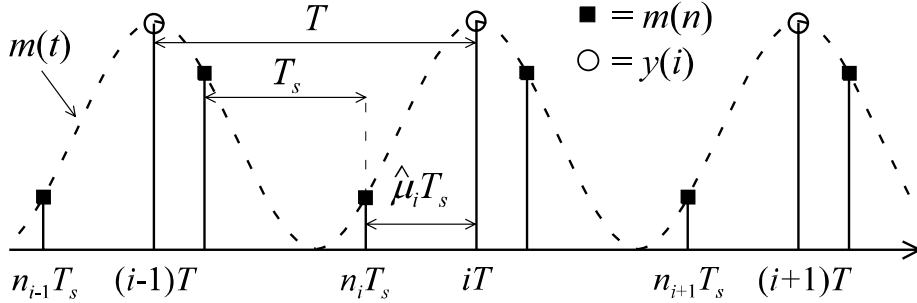


Fig. 2.7 Example of the input and output samples for the Farrow structure. Here the over-sampling ratio is $\beta = T/T_s = 2$.

where

$$v_l(n_i) = \sum_{k=I_1}^{I_2} m(n_i - k)c_l(k). \quad (2.25)$$

The FIR filter coefficients for the Lagrange interpolation are given, e.g., in [14] and for more general interpolation techniques, see [17], [22], [23].

The idea of the Farrow structure is that the output samples of the FIR filters $v_l(n_i)$ as given by Eq. (2.25) form a polynomial approximation for the continuous-time signal $m(t)$ in the interval $n_i T_s \leq t < (n_i + 1)T_s$. The output sample $y(i)$ is then calculated by evaluating the value of the polynomial at the time instant determined by $\hat{\mu}_i$ according to Eq. (2.24). Therefore, the time instant for the output sample $y(i) = y(iT)$ is determined by (see Fig. 2.7)

$$iT = (n_i + \hat{\mu}_i)T_s \quad \text{with } 0 \leq \hat{\mu}_i < 1. \quad (2.26)$$

The advantage of the Farrow structure is that the filter coefficients $c_l(k)$ are fixed and the time instant for the output sample can be easily controlled by the fractional interval $\hat{\mu}_i$.

2.5 POLYNOMIAL APPROXIMATION FOR THE LOG-LIKELIHOOD FUNCTION

In this section, we derive the polynomial approximation for the log-likelihood function for both DA and NDA cases. We consider the case of a non-synchronized receiver where the sampling rate is twice the symbol rate ($T = 2T_s$), consequently, we are going to use τ and μ in the following to denote the timing error as fractions of the symbol and sampling interval, respectively. The function of the interpolation filter is to calculate the correct output sample, $y(i) = y(iT)$, at a time using a set of adjacent input samples, $m(n) = m(nT_s)$, obtained from the output of the matched filter based on a timing error estimate $\hat{\mu}$. Here n denotes the largest integer for which $nT_s \leq iT$.

2.5.1 Data-Aided Estimator

In the following, the polynomial approximation for the log-likelihood function is derived by utilizing the fact that the output samples of the FIR filters in the Farrow structure, denoted by $v_l(n)$, form an L^{th} order polynomial approximation for the input signal $m(n)$. This approximation is piecewise polynomial, i.e., there are different polynomial approximations for each sample interval. Because we are using two samples per one symbol interval, there are two different polynomial approximations of the log-likelihood function [P2] corresponding to the two halves of the symbol interval. Consequently, from expression (2.16) the symbol timing is estimated by

$$\hat{\tau} = \arg \max_{\tau} \begin{cases} |\Gamma_1(2\tau)| & \text{for } 0 \leq \tau < T/2 \\ |\Gamma_2(2\tau - 1)| & \text{for } T/2 \leq \tau < T \end{cases} \quad (2.27)$$

where the LLF functions $\Gamma_1(2\tau)$ and $\Gamma_2(2\tau - 1)$ are generated using odd and even samples of the matched filter output $m(n, \tau)$, as follows

$$\begin{cases} \Gamma_1(2\tau) = \sum_{n=1}^N a^*(n)m(2n - 1, 2\tau) & \text{for } 0 \leq \tau < T/2 \\ \Gamma_2(2\tau - 1) = \sum_{n=1}^N a^*(n)m(2n, 2\tau - 1) & \text{for } T/2 \leq \tau < T. \end{cases} \quad (2.28)$$

Also, by using the timing estimate $\hat{\tau}$ in the corresponding symbol time interval, the carrier phase estimate (Eq. (2.17)) becomes

$$\hat{\theta} = \begin{cases} \arg \Gamma_1(2\hat{\tau}) & \text{for } 0 \leq \hat{\tau} < T/2 \\ \arg \Gamma_2(2\hat{\tau} - 1) & \text{for } T/2 \leq \hat{\tau} < T. \end{cases} \quad (2.29)$$

The above expressions can be rewritten with respect to the sample interval denoted here by the fractional interval μ . The LLF equation (2.28) becomes

$$\begin{cases} \Gamma_1(\mu T_s) = \sum_{n=1}^N a^*(n)m(2n - 1, \mu T_s) \\ \Gamma_2(\mu T_s) = \sum_{n=1}^N a^*(n)m(2n, \mu T_s). \end{cases} \quad (2.30)$$

The values of $m(n, \mu T_s)$ can be interpolated for different values of $\mu \in [0, 1)$ by utilizing the Farrow structure and the original samples $m(n)$. Thus, the interpolated sample values

expressed as a function of the FIR branch filter outputs in the Farrow structure, $v_l(n)$, and the fractional interval, μ , are given by [P2]

$$\begin{cases} m(2n-1, \mu T_s) = \sum_{l=0}^L v_l(2n-1)\mu^l \\ m(2n, \mu T_s) = \sum_{l=0}^L v_l(2n)\mu^l. \end{cases} \quad (2.31)$$

where L is the degree of polynomial approximation. Finally, by substituting Eq. (2.31) into (2.30), the polynomial approximation of the log-likelihood function can be written as:

$$\begin{cases} \Gamma_1(\mu T_s) = \sum_{l=0}^L \left(\sum_{n=1}^N a^*(n)v_l(2n-1) \right) \mu^l \\ \Gamma_2(\mu T_s) = \sum_{l=0}^L \left(\sum_{n=1}^N a^*(n)v_l(2n) \right) \mu^l. \end{cases} \quad (2.32)$$

Consequently, the symbol timing and the carrier phase estimation can be performed easily with the aid of the Farrow structure. First, the polynomial coefficients of the log-likelihood functions are calculated by averaging the product of $a^*(n)$ and $v_l(n)$ over N symbols according to Eq. (2.32). It has turned out through simulations that the values of N between 16 and 64 provides good results. Second, the value of the timing error estimate $\hat{\mu}$ that maximizes either of the log-likelihood functions $\{\Gamma_1(\mu T_s), \Gamma_2(\mu T_s)\}$ is computed. Finally, by using the timing estimate, the carrier phase estimate $\hat{\theta}$ is calculated. A formal description of this algorithm is written as follows:

```

If  $\max |\Gamma_1(\mu T_s)| > \max |\Gamma_2(\mu T_s)|$  then
     $\hat{\mu} = \arg \max_{\mu} |\Gamma_1(\mu T_s)|$ 
     $\hat{\theta} = \arg[\Gamma_1(\hat{\mu} T_s)]$ 
else
     $\hat{\mu} = \arg \max_{\mu} |\Gamma_2(\mu T_s)|$ 
     $\hat{\theta} = \arg[\Gamma_2(\hat{\mu} T_s)]$ 
end If
    
```

The overall scheme of the proposed DA block-based symbol timing and carrier phase recovery is illustrated in Fig. 2.8. After the parameters $\hat{\mu}$ and $\hat{\theta}$ are estimated, timing adjustment is performed by evaluating the value of the polynomial at the given value of $\hat{\mu}$. Subsequently, the carrier phase is corrected by the factor $e^{-j\hat{\theta}}$.

The efficiency of this algorithm is due to the fact that here the block averaging of the likelihood function is done in the polynomial coefficient domain, and the multiplications with $\hat{\mu}$ are needed only for the whole estimation block. The above procedure can be used as such in the data-aided (DA) systems where the symbol values are known in advance. For example, GSM does have a known synchronization symbol sequence. In case of decision-directed (DD) systems, a reasonably good initial estimate for the sampling phase must be known. This scheme can also be utilized in non-data-aided (NDA) systems with some modifications as shown in the following section.

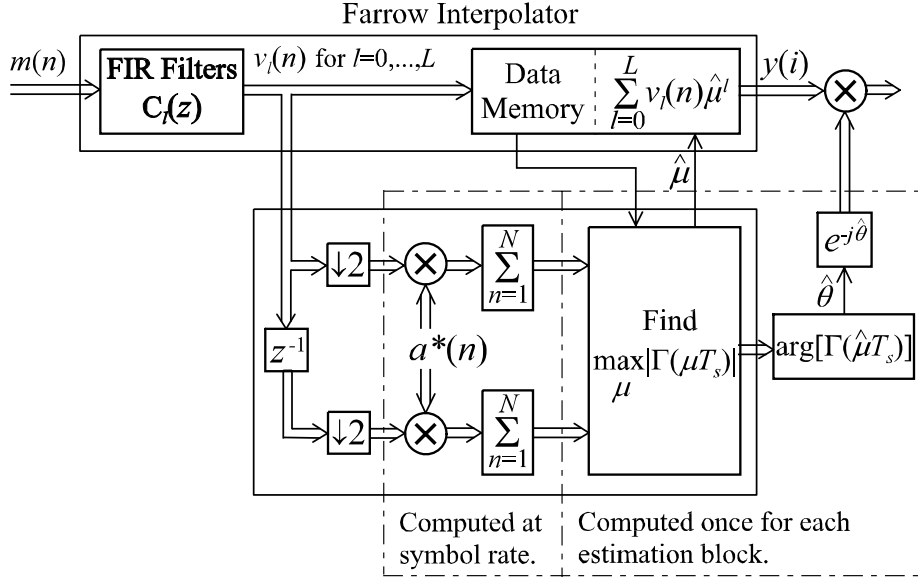


Fig. 2.8 DA symbol timing and carrier phase synchronization scheme.

2.5.2 Non-Data-Aided Estimator

Similarly to the DA estimators, the symbol timing for the NDA case is derived from expression (2.20) as follows [P3]

$$\hat{\tau} = \arg \max_{\tau} \begin{cases} \Lambda_1(2\tau) & \text{for } 0 \leq \tau < T/2 \\ \Lambda_2(2\tau - 1) & \text{for } T/2 \leq \tau < T \end{cases} \quad (2.33)$$

where the likelihood functions $\Lambda_1(2\tau)$ and $\Lambda_2(2\tau - 1)$ are given by

$$\begin{cases} \Lambda_1(2\tau) = \sum_{n=1}^N |m(2n - 1, 2\tau)|^2 & \text{for } 0 \leq \tau < T/2 \\ \Lambda_2(2\tau - 1) = \sum_{n=1}^N |m(2n, 2\tau - 1)|^2 & \text{for } T/2 \leq \tau < T. \end{cases} \quad (2.34)$$

The likelihood functions (2.34) can also be expressed as a function of the fractional interval and interpolation filter branches as follows;

$$\begin{cases} \Lambda_1(\mu T_s) = \sum_{n=1}^N \left| \sum_{l=0}^L v_l(2n - 1) \mu^l \right|^2 \\ \Lambda_2(\mu T_s) = \sum_{n=1}^N \left| \sum_{l=0}^L v_l(2n) \mu^l \right|^2. \end{cases} \quad (2.35)$$

The carrier phase estimate for an M-PSK signal is deduced by using the above timing estimate $\hat{\tau}$, as follows

$$\hat{\theta} = \begin{cases} \frac{1}{M} \arg \sum_{n=1}^N \left(\sum_{l=0}^L v_l(2n - 1) \hat{\mu}^l \right)^M \\ \frac{1}{M} \arg \sum_{n=1}^N \left(\sum_{l=0}^L v_l(2n) \hat{\mu}^l \right)^M. \end{cases} \quad (2.36)$$

By noticing that the summation inside the parentheses is actually the output sample of the Farrow structure $y(i)$ for both $0 \leq \tau < T/2$ and $T/2 \leq \tau < T$, Eq. (2.36) can be rewritten

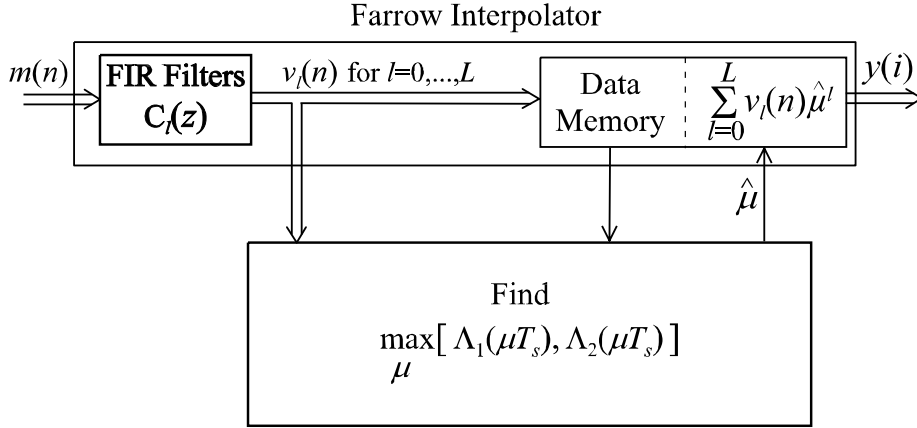


Fig. 2.9 NDA symbol timing recovery scheme.

as

$$\hat{\theta} = \frac{1}{M} \arg \sum_{n=1}^N (y(i))^M. \quad (2.37)$$

Finally, the symbol timing estimate is reduced to the search of the value of $\hat{\mu}$ that maximizes either of the likelihood functions $\{\Lambda_1(\mu T_s), \Lambda_2(\mu T_s)\}$. Then, the timing estimate is used for computing the carrier phase estimate $\hat{\theta}$. Alternatively, this algorithm is described as follows;

If $\max[\Lambda_1(\mu T_s)] > \max[\Lambda_2(\mu T_s)]$ **then**
 $\hat{\mu} = \arg \max_{\mu} [\Lambda_1(\mu T_s)]$
 $\hat{\theta} = \frac{1}{M} \arg \sum_{n=1}^N (y(i))^M$
else
 $\hat{\mu} = \arg \max_{\mu} [\Lambda_2(\mu T_s)]$
 $\hat{\theta} = \frac{1}{M} \arg \sum_{n=1}^N (y(i))^M$
end If

The overall scheme of the NDA block-based symbol timing and carrier phase recovery is illustrated in Figs. 2.9 and 2.10. Notice that the influence of the data symbols of this NDA feed-forward phase estimator is removed by the M^{th} power. Remark also that in this case, the averaging of the likelihood function cannot be done in the polynomial coefficient domain. Consequently, the algorithm is not as efficient as in the DA case with respect to the computational complexity.

2.6 SUMMARY OF SIMULATION RESULTS

Simulations have been performed to analyze the performance of digital receivers with non-synchronized sampling using the proposed polynomial-based ML synchronization algorithms for both DA and NDA cases and the results are shown in the publications [P1]-[P5]. The proposed schemes are simulated using an AWGN channel model, and different signal constellation types (i.e., PAM, QPSK, 16-QAM, and 64-QAM) for different block lengths

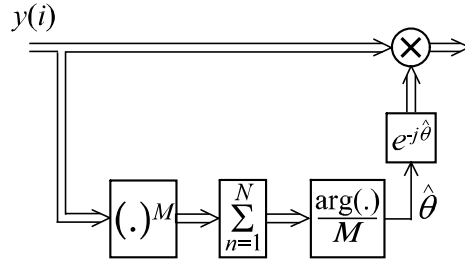


Fig. 2.10 NDA carrier phase estimation scheme for M-PSK modulations.

N . The transmitter and receiver pulse-shaping filters are square root raised cosine filters with excess bandwidth of 35%.

A frequency domain optimized third order interpolation filter ($L = 3$) of length 8 designed by using a minimax synthesis technique [24] is compared in the simulations with the conventional cubic Lagrange interpolator [13]. The length of the FIR filters in the Farrow structure for the optimized interpolator is twice as long as for the Lagrange interpolator. However, the filter coefficients are symmetrical for this optimized design which makes its complexity of the same order with the Lagrange interpolator. The number of the FIR filter branches is four for both interpolators. Also, the simulations are done using the worst-case timing offset and some selected values of the phase error.

Several sets of experiments have been conducted for both DA and NDA synchronization approaches. Theoretical expectations are compared with simulated worst case (with respect to timing offset) SEP as a function of E_b/N_0 using different types of modulations. Also, variance and mean of the timing jitter as well as symbol error probability (SEP) of both interpolators are compared. The effect of a relatively small frequency error, compared to the symbol rate, on the synchronization scheme is analyzed in [P4]. The simulation results demonstrate the efficiency and excellent performance of the proposed block-based feedforward estimators even in the presence of a small frequency error. Also, the results show the excellent performance of the frequency domain optimized interpolator compared to the traditional Lagrange interpolator specially if we want to make use of shorter block lengths which provide fast acquisition. In [P5], a new frequency estimator for fine acquisition suitable for this digital receiver type is derived. The simulation results of this work are given in the publications [P1]-[P5] included in the appendices, and a summary of the main results is presented in Chapter 4.

Chapter 3

Multipath Delay Estimation for Accurate Positioning

3.1 INTRODUCTION

In this chapter, we provide an overview of the most promising geolocation positioning techniques for wireless systems that are being standardized, including a survey of fundamental concepts and major problems in positioning. Then we briefly review the GPS system. Finally, we discuss and introduce new techniques with subchip resolution capabilities for estimating closely-spaced multipath delays in spread spectrum CDMA systems. Generally, multipath delays caused by distant reflectors have relatively large delay spread, more than one chip interval, that can be detected using conventional techniques [25], [26]. However, shorter excess path delays result in overlapped fading multipath components that introduce significant errors to the LOS path time and gain estimation. The proposed algorithms are intended to improve the accuracy of location estimates of GPS, as well as, mobile phone positioning using the cellular network assisted GPS technology by estimating correctly the LOS path. In the sequel, we will focus our study mainly on the GPS case.

3.2 TECHNIQUES FOR PERSONAL POSITIONING: PRINCIPLES AND PROBLEMS

Although mobile location is an enhanced feature of cellular systems which are primarily designed only for voice and data transmission, there exist some basic parameters available to the network that can be used to generate a rough position estimate. These available pieces of information, such as serving cell identity (CI), timing advance, and measured signal strengths of the serving and neighboring cells, can provide only a limited precision of location which cannot in any case satisfy the FCC requirements [1]. Even though, mobile positioning is a rather new concept and it is still in its infancy, various geolocation technologies have been recently devised using either *cellular network-based*, *mobile-based*,

or *hybrid* approaches [2]. Hereafter, we briefly discuss the most prominent positioning methods that have been approved for standardization within the 3rd Generation Partnership Project (3GPP)¹, by the sub-committee T1P1.5 of the American T1 Standards Committee, and subsequently in ETSI Technical Committee SMG. The methods that are being standardized by T1P1.5 for GSM are Time of Arrival (TOA), Enhanced Observed Time Difference (E-OTD), and Assisted GPS (A-GPS) [27]. In addition, Observed time difference of Arrival - Idle Period Down Link (OTDOA-IPDL) and Cell Identity methods have been added to allow easy migration to the upcoming 3G systems [28].

- **Time of Arrival**

Time of Arrival positioning method with known time of transmission (TOT), is a multilateral and pure network-based approach where multiple base stations listen to handover access bursts and triangulate the position of the mobile. Measurements of the exact time of arrival of at least three MS to BSs radio links has to be performed with respect to a synchronized and common reference time clock [53]. The location of the user equipment is consequently given by the intersection of the three TOA circles. TOA positioning requires full network synchronism, which is not the case for GSM and the forthcoming 3G networks [2].

A more practical and suitable technique for the asynchronous networks is the *Time Difference of Arrival* (TDOA) positioning where TOA differences are used in order to eliminate the unknown TOT from the observations. TDOA technique relies simply on the time difference at which signal arrives at multiple BSs, rather than on the absolute arrival time like the TOA method [29]. TOA estimates of a serving BS and its neighbor yield one TOA difference which result in a hyperbola that lies between the two BSs. Measurements of TOA from at least four serving neighbor BSs result in three hyperbolas. The intersection of the three hyperbolas determines the mobile device position, and this is known as hyperbolic trilateration [29].

- **Enhanced Observed Time Difference**

Enhanced Observed Time Difference is basically reversed TOA or mobile terminal based TOA, where the handset is much more actively involved in the positioning process. E-OTD is a unilateral approach that involves the mobile station in estimating the timing differences between the various base stations [30]. In E-OTD, the mobile station listens to bursts from several base stations and measures the observed time differences, which are then used for trilateration of the mobile position as shown in Figure 3.1.

Unilateral E-OTD principle has been approved for standardization in different cellular systems. For GSM it is called E-OTD, in 3G systems it is OTDOA-IPDL, and in US-CDMA it is called Advanced Forward Link Trilateration (AFLT). These systems have different names mainly because of the different network types and measurement processes of TOA signals [27].

- **Assisted Global Positioning System (A-GPS)**

¹3GPP is a joint activity of the European ETSI, American National Standards Institute, and Japanese ARIP to standardize next generation wireless communication systems.

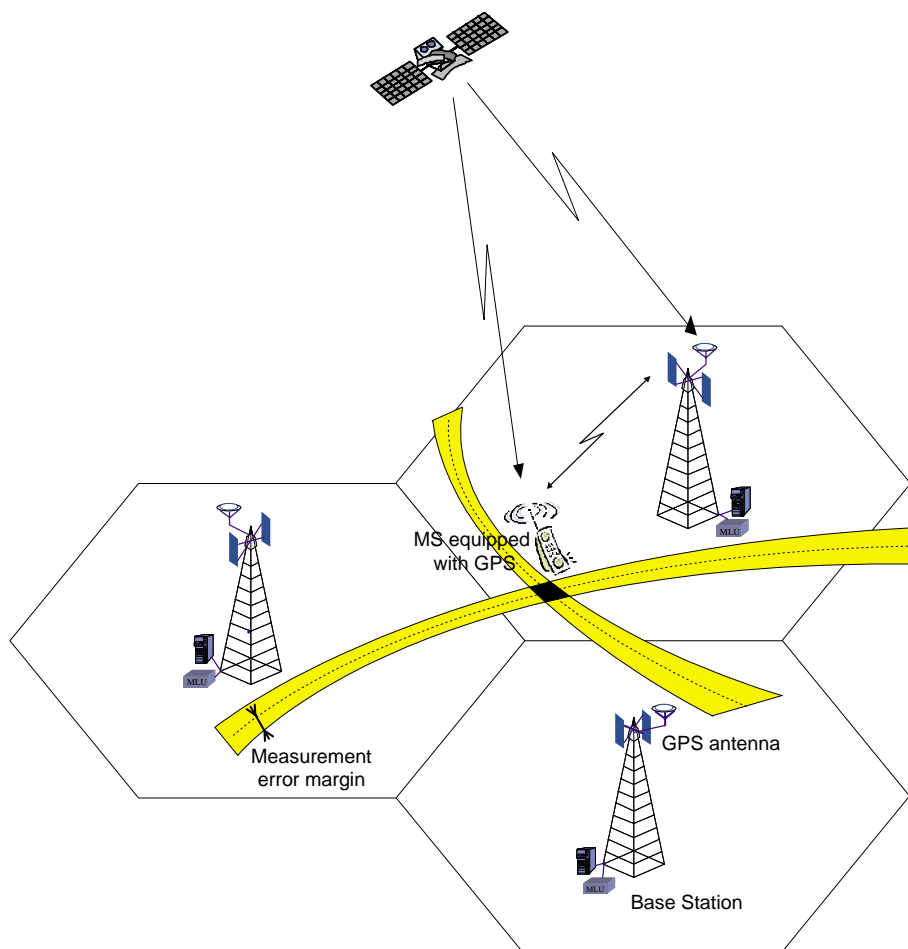


Fig. 3.1 Principles of E-OTD and A-GPS methods in cellular network.

Assisted Global Positioning System relies on mobile stations having an integrated GPS receiver aided by the cellular network assistance and support to enhance the positioning, especially for the non-line-of-sight (NLOS) conditions and indoor environments. Assistance data is transmitted from the network to the MS in order to expedite the GPS signal acquisition search and therefore shortening the time-to-first-fix from minutes to a second or less [31]. GPS-based positioning appears to be the most prominent and the leading candidate for wireless systems in terms of accuracy, reliability, latency, availability, and continuity of service [2].

The major problem of the above described geolocation solutions, with the exception of A-GPS, is that they are unable to deliver reliable positioning to the end user with homogeneous performance in urban, suburban, rural, and indoor environments. Currently, the efforts are aiming at defining hybridised solutions that satisfy all the imposed requirements, involving the lowest possible cost and minimal impact on the network and handset equipment. For example, network-based positioning systems have the advantage of working with all existing mobiles, but have the disadvantage of limited accuracy and requiring additional investments in the supporting infrastructure. Similarly, mobile station based on stand-alone GPS provides location capability with high accuracy, also in the absence of wireless coverage or network assistance using the same infrastructure, but requires handset modifications,

receiver could take several minutes to acquire the satellite signals, and generally fails in radio shadows and indoor environments.

Another major source of error that has a strong impact on the accuracy of most geolocation solutions, including GPS, is due to the multipath signal propagation that may be due to atmospheric reflection or refraction, or reflections from buildings and other objects. Commonly, in most applications of radio communications and navigations [25], the line of sight (LOS) signal is succeeded by multipath components that arrive at the receiver within a short delay spread, that can be less than one chip interval. This causes overlapping fading multipath components and introduces significant errors in the LOS path time of arrival and gain estimation. In spread spectrum CDMA systems, such as third generation mobile communications or GPS receivers, it is important to achieve accurate delay estimation (or code synchronization) before despreading and data detection. Also, most spread spectrum systems use spreading codes with non-ideal correlation properties which result in co-channel interference, or multiuser-interference, for radio communication systems, which is also called multi-transmitter interference in radio-navigation systems [25]. Generally, the performance of radio communication systems is heavily affected by the multipath and multiuser-interferences.

3.3 FUNDAMENTALS OF GPS

The principle of GPS positioning is based on the concept of TOA ranging to determine the user location. This concept entails measuring the propagation time of signals broadcast simultaneously from satellites at known locations. Ideally, the distance between a satellite and a user receiver is obtained by multiplying the propagation-time (or transit-time) with the speed of light. The GPS satellites, or space vehicles (SVs), are put in medium earth orbital planes and they are moving in space at a speed of about 4 km/s along their orbits, repeating almost the same ground track once each day. Although each SV is equipped onboard by a pair of ultra-stable atomic clocks, the satellite clocks are maintained in synchronism by the monitoring control segment that uploads the updated parameters for each SV clock, together with the navigation message broadcast by each satellite [32].

In theory, a receiver can estimate its position using three TOA measurements if the satellite and receiver clocks are synchronized. However, in practice the user's receivers typically employ inexpensive and low-accuracy quartz oscillators as local clocks, which are set approximately to GPS time. Therefore, the receiver clock introduces certain timing offset or clock-bias to the true GPS time which affects the observed transit-time for all satellites equally. The receiver can overcome this problem by measuring the distance to four SVs in view. These measured distances are usually too short, or too long, compared to the 'real' range by a common amount and they are called pseudo-ranges. In addition to the 3-dimensional coordinates of spatial position, a user needs to estimate the receiver clock offset. The user position can then be determined by solving the four pseudo-ranges for the four unknowns [33].

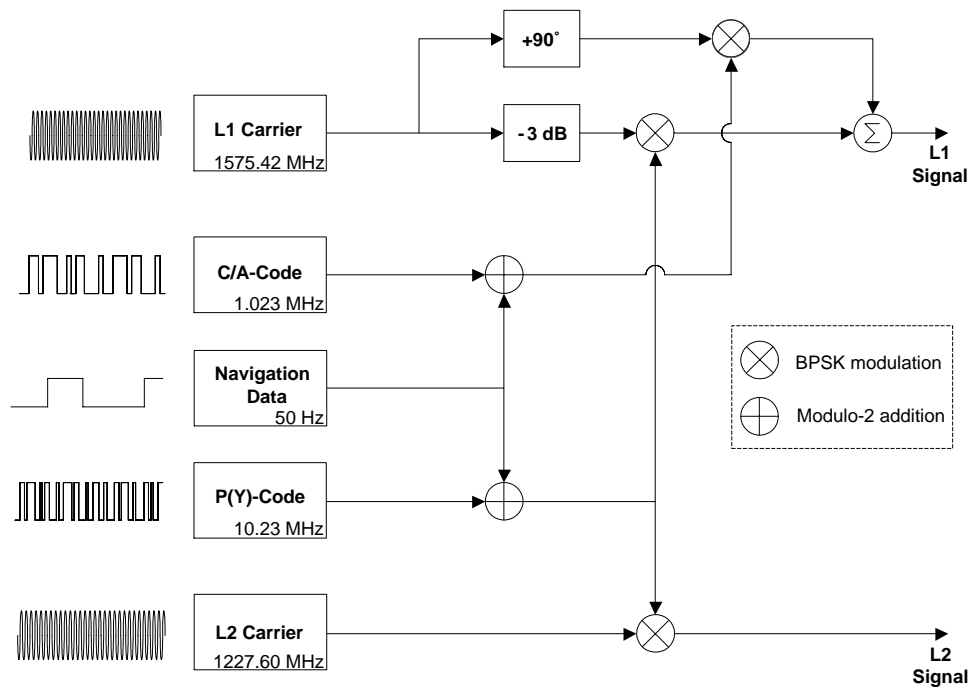


Fig. 3.2 GPS signal structure.

3.3.1 Satellite Signals

GPS satellite transmissions utilize direct sequence spread spectrum (DS-SS) modulation [32]. Spread spectrum techniques have been widely in military use because they can combat strong interference and prevent message recovery by unauthorized receivers, and they have also been adopted for commercial applications [16]. Spread spectrum communication systems involve the transmission of a signal in a radio frequency bandwidth much greater than the data information bandwidth to be conveyed. These systems spread the transmitted signal spectrum over a frequency range substantially greater than the bandwidth of the modulating data message. In Direct sequence (DS) systems, the spectral spreading is performed by multiplying the data signal by an auxiliary pseudo random-noise (PRN) code [34].

Each SV broadcasts two types of PRN ranging signals, as well as navigation data which consists of satellite ephemeris data and satellite health data, allowing users to measure their pseudo-ranges and hence estimating their positions, velocity, and time [32]. Figure 3.2 illustrates the GPS signal structure. The ranging signals are pseudo-random noise codes that modulate the satellite carrier frequencies using binary phase shift keying (BPSK). Each satellite transmits continuously two microwave carrier signals called the primary carrier, $L_1 = 1575.42$ MHz, and secondary carrier, $L_2 = 1227.60$ MHz. The carrier frequencies are modulated by spread spectrum codes with a unique PRN sequence associated to each satellite and by the navigation data [33]. The near orthogonality of the PRN code sequences permits all the satellites to transmit on the same carrier frequencies without incurring significant mutual interference [34]. PRN codes are simply deterministic binary sequences with specific statistical random noise-like properties [34]. The family of PRN codes is mainly characterized by the low cross-correlation between the codes, they are nearly orthogonal, and the autocorrelation function is almost zero except at zero delay [32].

3.3.2 Signal Characteristics

The carrier frequency L_1 is BPSK modulated by two PRN codes, the coarse acquisition code (C/A-code) and the precision code (P-code), while L_2 is BPSK modulated only by the P-code. Low rate navigation data is modulated to both carriers. The P-code is available only for USA Department of Defense (DoD) authorized users and, when encrypted, is called Y-code. P-code is a very long PRN code with a repetition period of one week and chipping rate of 10.23 MHz and is the basis for precise position services (PPS). The C/A-code is a gold code sequence of length 1023 chips, with a repetition period of 1 ms, and a null to null bandwidth of about 2.046 MHz, ten times smaller that of the P-code [32]. C/A codes are intended for civil standard position services (SPS) and available for all users. The L_1 carrier is modulated by C/A code sequence combined with the navigation data inphase quadrature with the precision P-code combined with the data [36]. Thus, as shown in Fig. 3.3, the modulation of the civil C/A-code combined with the data is orthogonal to the modulation of the P-code added with the data on the L_1 signal. The navigation data consists of a low-rate (50 bits/sec) bit-stream describing the satellite orbits (ephemeris and almanac), clock corrections, and other parameters.

The received power levels on earth of the three GPS signals transmitted by the SVs are extremely weak and depend on the user elevation angle [32]. The minimum received signal power level, correspond at an elevation angle of 5° from the user's horizon are -160 dBW for the C/A-code, -163 dBW for P(Y)-code at L_1 , and -166 dBW for P(Y)-code at L_2 . Table 3.1 summarizes the GPS signal structure and the minimum received signal power at

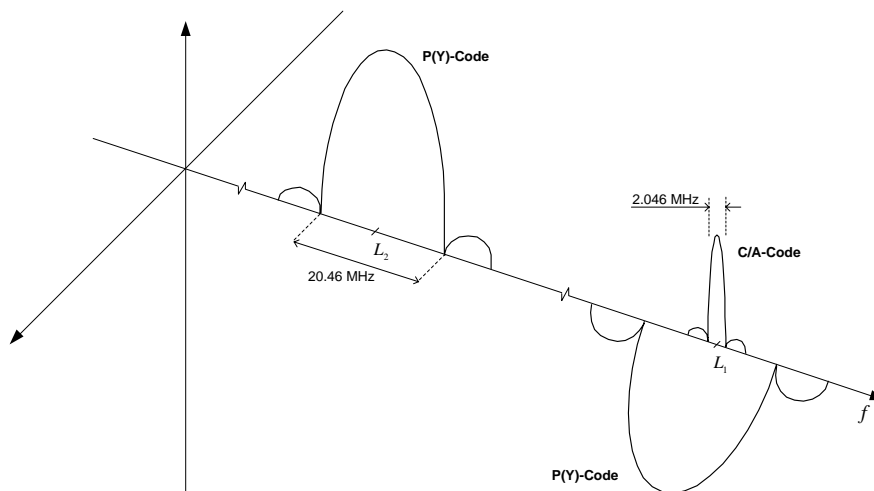
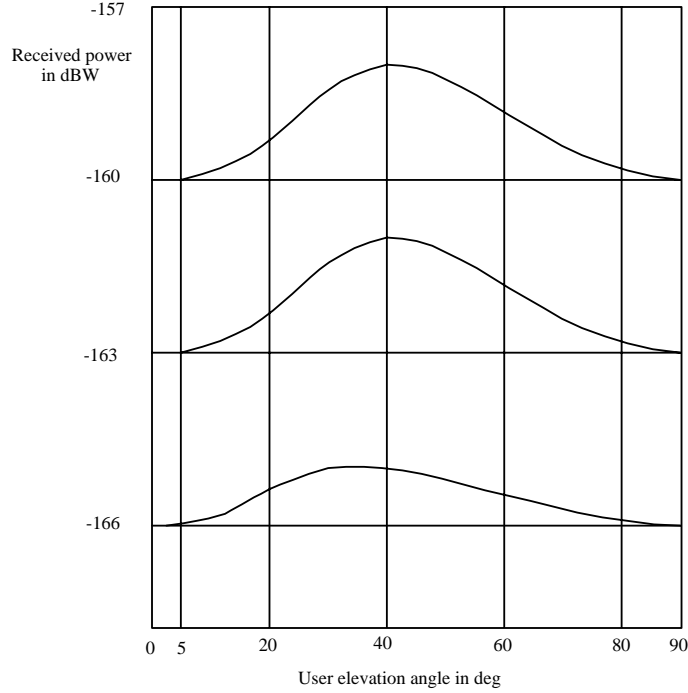


Fig. 3.3 GPS signal spectrum (positive side).

an elevation of 5° . The change in the received power levels with respect to the user elevation angle and signal structure is illustrated in 3.4. GPS is limited by the weak penetration indoor of the satellite signal. Multipath effects are considered as one major sources of error in precise GPS positioning services. It affects the code range, the carrier phase measurements, and also the signal power which is an average of the composite of signal power of the direct and multipath components.

Table 3.1 GPS signal structure and minimum received signal power.

Signal	P(Y) & L ₁	C/A & L ₁	P(Y) & L ₂
Carrier Frequency (MHz)	1575.42	1575.42	1227.60
PRN Codes (Mchips/sec)	10.23	1.023	10.23
Navigation Data (bits/sec)	50	50	50
Minimum Received Power (dBW)	-163	-160	-166


Fig. 3.4 User received minimum power levels with respect to the user elevation angle and signal structure.

3.4 MULTIPATH DELAY ESTIMATION TECHNIQUES

3.4.1 Channel Models

In a multipath fading environment, the channel can be modeled by a linear time-variant filter characterized by the complex-valued lowpass equivalent impulse response [26]

$$h(\tau, t) = \sum_{n=0}^N \alpha_n(t) e^{j\phi_n(t)} \delta(\tau - \tau_n(t)) \quad (3.1)$$

where N represents the number of propagation paths, $\alpha_n(t)$, $\phi_n(t)$ and $\tau_n(t)$ are the amplitude, the phase, and the propagation delay of n^{th} path, respectively. The channel is assumed to remain stationary during the considered observation time interval. In the sequel, the notation α_n , ϕ_n and τ_n will be adopted for simplicity.

By assuming that $h(\tau, t)$ is a zero mean, complex Gaussian random variable and wide-sense stationary, it can be described by the following fading autocorrelation function [16]

$$R_h(\tau, \Delta t) \triangleq E[h^*(\tau; t)h(\tau; t + \Delta t)] \quad (3.2)$$

which gives a measure of the speed of channel variations. For $\Delta t = 0$, the autocorrelation reduces to $R_h(\tau, 0) \equiv R_h(\tau)$, called the intensity profile of the channel measuring the expected received power as a function of the delay τ . The delay-spread of the channel, denoted by T_m , is given by the region over which the $R_h(\tau)$ is not equal to zero and it indicates the degree of the time spreading in the channel. Thus, the reciprocal $B_c = 1/T_m$ is defined as the coherence bandwidth of the channel and it is a measure of the frequency selectivity. The multipath components have different path lengths resulting in different propagation delays. The delay spread of a channel depends in part on the proximity of scattering objects to the transmitter and receiver.

Due to the time variations in the medium structure, multipath delays are generally time-varying. The rate at which these-time delays vary, influences strongly the multipath channel effects on the signal. Time-variant multipath characteristics of the channel are analyzed using the spaced-time spaced-frequency correlation function of the channel given by [16]

$$R_H(\Delta f; \Delta t) \triangleq E[H^*(f; t)H(f + \Delta f, t + \Delta t)]. \quad (3.3)$$

Here $H(f; t)$ is the Fourier transform of $h(\tau; t)$ and the time variations in the channel are measured by the time spacing parameter Δt .

Another way to express the rapidity of the channel variations and to reflect the Doppler effects, is by means of the Fourier transform of $R_H(\Delta f; \Delta t)$ with respect to the time spacing Δt as follows [26]

$$S_H(\Delta f; \nu) \triangleq \int_{-\infty}^{+\infty} R_H(\Delta f; \Delta t) e^{-j2\pi\nu \Delta t} d\Delta t. \quad (3.4)$$

In particular for $\Delta f = 0$, the Doppler power spectrum of the channel is defined by

$$S(\nu) \equiv S_H(0, \nu) = \int_{-\infty}^{+\infty} R_H(\Delta t) e^{-j2\pi\nu \Delta t} d\Delta t. \quad (3.5)$$

The width of the region over which $S(\nu)$ is non-zero, is called the Doppler spread of the channel, denoted here by B_d , and its reciprocal is called the coherence time $(\Delta t)_c = 1/B_d$. The Doppler spread function characterizes the rapidity of the fading and is used in modeling Doppler shifts in the frequency domain caused by the relative motion of the transmitter, scatterers, and receiver. Slowly fading channel has a small Doppler spread B_d , which corresponds to a long coherence time.

Different types of fading channels do exist depending on the value of spread factor $T_m B_d$ of the channel, as well as, on the bandwidth $W = 1/T$ of the lowpass equivalent received signal [35]. For example, for a frequency nonselective flat and slowly fading channel, the spread factor is less than unity, $T_m B_d < 1$. In this case, the signal bandwidth is very small compared to the coherence bandwidth of the channel $W \ll B_c$, also the signalling interval is very small compared to the coherence time $T \ll (\Delta t)_c$ and the channel properties remains constant during a symbol interval. Similarly, if the spread factor is greater than unity $T_m B_d > 1$, it indicates that we have either a frequency selective channel $W > B_c$ or a fast fading channel $T > (\Delta t)_c$.

3.4.2 Conventional ML Based Approaches

After down-conversion of the received civil signal to baseband through mixing and filtering, the received GPS signal from one satellite in the presence of M -path channel can be modeled as [25], [37]

$$\begin{aligned} r(t) &= x(t) + n(t) \\ &= \sum_{i=0}^{M-1} a_i C(t - \tau_i) e^{j\theta_i} + n(t), \end{aligned} \quad (3.6)$$

where $C(t)$ is the real spread-spectrum code with a chipping rate $1/T_C$ much higher than the navigation data stream rate $1/T_D = 50$ bits/s, and $n(t)$ is an additive white Gaussian noise with power spectral density N_0 . The time-variant a_i , τ_i and θ_i represent the attenuation factor, time delay, and phase for the i^{th} path, respectively. The estimation of the set of parameters $\{a_i, \tau_i, \theta_i\}$ is very essential for locating the line-of-sight path, and consequently for determining the GPS position, velocity and/or time.

Assuming that the down-converted signal $r(t)$ is completely defined in the observation time interval T_D , the conditional likelihood function based on the observation vector \mathbf{r} for a given set of synchronization parameters $\Phi = \{a, \tau, \theta\}$ is given by

$$p[\mathbf{r}|\Phi] = \xi \exp \left\{ -\frac{1}{N_0} \int_{T_D} [r(t) - \hat{x}(t)]^2 dt \right\} \quad (3.7)$$

where ξ is just a positive constant independent of the synchronization parameters which can be neglected, and $\hat{x}(t)$ is the local trial signal replica generated at the receiver, modeling the estimated line-of-sight and multipath signals

$$\hat{x}(t) = \sum_{i=0}^{M-1} \hat{a}_i C(t - \hat{\tau}_i) e^{j\hat{\theta}_i}. \quad (3.8)$$

Multipath delay estimation techniques are based on the maximum likelihood theory [25] which are trying to estimate the set of parameters $\{\hat{a}, \hat{\tau}, \hat{\theta}\}$ by minimizing the mean squared error of the log-likelihood function (LLF) given by

$$L_{ML}(\hat{a}, \hat{\tau}, \hat{\theta}) = \text{Re} \left\{ \int_{T_D} [r(t) - \hat{x}(t)]^2 dt \right\}. \quad (3.9)$$

Thus, the synchronization parameters are determined by differentiating the above LLF function with respect to the synchronization parameters, then setting the partial derivatives equal to zero. The partial derivative with respect to the time-delay estimate is given by [25]

$$\left. \frac{\partial}{\partial \tau} L_{ML}(\hat{a}_i, \tau, \hat{\theta}_i) \right|_{\tau=\tau_i} = 2 \frac{\partial}{\partial \tau} \left[\text{Re} \left\{ \left[R_{rc}(\tau) - \sum_{l=0, l \neq i}^{M-1} \hat{a}_l R_c(\tau - \hat{\tau}_l) e^{j\hat{\theta}_l} \right] e^{-j\hat{\theta}_i} \right\} \right]_{\tau=\tau_i}. \quad (3.10)$$

In the above equation, $R_{rc}(\tau)$ is the inphase/quadrature time-average cross-correlation function over the observation time interval T_D , given by

$$R_{rc}(\tau) = \frac{1}{T_D} \int_{T_D} r(t) C(t - \tau) dt, \quad (3.11)$$

and $R_c(\tau)$ is the reference time-average correlation function of the spreading code, given by

$$R_c(\tau) = \frac{1}{T_D} \int_{T_D} C(t)C(t - \tau)dt. \quad (3.12)$$

Different methods have been derived for finding the multipath delays, including coherent and non-coherent delay locked loops (DLLs) with proper early and late code spacings [34], [37] [38]. These methods are just trying to track the delay of the line-of-sight path by correlating the down-converted received signal with replicas of spreading codes locally generated by the DS-SS receiver.

Normally, by spreading the transmitted signal over a bandwidth larger than the coherence bandwidth of the channel, we can decrease the effects of multipath fading. The bandwidth spread makes it possible to separate different multipath signals if their relative delay difference exceeds one chip interval. Typically, distant reflectors have relatively large delay spread with more than one chip interval between successive paths, therefore, resulting multipaths can be removed by correlator-based mitigation techniques [25]. Thus, by maximizing the partial derivative equation of the LLF (3.9) with respect to the time-delay, the desired i^{th} path estimate can be written as follows,

$$\hat{\tau}_i = \arg \max_{\tau} \left[\text{Re} \left\{ \left[R_{rc}(\tau) - \sum_{l=0, l \neq i}^{M-1} \hat{a}_l R_c(\tau - \hat{\tau}_l) e^{j\hat{\theta}_l} \right] e^{-j\hat{\theta}_i} \right\} \right]. \quad (3.13)$$

Similarly, by differentiating equation (3.9) with respect to the carrier phase and amplitude, and by solving the partial derivative equations for the M multipath components, the estimated carrier phase and amplitude for the i^{th} path are, respectively, given by [25]

$$\hat{\theta}_i = \arg \left[R_{rc}(\hat{\tau}_i) - \sum_{l=0, l \neq i}^{M-1} \hat{a}_l R_c(\hat{\tau}_i - \hat{\tau}_l) e^{j\hat{\theta}_l} \right] \quad (3.14)$$

$$\hat{a}_i = \text{Re} \left\{ \left[R_{rc}(\hat{\tau}_i) - \sum_{l=0, l \neq i}^{M-1} \hat{a}_l R_c(\hat{\tau}_i - \hat{\tau}_l) e^{j\hat{\theta}_l} \right] e^{-j\hat{\theta}_i} \right\}. \quad (3.15)$$

Basic DLLs can estimate efficiently the multipath propagation delays if they are not overlapping and spaced at more $(1 + \Delta)T_C$, where Δ being the loop discriminator value or early-late code spacing. However, the effects of offset paths are ignored. Several studies have been conducted to analyze the effects of multipath delays on coarse acquisition techniques [39] and fine acquisition techniques [40]. Delay locked loop (DLL) circuits generally fail to estimate closely-spaced multipaths with less than one chip interval, besides their convergence can be quite slow [25], [26], [37], [38]. Fig. 3.5 shows an example of S-curves obtained via a non-coherent DLL (NCDLL) with $SNR = 20$ dB for half chip and two chips spaced taps. We clearly notice that NCDLL fails to detect very closely spaced multipaths [35].

Another illustrative example in Fig. 3.6 shows the effect of multipath propagation on the S-curve with different early-late spacing values. Notice that the multipath components bias the tracking of the DLL. Smaller discriminator values may reduce this bias effect but are not able to eliminate it completely. However, as the excess path delays becomes smaller, they

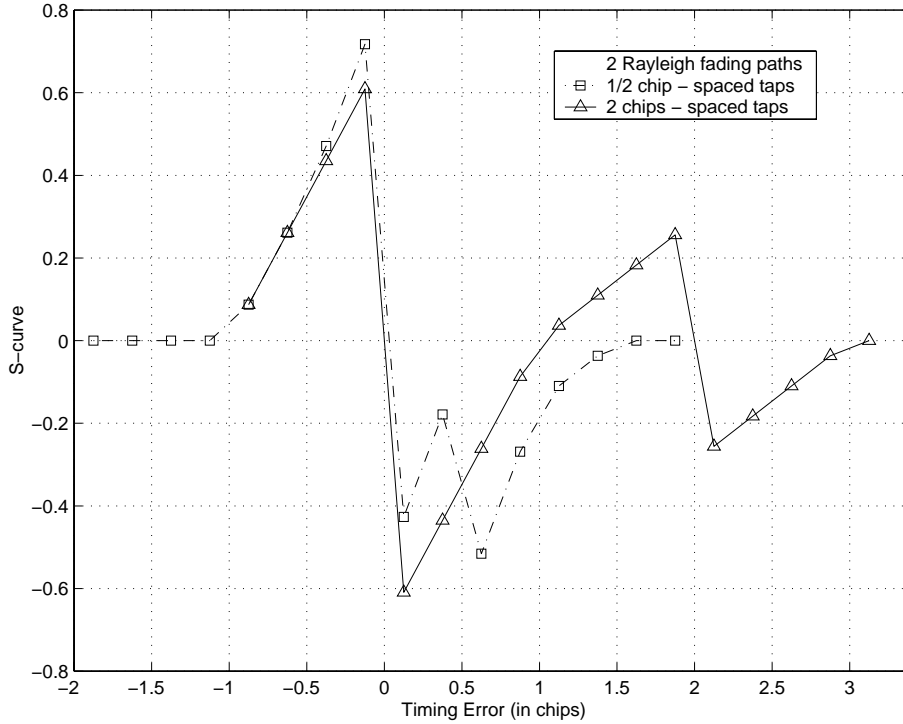


Fig. 3.5 Non-coherent DLL S-curve for a multipath channel.

result in shorter delays spread. Consequently, the LOS signal overlaps with the succeeding multipath components of short delays introducing significant error to the LOS path time and gain estimation.

Generally, multipath delay estimation techniques are based on the cross-correlation function (Eq. 3.11) of the down-converted signal de-spread with a copy of the spreading code locally generated by the DS-SS receiver. The advanced multipath estimating DLL techniques [38] are trying to approximate the overall cross-correlation using a set of reference correlation functions (Eq. 3.12) with certain delays, phases and amplitudes according to Eqs. (3.13), (3.14) and (3.15).

Many other techniques for mitigating the effects of multipath delays have been developed, including several subspace-based approaches. However, they are usually too complex for practical purposes and suitable only for systems employing short codes [41], [43], and the topic remains still an open area of research.

3.4.3 Multipath Delay Estimation Using Peak Tracking with Pulse Subtraction

Assuming that the locally generated code at the receiver side is locked to the received signal code (locally generated real code corresponds to the SV received signal code), by substituting equation (3.6) into (3.11), the cross-correlation function is simply expressed by

$$R_{rc}(\tau) = \frac{1}{T_D} \sum_{i=0}^{M-1} a_i e^{j\theta_i} \int_{T_D} C(t - \tau_i) C(t - \tau) dt + \frac{1}{T_D} \int_{T_D} n(t) C(t - \tau) dt. \quad (3.16)$$

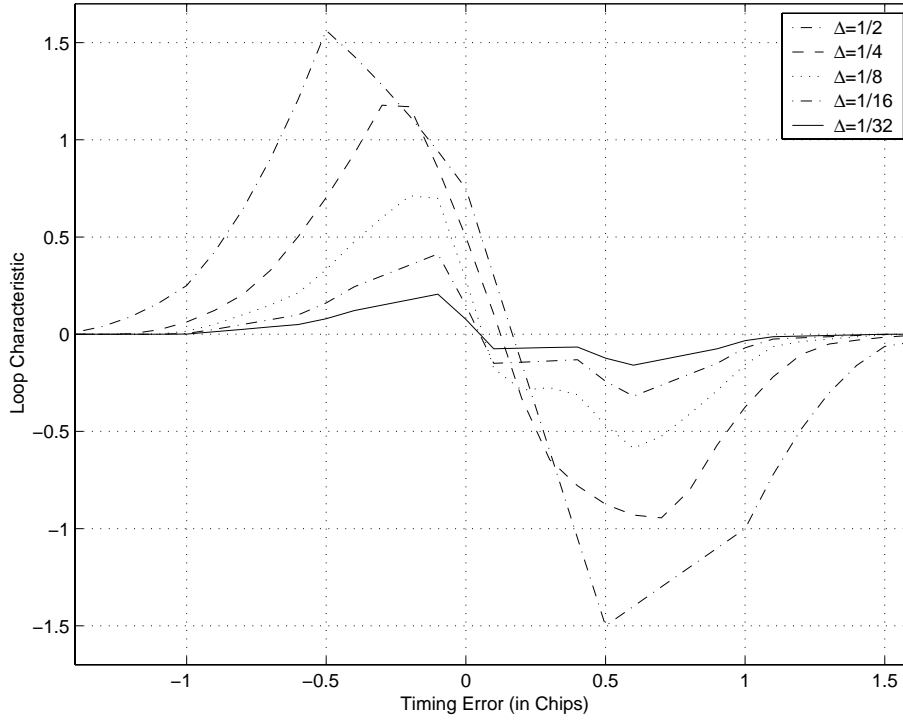


Fig. 3.6 Effect of multipath propagation on the S-curve of a non-coherent DLL using different discriminator values Δ and two paths channel.

Generally, practical GPS receivers perform averaging over short-time observation intervals less than the navigation data interval T_D to speed up the SV signals tracking. Normally, even-though we are considering averaging over a sufficiently large observation time interval, we shall consider the following biased estimator

$$R_{T'_D}(\tau) = \begin{cases} \frac{1}{T'_D} \int_{T'_D} C(t)C(t - \tau)dt & \text{for } |\tau| < T'_D \\ 0 & \text{otherwise} \end{cases}$$

whose expected value or mean is given by [42]

$$E\{R_{T'_D}\} = R(\tau) \left(1 - \frac{|\tau|}{T'_D}\right) = R(\tau) \Delta(\tau, T'_D). \quad (3.17)$$

Here, $\Delta(\tau, T'_D)$ denotes a triangular function defined as follows

$$\Delta(\tau, T'_D) = \begin{cases} 1 - |\tau|/T'_D & |\tau| \leq T'_D \\ 0 & \text{otherwise.} \end{cases} \quad (3.18)$$

Recalling the Gaussian nature of the random process as well as the mean of the biased estimator (3.17), the expectation of the above cross-correlation function (3.16) becomes

$$\begin{aligned} E\{R_{rc}(\tau)\} &= \sum_{i=0}^{M-1} a_i e^{j\theta_i} R_c(\tau - \tau_i) \left(1 - \frac{|\tau - \tau_i|}{T'_D}\right) \\ &= \sum_{i=0}^{M-1} a_i e^{j\theta_i} R_c(\tau - \tau_i) \Delta(\tau - \tau_i, T'_D). \end{aligned} \quad (3.19)$$

Notice that the expected value of the cross-correlation function is expressed simply as a weighted sum of delayed correlation functions times triangular windows with certain amplitude and phase specific to each signal path. The correlation effectively amplifies the underlying BPSK data signal, with an amplification factor equal to the length of the PRN Gold code sequence.

The proposed peak tracking with pulse subtraction approach for estimating the multipath delays is analogous to the advanced DLL techniques [25] in the sense that it is trying to estimate the overall cross-correlation function using a set of reference functions, but with different and simpler implementation. This approach is based on the search of the global maxima of the cross-correlation function (Eq. 3.16). Then, the contribution of each selected maximum is reduced from the overall cross-correlation using the autocorrelation function of a rectangular pulse [54]. The proposed technique is described further by the following algorithm:

- find the global maximum

$$\hat{\tau}_1 = \arg \max_{\tau} [|R_{rc}(\tau)|].$$
- compute the residual cross-correlation function

$$R_{rc,1}(\tau) = |R_{rc}(\tau) - R_{rc}(\hat{\tau}_1) \Delta(\tau - \hat{\tau}_1)|.$$
- find the global maximum of the residual cross-correlation function

$$\hat{\tau}_2 = \arg \max_{\tau} [|R_{rc,1}(\tau)|].$$
- estimate successively the next $M_{est} - 1$ maxima

$$\hat{\tau}_k = \arg \max_{\tau} \left[\left| R_{rc}(\tau) - \sum_{l=1}^{k-1} R_{rc,l}(\hat{\tau}_l) \Delta(\tau - \hat{\tau}_l, T_C) \right| \right], \quad k = 2, 3, \dots, M_{est}.$$

Here $R_{rc,l}(\tau)$ is the residual cross-correlation function after l^{th} peak subtraction, M_{est} is an estimate for the number of multipaths of the channel (it can be taken equal to the number of fingers (or correlators) as in a Rake receiver). By using the ideal code correlation pulse for subtracting the contribution of each channel path, we are able to detect very closely-spaced multipaths within less than one chip period ($|\tau_l - \tau_k| < T_C$) [54].

Only a simplified generic structure is presented above to describe the algorithm. However, instead of choosing the global maximum of the envelope of the residual correlation function as a true multipath component, we can take into account the merging phenomena. Hence, we try a set of multipath delays within a certain window around the global maxima with different weights, and the final estimates are those which give the best approximation of the correlation function in the mean square error sense.

3.4.4 Multipath Delay Estimation Based on Teager-Kaiser Operator

In this section, we introduce an innovative multipath delay estimation approach based on the nonlinear quadratic Teager-Kaiser operator that exploit the structure of the cross-correlation function (Eq. 3.11) for estimating sub-chip spaced multipath components.

The nonlinear quadratic TK operator was first introduced for measuring the real physical energy of a system [44], [45]. The energy of a generating system of a simple oscillation

signal was computed as the product of the square of the amplitude and the frequency of the signal. It was found that this nonlinear operator exhibits several attractive features such as simplicity, efficiency and ability to track instantaneously-varying spatial modulation patterns. Since its introduction, several applications have been derived for one-dimensional signal processing [S3], [46] (note that proposition 3 in [46] is erroneous as pointed in [47]) and two-dimensional signal processing [48], [55].

The continuous-time TK energy operator of a complex-valued signal $x(t)$ is defined as follows [S3]

$$\Psi_c[x(t)] = \dot{x}(t)\dot{x}^*(t) - \frac{1}{2}[\ddot{x}(t)x^*(t) + x(t)\ddot{x}^*(t)]. \quad (3.20)$$

Similarly, the discrete-time Teager operator of a complex valued signal is given by

$$\Psi_d[x(n)] = x(n-1)x^*(n-1) - \frac{1}{2}[x(n-2)x^*(n) + x(n)x^*(n-2)]. \quad (3.21)$$

Many useful properties of this nonlinear quadratic operator have been derived, and the analogy with the discrete-time domain has also been established [49], [56].

We notice that applying the continuous-time TK operator to the ideal reference correlation function of the spreading code which is characterized by the triangular shape (Eq. 3.18), we obtain

$$\Psi_c[\Delta(t, T_C)] = \frac{\Pi(t, T_C)}{T_C^2} + \frac{\Delta(t, T_C)\delta(t)}{T_C}, \quad (3.22)$$

where $\delta(t)$ is the Dirac function, and $\Pi(t, T_C)$ stands for a rectangular function with unit amplitude and duration $2T_C$ centered at $t = 0$ defined as

$$\Pi(t, T_C) \triangleq \begin{cases} 1 & |t| \leq T_C \\ 0 & \text{otherwise.} \end{cases}$$

Obviously, Eq. (3.22) shows that the TK operator applied to a triangular function provides a clear time-aligned peak location of the triangular pulse in the presence of a certain 'noise' floor.

Assuming now that the cross-correlation function is the sum of M triangular pulses as follows

$$R(t) = \sum_{i=0}^M a_i \Delta(t - t_i, T_C) e^{j\theta_i}, \quad (3.23)$$

where a_i , t_i and θ_i denote the amplitude, delay and phase, respectively. By applying the TK operator to the above equation we obtain

$$\begin{aligned} \Psi_c[R(t)] = & \frac{1}{T_C^2} \left[\left(\sum_{i=0}^M a_i \text{sign}(t - t_i) \Pi(t - t_i, T_C) \cos \theta_i \right)^2 \right. \\ & \left. + \left(\sum_{i=0}^M a_i \text{sign}(t - t_i) \Pi(t - t_i, T_C) \sin \theta_i \right)^2 \right] \\ & + \frac{1}{2T_C} \left[R^*(t) \left(\sum_{i=0}^M a_i \delta(t - t_i) e^{j\theta_i} \right) + R(t) \left(\sum_{i=0}^M a_i \delta(t - t_i) e^{-j\theta_i} \right) \right]. \end{aligned} \quad (3.24)$$

Notice that the above expression becomes very large if the time variable t is equal to one of the true delays t_i . Thus, equation (3.24) shows that the TK operator is capable of tracking very accurately the peak locations of the triangular pulses within certain 'noise' floor [57] independently of the delay spacing between the multipaths.

By exploiting the above properties of the quadratic operator, we found out that by applying this nonlinear TK operator to the specific cross-correlation function (Eq. 3.11) of a GPS receiver, one can easily estimate the multipath delays introduced by the channel. The multipath delays are simply estimated by selecting the time location of the highest (strongest) peaks of the Teager-Kaiser operator output function (equal to the number of fingers in the Rake receiver). Simulation results provided in publications [P6]-[P8] show the high performance of this innovative technique.

Chapter 4

Summary of Publications

4.1 RECEIVER SYNCHRONIZATION STUDIES

A general approach for discrete-time modeling and simulation of continuous-time signals and systems based on digital interpolation techniques is introduced in [P1]. We demonstrate that polynomial interpolation utilizing the generalized Farrow structure results in efficient polynomial signal processing models with moderate computational complexity. Normally, the lowest sampling rates which are sufficient for system modeling, are not sufficient for obtaining informative and accurate models. In cases where computational efficiency is an issue, different sampling rates can be used in different blocks to reduce the computational burden. In cases where there is a need to locate, e.g., the local maxima, minima, or zero crossings of a signal, higher order oversampling rate is needed. It is common practice also to use oversampling factors which are an order of magnitude higher than what is required from the sampling theory point of view.

The generalized Farrow structure allows, with low additional computational complexity, to compute several new samples at arbitrary points between the existing samples. Thus, it is very easy to get the signal sample values in a flexible way in what ever time instances they are needed. Furthermore, it is possible also to implement iterative procedures for estimating accurately, e.g., the maximum value of a continuous-time signal as well as the location of the maximum. In [P1] we also develop simple modifications of the Farrow structure which result in efficient polynomial-based differentiators for approximating the continuous-time derivative of a signal from its discrete-time samples. The Farrow structure discussed in [P1] is the basis of the proposed ML-based synchronization algorithms. As another potential application and a topic for future studies, Farrow-based derivative approximations could be utilized for efficiently calculating the continuous-time Teager function of a discrete-time signal. This could lead to efficient implementation structures for the Teager-based delay estimation techniques.

In [P2], a polynomial-based maximum likelihood technique for jointly estimating the symbol timing and carrier phase of digital receivers for the data-aided case is established. This technique is based on low order polynomial approximation of the log-likelihood func-

tion by using the Farrow structure. An extension of the proposed polynomial-based ML technique to the non-data-aided systems is derived in [P3]. Different simulations using the Lagrange and optimized interpolator are performed for both DA and NDA systems and compared with the theoretical case. The results show the high performance of the optimized interpolator compared to the Lagrange interpolator especially if we want to make use of shorter block lengths to obtain fast acquisition. However, the NDA approach requires more computation than the DA approach for estimating the polynomial-based likelihood function. Also, NDA based phase estimation is feasible only in case of PSK modulations.

In [P4], the effect of the frequency offset or Doppler shift on the performance of the digital receiver is analyzed while adjusting the symbol timing and the carrier phase. We demonstrated that the proposed synchronization scheme performs quite well within a relatively small range of frequency offset values with respect to the symbol period. Under the same assumption that the frequency offset is much smaller than the symbol period, symbol timing and carrier phase recovery can be done prior to the frequency error correction. Thus, we introduced in [P5] a frequency estimator that is directly derived from the carrier phase estimate. The proposed estimator is simple to implement and is particularly suited for this type of digital receiver architectures. Also, it performs fairly well when compared with the Fitz [50] and the Luise-Reggiannini [15] frequency estimators, in the presence of substantial carrier frequency offset.

4.2 MULTIPATH DELAY ESTIMATION STUDIES

Correlation estimation properties related to DS-CDMA receivers have been studied in [P6]. We showed the influence of the coherent integration and the non-coherent averaging length on multipath delay estimation, and the importance of the considered observation time interval length. In [P7], we introduced two techniques with subchip resolution capability for estimating closely-spaced overlapped multipath components suited for GSP system as well as for other spread spectrum CDMA systems. The first innovative technique is very simple and quite efficient based on Teager-Kaiser operator. It exploits the properties of the cross-correlation function between the received signal and the reference despreading code replica generated at the receiver in order to estimate accurately overlapped multipath delays independently of the delay spacing between the multipaths. The second algorithm is based on peak tracking with pulse subtraction which approximates the input correlation function using the superposition of a set of reference correlation pulses. Simulation results of a GPS receiver using different Rayleigh fading channels show the good performance of the proposed techniques. Also the obtained results are considered to be remarkable considering the computation complexity of these approaches in comparison to the advanced maximum likelihood based DLL techniques. Extension of the proposed algorithms to the case of asynchronous multiuser WCDMA systems is presented in [P8]. Simulation results in the presence of multiple interfering users and Rayleigh fading multipath channels are presented. It is demonstrated that the Teager-Kaiser technique is near far-resistant, and its performance in the presence of closely spaced multipaths is much better compared to the peak tracking with subtraction method.

The problem of resolving closely-spaced overlapped multipath components can be considered new, and has recently raised up the interest after its strong influence on the high

precision accuracy of geolocation solutions. Few good research articles exist in the literature dealing with this problem, they generally treat the case of only two paths that are present, and not very practical for implementation [37], [43], [51], [52].

4.3 AUTHOR'S CONTRIBUTION TO THE PUBLICATIONS

The research work of this thesis was carried out at the Institute of Communications Engineering (formerly Telecommunications Laboratory), Tampere University of Technology as one partner in the projects "Advanced Transceiver Architectures and Implementations for Wireless Communications" and "Analog and Digital Signal Processing Techniques for Highly Integrated Transceivers". The author has been a member of an active research group involved in studying and developing DSP algorithms for highly integrated digital receivers, as well in building COSSAP and Matlab simulation models. The members of the research group have been in close collaboration with the author and the whole project has been supported and guided by the thesis supervisor Prof. Renfors. However, the author's contribution to all of the publications has been essential in that he developed the theoretical framework, prepared the manuscript, and performed the experiments.

This thesis includes eight publications [P1]-[P8]. They are categorized under two main topics: estimation of the synchronization parameters for digital receivers with non-synchronized sampling clock [P1]-[P5], and estimation of closely-spaced multipath delays in CDMA systems [P6]-[P8]. In particular, the author's main contributions to these publications are as follows. In [P1], the author formulated and simulated the general approach for discrete-time modeling of continuous-time signals and systems based on the generalized interpolation technique which is efficiently implemented using minor modifications to the Farrow structure. Originally, the author introduced the concept of derivative approximation and the preliminary idea for integration using simple modifications of the Farrow structure. In [P2] and [P3], the author derived the likelihood functions for systematic synchronization schemes, made the extension for jointly estimating the symbol timing and carrier phase for both DA and NDA systems, and carried out the simulations. In [P4] and [P5], the author studied and simulated the effect of frequency offset on the synchronization scheme, and derived a new frequency estimator suitable for the proposed digital receiver type. Optimization of the Farrow structure based filters, needed in [P1]-[P5], are performed by Dr. Vesma.

In [P6] and [P7], the author is the founder of the multipath delay estimation techniques based on Teager-Kaiser operator. The idea of pulse subtraction technique was originally proposed by Prof. Renfors. The author derived and simulated the algorithms. In [P8], these algorithms have been applied and tested in the WCDMA multiuser environment using existing COSSAP simulation model. The author conducted experimental studies and wrote the manuscript.

Chapter 5

Conclusions

Currently, the main driving force behind the software radio development is the coexistence of several radio communication systems as a result of the high competition between Americans, Asians, and Europeans. The ultimate goal of designing a single-chip, flexible wireless transceiver supporting multimode and multistandard compatibility introduced new challenges in receiver architecture designs. The current trend is to push the analog/digital interface towards the antenna to simplify the analog parts and allow the implementation of most receiver functions digitally, increasing therefore the flexibility, configurability, and integrability. In fact, existing communication standards are using different data rates, and consequently they employ different master clock rates. By using a digital receiver architecture with a free running clock oscillator, receiver complexity can be substantially reduced by employing only a single master clock, and the other needed clock rates can be generated virtually by means of sampling rate conversion. As one important functionality, these new receivers require flexible and efficient synchronization algorithms which depend on the system requirements and receiver architecture design.

The first part of this research work introduces new maximum likelihood based symbol timing and carrier phase estimators suitable for digital receivers with non-synchronized sampling clock. Polynomial approximations of the likelihood functions using the Farrow-based interpolation technique were established for both DA and NDA forms. The simulations demonstrate the efficiency and excellent performance of the block-based feedforward estimators. The proposed approach provides an efficient and practical way for approximating very closely the ideal maximum likelihood estimate, especially for the DA case. The Farrow structure we are considering is particularly suitable for digital implementation.

However, the NDA case requires more computational burden because the averaging of the likelihood function can not be done in the polynomial coefficient domain as for the DA case. Therefore, further studies with respect to the computational complexity of the NDA technique are needed for practical applications.

Another essential receiver functionality closely related to synchronization is propagation delay estimation which is the basis for geolocation positioning solutions. The rapid evolution of digital communication systems and the new requirements imposed by the standardization authorities brought various consumer electronics device types and a high demand on

new communication services, such as mobile phone positioning with high and reliable accuracy. Even if safety was the primary motivation for mobile positioning, a lot of commercial applications have already emerged in the market.

However, multipath effects of the mobile channel could degrade the location estimate substantially, specially in the case of shorter excess path delays which result in overlapped fading multipath components that introduce significant errors to the LOS path time and gain estimation. Estimation of closely-spaced multipath components is regarded as a killer issue in location estimation, considered as one of the major sources of errors in high precision geolocation solutions, and still it is an open topic for research work.

In the second part of this thesis work, we introduced innovative techniques with sub-chip resolution capability for multipath delay estimation based on peak tracking with pulse subtraction and Teager-Kaiser quadratic operator both suited for spread spectrum CDMA systems, and we focused our study to the case of GPS receivers. Simulations results confirmed the high performance of Teager-based technique compared to the peak tracking with pulse subtraction method for all cases of closely-spaced multipaths within less than half chip period. The ability of solving closely-spaced paths in the presence of overlapped multipath components comes from the exploitation of the properties of the cross-correlation function. This new techniques are extremely simple and very efficient for estimating closely-spaced multipaths with much less computational complexity compared, e.g., to the conventional delay-locked loops and subspace-based multipath delay estimation methods [25], [41].

In general, for each shape of the reference correlation function or pulse shaping filter used, there may exist a linear or nonlinear operator capable of estimating easily the multipath delays. It remains as a challenging topic for future work is to generalize the Teager-based technique, and to derive other linear or nonlinear operators capable of tracking multipath delays in different communication systems.

References

- [1] FCC docket No. 94–102, Fourth memorandum opinion and order, September 8th, 2000.
- [2] J. Syrjärinne, *Studies of modern techniques for personal positioning*. PhD Thesis, Tampere University of Technology, 2001.
- [3] Benefon Oyj., "Personal navigation phone GSM + GPS," <http://www.benefon.com>.
- [4] Cellpoint Inc., "Mobile location system," <http://www.cellpoint.com/pdf/MLS.pdf>.
- [5] G. Christensen, "Location based services," <http://www.mobilein.com>.
- [6] R. Baines, "The DSP bottleneck," *IEEE Communications Magazine*, vol. 33, pp. 46–54, May 1995.
- [7] R.J. Lackey and D.W. Upmal, "Speakeasy: the military software radio," *IEEE Communications Magazine*, vol. 33, pp. 56–68, May 1995.
- [8] J. Mitola, "The software radio architecture," *IEEE Communications Magazine*, vol. 33, pp. 24–38, May 1995.
- [9] M. Laddomada, F. Daneshgaran, M. Mondin and R.M. Hickling, "A PC-based software receiver using a novel front-end technology," *IEEE Communications Magazine*, vol. 39, pp. 136–145, August 2001.
- [10] T. Hentshel and G. Fettweis, "Sample rate conversion for software radio," *IEEE Communications Magazine*, August, 2000, pp. 142–150.
- [11] Harris Corporation, "RF communications," *Annual Report 2001*, <http://www.harris.com/harris/ar/01/rfcomm.html>.
- [12] H. Meyr and G. Ascheid, *Synchronization in digital communications, phase, frequency locked loops, and amplitude control*. Wiley Sons, 1989.
- [13] F. M. Gardner, "Interpolation in digital modems - Part I: fundamentals," *IEEE Trans. Commun.*, vol. 41, pp. 501–507, March 1993.

- [14] L. Erup, F. M. Gardner, and R. A. Harris, "Interpolation in digital modems - Part II: implementation and performance," *IEEE Trans. Commun.*, vol. 41, pp. 998–1008, June 1993.
- [15] U. Mengali and A. N. D'Andrea, *Synchronization techniques for digital receivers*. Plenum Press, 1997.
- [16] J. G. Proakis, *Digital communication*. McGraw-Hill, 1989.
- [17] C. W. Farrow, "A continuously variable digital delay element," in *Proc. IEEE Int. Symp. Circuits & Syst.*, Espoo, Finland, June 1988, pp. 2641–2645.
- [18] L.P. Sabel and W.G. Cowley, "Block processing feedforward symbol timing estimator for digital modems," *Electronics Letters*, vol. 30, pp. 1273–1274, August 1994.
- [19] W.G. Cowley and L.P. Sabel, "The performance of two symbol timing recovery algorithms for PSK demodulators," *IEEE Transactions on Communications*, vol. 42, pp. 2345–2355, June 1994.
- [20] H. Meyr, M. Moeneclaey, and S. A. Fechtel, *Digital communication receivers: synchronization, channel estimation and signal processing*. John Wiley & Sons, 1998.
- [21] F. M. Gardner, "Demodulator reference recovery techniques suited for digital implementation," *ESA Final Report*, Aug. 1988.
- [22] J. Vesma, *Optimization and applications of polynomial-based interpolation filters*. Ph.D. Thesis, Tampere University of Technology, Tampere, Finland, May 1999.
- [23] T.I Laakso, V. Välimäki, M. Karjalainen, and U.K. Laine, "Splitting the unit delay," *IEEE Signal Processing Magazine*. vol. 13, pp. 30–60, January 1996.
- [24] J. Vesma and T. Saramäki, "Interpolation filters with arbitrary frequency response for all-digital receivers," *Proc. IEEE Int. Symp. Circuits & Syst.*, Atlanta, GA, May 1996, pp. 568–571.
- [25] R. Van Nee, *Multipath and multi-transmitter interference in spread-spectrum communication and navigation system*. Delft University Press, 1995.
- [26] M.K. Simon and M.S. Alouini, *Digital communication over fading channels; a unified approach to performance analysis*. John Wiley & Sons, Inc., 2000.
- [27] 3rd Generation Partnership Project, *Technical Report 25.827*, 2001-03, <http://www.3gpp.org>.
- [28] K. Kalliojärvi, "Terminal positioning in WCDMA," in *Proc. EUSIPCO 2000*, Tampere, Finland, September 2000, pp. 2269–2272.
- [29] T.S. Rappaport, J.H. Reed and B.D. Woerner, "Position location using wireless communications on highways of the future," *IEE Communications Magazine*, October, 1996, pp. 33–41.

- [30] L. Lopes, E. Villier and B. Ludden, "GSM standards activity on location," *IEE Colloquium on Novel Methods of Location and Tracking of Cellular Mobiles and Their System Applications*, 1999, pp. 1–7.
- [31] M. D. Goran and R. E. Richton, "Geolocation and assisted GPS," *IEEE Communications Magazine*, Feb. 2001, pp. 123–125.
- [32] E.D. Kaplan, *Understanding GPS; principles and applications*. Artech House Inc., 1996.
- [33] P. Enge and Pratap Mistra, "Scanning the issue/technology; special issue on GPS," *Proc. of the IEEE*, vol. 87, No. 1, January 1999, pp. 3–15.
- [34] M. Braasch and A.J.V. Dierendonck, "GPS receiver architectures and measurements," *Proc. of the IEEE*, vol. 87, No. 1, January 1999, pp. 48–64.
- [35] J.S. Lee and L.E. Miller, *CDMA systems engineering handbook*. Artech House, 1998.
- [36] <http://www.colorado.edu/geography/gcraft/notes/gps/>
- [37] M.C. Laxton and S.L. DeVilbis, "GPS multipath mitigation during code tracking," in *Proc. of the American Control Conference*, Albuquerque, New Mexico, pp. 1429–1433, June 1997.
- [38] R. Van Nee, J. Sierveld, P. Fenton, and B. Townsend, "The multipath estimating delay lock loop: approaching theoretical accuracy limits," in *Proc. of IEEE Position, Location, and Navigation Symposium*, April 1994, pp. 246–251.
- [39] B. Ibrahim and A. Aghvami, "Direct sequence spread spectrum matched filter acquisition in frequency-selective Rayleigh fading channels," *IEEE Journal on Selected Areas in Communications*, vol. 12, pp. 885–890, June 1994.
- [40] W. Sheen and G.L. Stüber, "Effects of multipath fading on delay-locked loops for spread spectrum systems," *IEEE Trans. on Communications*, vol. 42, pp. 1947–1956, February/March/April 1994.
- [41] P. Luukkanen, and J. Joutsensalo, "Comparison of MUSIC and matched filter delay estimators in DS-CDMA," in *Proc. of IEEE Personal, Indoor and Mobile Radio Communications*, vol. 3, 1997, pp. 830–834.
- [42] A. Papoulis, *Signal analysis*. McGraw-Hill, 1988.
- [43] Z. Kostić, G. Pavlović, "Resolving sub-chip spaced multipath components in CDMA communication systems," in *Proc. of IEEE VTC*, vol. 1, 1993, pp. 469–472.
- [44] J. F. Kaiser, "On a simple algorithm to calculate the 'energy' of a signal," *Proc. IEEE ICASSP-90*, Albuquerque, New Mexico, pp. 381–384, April 1990.
- [45] J. F. Kaiser, "On Teager's energy algorithm and its generalization to continuous signals," *Proc. 4th IEEE Digital Signal Processing Workshop*, Mohonk (New Paltz), NY, September 1990.

- [46] P. Maragos, J. F. Kaiser, and T. F. Quatieri, "Energy separation in signal modulations with application to speech analysis," *IEEE Trans. Signal Processing*, vol. 41, no. 10, pp. 3024–3051, October 1993.
- [47] V.P. Stokes and P. Händel, "Comments on "On amplitude and frequency demodulation using energy operators," *IEEE Transactions on Signal Processing*, vol. 46, no. 2, pp. 506–507, February 1998.
- [48] J. Fang and L. Atlas, "Quadratic detectors for energy estimation," *IEEE Transactions on Signal Processing*, vol. 43, no. 11, pp. 2582–2594, November 1995.
- [49] J. F. Kaiser, "Some useful properties of Teager's energy operators," *Proc. IEEE ICASSP-93*, vol. III, pp. 149–152, April 27–30, 1993.
- [50] M.P. Fitz, "Further results in the fast estimation of a single frequency," *IEEE Trans. Commun.*, Vol. 42, pp. 862–864, March 1994.
- [51] J. Soubielle and I. Fijalkow, "GPS positioning in a multipath environment," *IEEE Transactions on Signal Processing*, vol. 50, no. 1, pp. 141–150, January 2002.
- [52] G. Fock, J. Baltersee, P. Schulz-Rittich and H. Meyr, "Channel tracking for Rake receivers in closely spaced multipath environment," *IEEE Journal on selected areas in communications*, vol. 19, no. 12, pp. 2420–2431, December 2001.
- [53] R. Hamila, M. Renfors, G. Gunnarsson, M. Alanen, "Data processing for mobile phone positioning," in *Proc. VTC'99*, Amsterdam, Netherlands, Sept. 1999, pp. 446–449.
- [54] R. Hamila, S. Lohan and M. Renfors, "Multipath delay estimation in GPS receivers," *In Proc. Nordic Signal Processing Symposium (Norsig'2000)*, Kolmården, Sweden, pp. 417–420, June 2000.
- [55] F. Alaya Cheikh, R. Hamila, M. Gabbouj and J. Astola, "Impulse noise removal in highly corrupted color images," *Proc. 1996 IEEE International Conference on Image Processing*, ICIP-96, Vol.1, pp. 997–1000, Lausanne, Switzerland, 1996.
- [56] R. Hamila, "Teager energy operator; theory and Applications," *Licentiate Thesis*, Tampere University of Technology, December 1998.
- [57] R. Hamila and M. Renfors, "Nonlinear operator for multipath channel estimation in GPS receivers," *In The 7th IEEE International Conference On Electronics, Circuits & Systems*, Jounieh, Lebanon, pp. 352–356, December 2000.

Publications

Publication 1

R. Hamila, J. Vesma, T. Saramäki and M. Renfors, "Discrete-Time Simulation of Continuous-Time Systems Using Generalized Interpolation Techniques," *in Proc. 1997 the Summer Computer Simulation Conference, SCSC'97, Arlington, Virginia, USA, July 1997*, pp. 914–919.

Copyright ©1997 by SCSC'97. Reprinted, with permission, from the proceedings of SCSC'97.

THE PROCEEDINGS OF THE
1997
SUMMER COMPUTER
SIMULATION CONFERENCE

*Simulation and Modeling Technology
for the Twenty-First Century*

Edited by
Mohammad S. Obaidat
John Illgen

ARLINGTON, VIRGINIA
JULY 13-17, 1997
KEY BRIDGE MARRIOTT



ISBN: 1-56555-123-0

SPONSORED BY THE SOCIETY FOR COMPUTER SIMULATION INTERNATIONAL

DISCRETE-TIME SIMULATION OF CONTINUOUS-TIME SYSTEMS USING GENERALIZED INTERPOLATION TECHNIQUES

Hamila Ridha, Jussi Vesma, Markku Renfors, and Tapio Saramäki
Telecommunications Laboratory
Tampere University of Technology
P. O. Box 553, FIN-33101 Tampere, Finland
E-mail: ridha@cs.tut.fi

Keywords: communications, signal processing, numerical methods, discrete simulation

ABSTRACT

This paper presents a general approach for modelling and computer simulation of continuous-time signals and systems. The idea is based on utilizing a polynomial approximation of the continuous-time signal between the existing discrete-time samples. The so-called Farrow structure provides a computationally efficient implementation making it possible to get the interpolated signal values at arbitrary time instances between the existing samples. This results in efficient overall simulation models, because with the aid of the proposed techniques it is possible to obtain visually correct continuous-time waveforms while using a modest oversampling factor. This paper proposes a family of optimized polynomial interpolators for modelling purposes and discusses the filter criteria in terms of the required accuracy and other simulation parameters. In addition, a numerical approach for estimating the derivative and integral of a discrete-time signal is established.

1. INTRODUCTION

Discrete-time modelling and simulation of continuous-time signals and systems is a common practice in many fields for research, development, and education purposes. From computational efficiency point of view, the smallest sampling rate sufficient for accurate system modelling is determined by the sampling theory. In cases where computational efficiency is an issue, different sampling rates can be used in different blocks to reduce the computational burden. Anyway, the lowest sampling rates which are sufficient for system modelling are typically not sufficient for obtaining informative and visually pleasing waveform plots of the signals. For this reason, it is a common practice to utilize oversampling factors which are an order of magnitude higher than what is needed for accurate system modelling.

Also in cases where there is a need to locate, e.g., the local maxima, minima, or zero-crossings of a signal, considerably higher sampling rates are needed. Other difficult cases are, for example, conversion between incommensurate sampling rates that might be used in different model blocks to be connected together.

Partial solutions to these problems are offered by "classical" *sampling rate conversion techniques* (Crochiere and Rabiner 1983) which allow sampling rate conversion by integer or fractional factors. Adjusting the sampling phase is difficult with these classical techniques, but the so-called fractional delay filters (Laakso *et al.* 1996; Vesma and Saramäki 1996a; Vesma and Saramäki 1996b; Vesma and Saramäki 1997; Saramäki and Ritonieni 1996) help in this task. Another classical approach is the Lagrange interpolation (Erup *et al.* 1993), which however also has its limitations.

In this paper, we consider polynomial interpolation with the so-called Farrow structure (Farrow 1988) implementation as a general-purpose solution to the above-mentioned tasks. The Farrow structure allows, with low additional computational complexity, to compute several new samples at arbitrary points between the existing samples. Thus, it is very easy to get the signal sample values in a flexible way in what ever time instances they are needed. Furthermore, it is possible also to implement iterative procedures for estimating accurately, e.g., the maximum value of a continuous-time signal as well as its location.

Also the Lagrange interpolation can be implemented using the Farrow structure, but we have demonstrated that a clearly better performance can be achieved by utilizing filter optimization techniques (Vesma and Saramäki 1996a; Vesma and Saramäki 1996b; Vesma and Saramäki 1997) and

also that the performance of the Lagrange interpolation is not sufficient for all purposes (Vesma *et al.* 1996).

In Section 2 of this paper, we first describe the ideas of polynomial interpolation and Farrow structure. In Section 3, we discuss the use of the Farrow-structured interpolators in signal and system modeling and give some examples of interpolation filters. In Section 4, we show how the derivative and integral functions of a continuous-time signal can be approximated using the Farrow-structured interpolators.

2. POLYNOMIAL INTERPOLATION

A continuous-time signal can be approximated at any point between the discrete-time samples using a polynomial-based interpolation. This is illustrated in Fig. 1. The approximating polynomial (solid line) is formed by adding together weighted and shifted basis functions (dashed line). These functions are weighted by the corresponding sample values (circles). The sample values which are used in the approximation form a base-point set. Now the value of the original continuous-time signal can be estimated by evaluating the value of the approximating polynomial at the desired point.

It should be pointed out that the best approximation is obtained in the middle interval of the base-point set, $[0,1)$ in the figure. In this paper, we use only basis functions which are piecewise polynomials because of the efficient implementation.

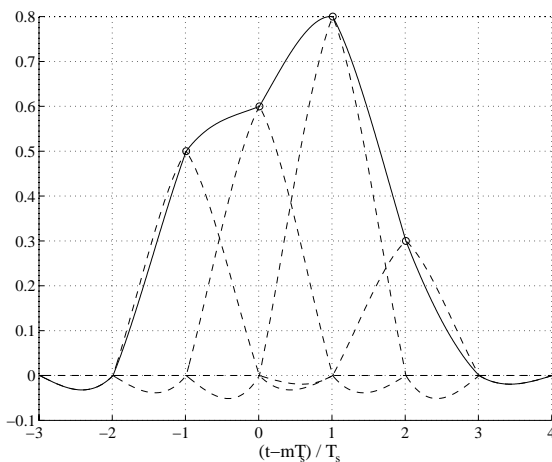


Fig. 1. Weighted basis functions (dashed line) and approximating polynomial (solid line).

The polynomial-based interpolation can be efficiently implemented using a special discrete-time filter structure (terms ‘interpolator’ and ‘interpolation filter’ are used). This filter is the so-called Farrow structure (Fig. 2) (Farrow 1988). In the Farrow structure, all the filter coefficients are fixed and the only changeable parameter is the fractional interval $\mu \in [0,1)$, which is defined by

$$t = mT_s + \mu T_s, \quad (1)$$

where T_s is the input sampling interval and

$$m = \lfloor t/T_s \rfloor. \quad (2)$$

Here $\lfloor x \rfloor$ stands for the integer part of x . In this case, $[mT_s, (m+1)T_s]$ forms the middle interval of the base-point set.

With different values of μ , the output of the Farrow structure gives the following approximation to the continuous-time signal:

$$\tilde{y}(t) = \sum_{l=0}^L f_l(m) \left(\frac{t - mT_s}{T_s} \right)^l = \sum_{l=0}^L f_l(m) \mu^l, \quad (3)$$

where L is the degree of the interpolation and the $f_l(m)$'s are given by

$$f_l(m) = c_l(m) * x(m) \quad (4)$$

with the $c_l(m)$'s being the coefficients of the Farrow structure. The total number of coefficients is $N(L+1)$, where N is the length of the branch filters.

In many applications, the output of the Farrow structure is computed at a fixed output rate, $1/T_i$, which may have an arbitrary ratio to the input sampling rate. In some other applications, the outputs may be needed at arbitrary time instances, e.g., according to some iterative search procedure.

The Farrow structure has a time-varying impulse response. The impulse response values of this digital filter are determined by the fractional interval μ and they are obtained from the underlying continuous-time impulse response $h(t)$ (Fig. 3). Actually, this continuous-time impulse response is the same as the basis function. Therefore, the Farrow structure can be analyzed and synthesized using this continuous-time filter $h(t)$. In the ideal case, the continuous-time filter is an ideal low-pass filter and in the time domain it is the sinc-function. This

fact can be utilized in the filter optimization (Vesma and Saramäki 1996a).

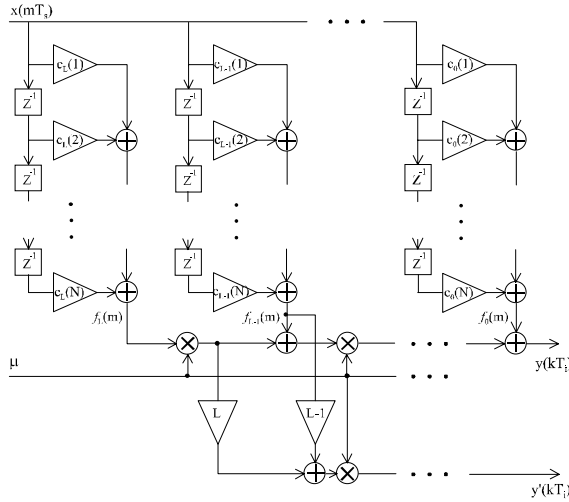


Fig. 2. The Farrow structure for the general case. N is the length of the filter and L is the degree of the interpolation. Also the modifications needed for the derivative approximation are shown.

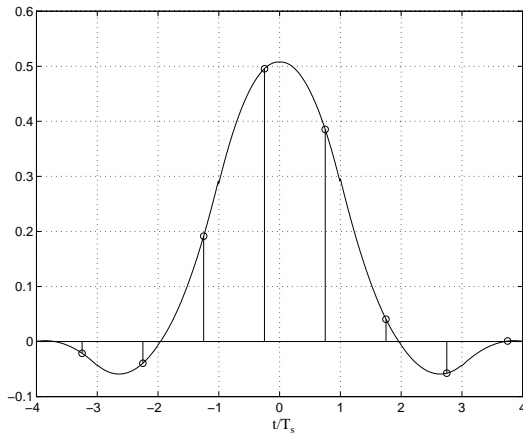


Fig. 3. Impulse response $h(t)$ and impulse response of the Farrow structure for $\mu = 0.25$.

3. POLYNOMIAL INTERPOLATION IN SIMULATIONS

The basic problem in the computer simulations is that we have just discrete-time samples from some, possibly stochastic, continuous-time system. There are also situations where the signal value is needed between these discrete-time samples. One solution is to increase the sampling rate. However, this makes the simulation very slow and the signal is still discrete time.

In this paper, we introduce a new approach to this problem. In this approach, the original continuous-time signal is estimated using polynomials, and the value of the signal can be approximated by evaluating the value of the polynomial at the desired point. This polynomial interpolation (or estimation) can be efficiently implemented using the Farrow structure as discussed earlier.

The block diagram of the interpolation function is shown in Fig. 4. $x(mT_s)$ is the input sample vector and $y(kT_i)$ is the output sample. The location of this output sample $t = kT_i$ is determined by the input parameters μ and m according Eq. (1).

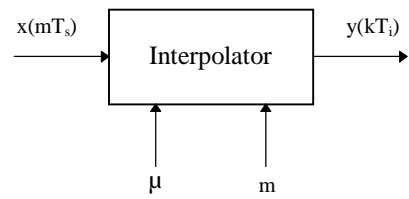


Fig. 4. The block diagram of the interpolation function and the input and output parameters.

What is inside the interpolation function in Fig. 4 is just the implementation of the Farrow structure with a suitable length N and order L (to be discussed later on). The advantage of this interpolation function when modelling some continuous-time system is that there is no need for high over-sampling factor at the input. In addition to that, the output is really continuous time because the fractional interval μ is practically continuous valued (of course this is limited by the number of bits used to represent μ).

3.1. Interpolation Filters

The complexity of the interpolation filter depends on the accuracy requirements of the simulation model. The approximation error in the interpolation (that is the error between the original continuous-time signal at point kT_i and the interpolated value $y(kT_i)$) can be decreased by increasing the length of the branch filters or the degree of the interpolation.

The design parameters of the interpolation filters are related to its frequency response, as normally in the case of linear filters. The parameters include the tolerated passband amplitude response variation, the minimum stopband attenuation, and the

passband and stopband cut-off frequencies. Basically, the task of the filter is to attenuate the aliasing/imaging components appearing due to the change of the sampling rate. Time-domain accuracy requirements cannot be converted easily to the corresponding frequency-domain requirements. In practice, the performance of candidate interpolation filters may be evaluated by trial simulations in order to be able to select the most suitable one.

As mentioned earlier, interpolation filters can be analyzed and synthesized using the continuous-time impulse response $h(t)$. In the filter design criteria, the frequency response of this filter $h(t)$ should approximate unity in the signal band and zero elsewhere.

Table I shows four different interpolation filters. For these filters, the stop band attenuation varies from 53 dB to 91 dB and the number of multiplications from 50 to 216. It should be noted that the complexity of these filters can be decreased by increasing the sampling rate by an integer factor which allows to use a wider transition band (Saramäki and Ritonniemi 1996). For example, by using the over-sampling factor of two, the highest component of the signal is below $0.25f_s$ which helps to reduce the filter complexity.

Table I. Four different interpolation filters. Passband ripple δ_p , stopband attenuation A_s , passband and stopband edges (normalized frequency), and the number of coefficients in the Farrow structure $N(L+1)$.

	δ_p	A_s [dB]	f_p	f_s	$N*(L+1)$
1	0.01	53	0.38	0.62	$10(4+1)=50$
2	0.009	80	0.38	0.62	$14(6+1)=98$
3	0.008	67	0.425	0.575	$20(7+1)=160$
4	0.012	91	0.425	0.575	$24(8+1)=216$

The frequency and impulse responses for the last filter in Table I are shown in Figs. 5 and 6. The impulse response in Fig. 6 is truly piecewise polynomial. This is difficult to see because it does not include high frequency components (see Fig. 5) which makes it very smooth.

Figure 7 shows a part of a discrete-time ECG signal and its approximated continuous-time waveform. This waveform is obtained using the

second interpolation filter in Table I. The ECG signal has been obtained from a patient during anaesthesia at Helsinki University Hospital.

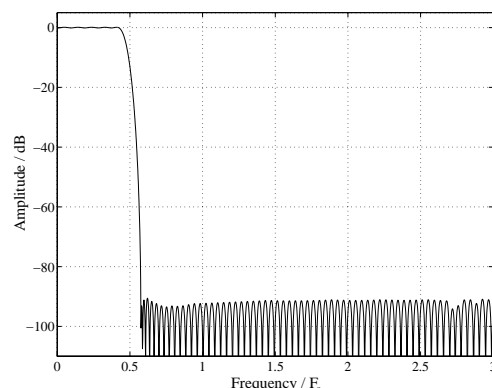


Fig. 5. Frequency response for the interpolation filter. $N = 24$ and $L = 8$ (the last entry in Table I).

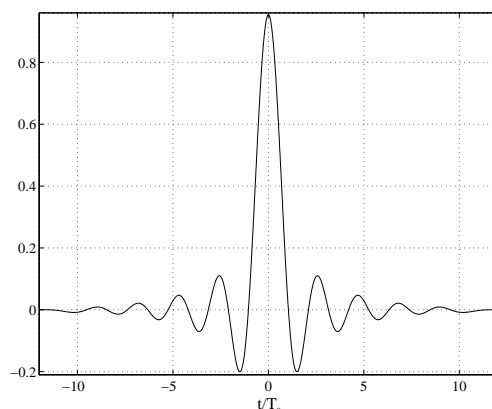


Fig. 6. Impulse response for the interpolation filter. $N = 24$ and $L = 8$ (the last entry in Table I).

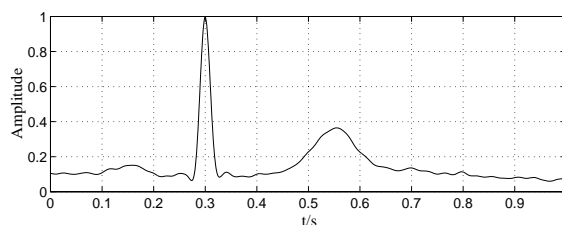
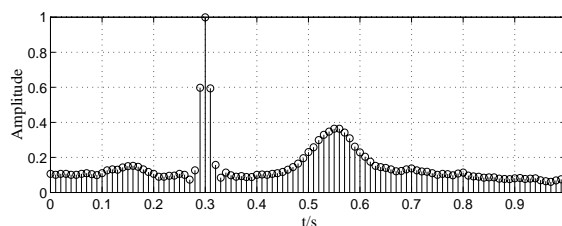


Fig. 7. Discrete-time ECG signal and its approximated continuous-time waveform.

4. POLYNOMIAL APPROXIMATION OF DERIVATIVE AND INTEGRAL

In this section, we will show how the polynomial based interpolation can be used for estimating the continuous-time derivative and integral from a sampled signal. The design criteria for polynomial-based differentiators have been discussed in (Ridha *et al.* 1997).

4.1. Differentiator

The derivative of the continuous-time approximating signal at an arbitrary time instant is obtained from Eq. (3) and it is expressible by

$$\frac{d\tilde{y}(t)}{dt} = \sum_{l=1}^L l f_l(m) \left(\frac{t - mT_s}{T_s}\right)^{l-1} = \sum_{l=1}^L l f_l(m) \mu^{l-1}. \quad (5)$$

From this equation it is seen that the Farrow structure used in the polynomial-based interpolation can also be used for approximating the derivative of the original continuous-time signal at any desired time instant.

The modifications needed in the Farrow structure are shown in Fig. 2, whereas the frequency and impulse responses for the differentiator are shown in Figs. 8 and 9, respectively in the case of the last interpolator in Table I. Figure 10 depicts the resulting approximated continuous-time derivative for the discrete-time ECG signal in Fig. 7.

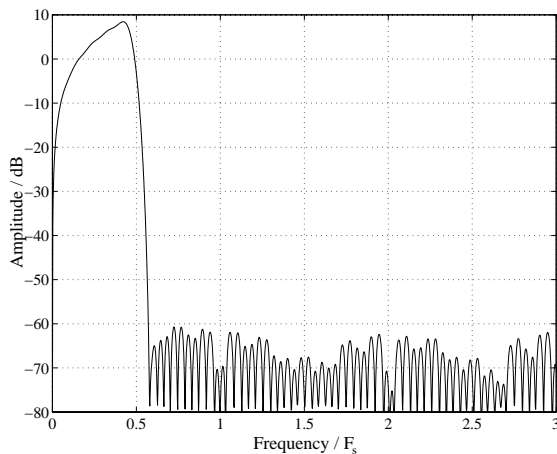


Fig. 8. Frequency response for the differentiator. $N = 24$ and $L = 8$ (the last entry in Table I).

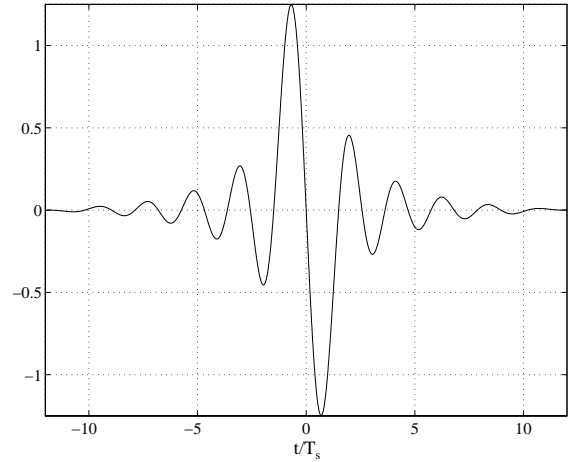


Fig. 9. Impulse response for the differentiator. $N = 24$ and $L = 8$ (the last entry in Table I).

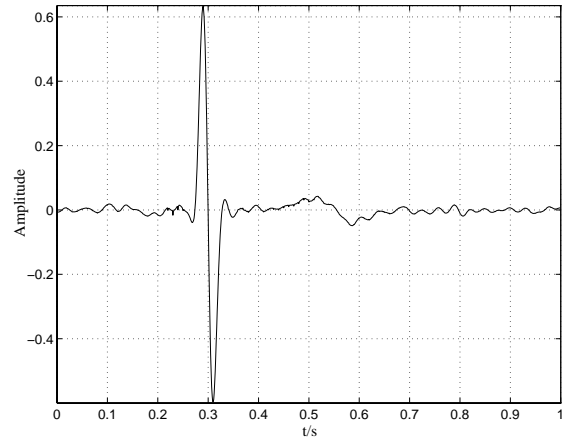


Fig. 10. Approximated continuous-time derivative for the discrete-time ECG signal in Fig. 7.

4.2. Integrator

In the following we introduce a new integration method for simulating continuous-time systems using discrete-time computations. The developed "integrator" is also based on the polynomial generalized interpolation techniques.

The continuous-time integration of a signal at an arbitrary time instant is approximated from the fundamental equation of digital interpolation, Eq. 3, as follows

$$\int \tilde{y}(t) dt = \sum_{l=0}^L f_l(m) \frac{\mu^{l+1}}{l+1}. \quad (6)$$

The above equation represents the continuous-time integrator and is easily implemented by intro-

ducing a small modifications to the Farrow structure used in the polynomial-based interpolation purpose.

Assuming that the frequency response of the interpolation filter is $H(\omega)$, then the ideal frequency response for the integrator filter is equal $H(\omega)/(j\omega)$ (see Fig. 11).

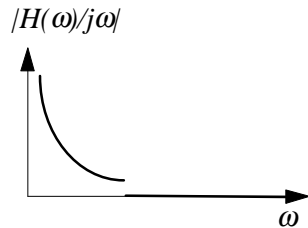


Fig. 11. Ideal frequency response for integrator.

Most of the developed digital integrators are designed from a polynomial perspective (Regolia 1993). Further work to treat the design aspects of the continuous-time integrator is needed.

5. CONCLUSION

In this paper a novel approach for modelling and computer simulation of continuous-time signals and systems has been introduced. We have shown how this approach is based on the fundamental equation of digital interpolation, and that it provides a generalized method for approximating the continuous-time derivative and integral of a discrete-time signal. Moreover, efficient and simple implementation are obtained using the Farrow structure.

Simulation results show that accurate and good continuous-time interpolation and derivative approximations can be obtained by designs based on optimized piecewise polynomial interpolators.

It remains as a topic for future work to devise efficient and sufficiently accurate polynomial-based integrators.

REFERENCES

Crochiere, R. E. and L. R. Rabiner. *Multirate Digital Signal Processing*. Englewood Cliffs, NJ: Prentice-Hall, 1983.

Erup, L.; F. M. Gardner; and R. A. Harris. "Interpolation in digital modems - Part II: Imple-

mentation and performance," *IEEE Trans. Commun.*, vol. 41, pp. 998-1008, June 1993.

Farrow, C. W. "A continuously variable digital delay element," in *Proc. IEEE Int. Symp. Circuits & Syst.*, Espoo, Finland, June 1988, pp. 2641-2645.

Gardner, F. M. "Interpolation in digital modems - Part I: Fundamentals," *IEEE Trans. Commun.*, vol. 41, pp. 501-507, Mar. 1993.

Laakso, T. I.; V. Välimäki; M. Karjalainen; and U. K. Laine. "Splitting the unit delay," *IEEE Signal Processing Magazine*, vol. 13, pp. 30-60, Jan. 1996.

Regolia, P. A. "Special filter design," chapter 13 in *Handbook for Digital Signal Processing* edited by S. K. Mitra and J. F. Kaiser., John Wiley & Sons, 1993.

Ridha, H.; J. Vesma; T. Saramäki; and M. Renfors. "Derivative approximations for sampled signals based on polynomial interpolation," to be presented at 13th *International Conference on Digital Signal Processing*, Santorini, Greece, July 1997.

Saramäki T. and M. Ritonieni. "An efficient approach for conversion between arbitrary sampling frequencies," in *Proc. IEEE Int. Symp. Circuits & Syst.*, Atlanta, GA, May 1996, pp. 285-288.

Vesma, J.; M. Renfors; and J. Rinne. "Comparison of efficient interpolation techniques for symbol timing recovery," in *Proc. IEEE Globecom 96*, London, UK, Nov. 1996, pp. 953-957.

Vesma, J. and T. Saramäki. "Interpolation filters with arbitrary frequency response for all-digital receivers," in *Proc. IEEE Int. Symp. Circuits & Syst.*, Atlanta, GA, May 1996, pp. 568-571.

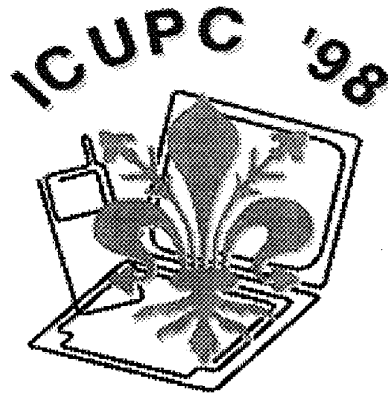
Vesma J. and T. Saramäki. "Optimization and efficient implementation of fractional delay FIR filters," in *Proc. Third IEEE Int. Conf. Electronics, Circuits, Syst.*, Rodos, Greece, Oct. 1996, pp. 546-549.

Vesma J. and T. Saramäki. "Optimization of efficient implementation of FIR filters with adjustable fractional delay," to be presented at 1997 *IEEE International Symposium on Circuits and Systems* Hong Kong, June 1997.

Publication 2

R. Hamila, J. Vesma, H. Vuolle, and M. Renfors, "Joint Estimation of Carrier Phase and Symbol Timing Using Polynomial-Based Maximum Likelihood Technique," *in the IEEE 1998 International Conference on Universal Personal Communications, ICUPC'98*, Florence, Italy, October 1998, pp. 369–373.

Copyright ©1998 IEEE. Reprinted, with permission, from the proceedings of ICUPC'98.



**IEEE 1998 International Conference
on
Universal Personal Communications**

5 – 9 October 1998
Florence, Italy

CONFERENCE PROCEEDINGS

VOLUME 2 OF 2

JOINT ESTIMATION OF CARRIER PHASE AND SYMBOL TIMING USING POLYNOMIAL-BASED MAXIMUM LIKELIHOOD TECHNIQUE

Ridha Hamila, Jussi Vesma, Hannu Vuolle, and Markku Renfors

Telecommunications Laboratory
Tampere University of Technology
P.O. Box 553, FIN-33101 Tampere, Finland
e-mail: ridha@cs.tut.fi

ABSTRACT

A new approach for joint clock and carrier phase synchronization in digital receivers using a data-aided block based feed-forward architecture is proposed. This approach is based on polynomial approximation of the log-likelihood function by using the Farrow structure. Thus, the maximum likelihood function is expressed in terms of the polynomial-based interpolator filter branches. Simulation results for different types of linear modulations using the conventional Lagrange interpolator and a new optimized interpolator are provided and compared with the theoretical case.

1. INTRODUCTION

In conventional receivers, the sampling of the received signal must be synchronized to the incoming data symbols. The synchronization is performed by using a feedback loop. Currently, there is a trend of using digital receivers where the sampling of the received signal is not synchronized to the incoming data symbols. With this approach, there is no need for the complex PLL circuits used in the conventional receivers.

In this receiver architecture, the sampling of the received signal is performed by a fixed sampling clock and thus sampling is not synchronized to the incoming symbols. Therefore, timing adjustment must be done by digital methods after sampling. The estimated timing is then used for the carrier phase recovery. One way to perform this timing is to calculate the value of the signal at the desired time instants using interpolation. One promising approach is polynomial-based interpolation based on the so-called Farrow structure. It is characterized by its efficiency and flexible realization [4]-[5].

The best synchronization algorithms for digital communication systems are based on the maximum likelihood (ML) estimation theory. Joint estimation of signal parameters using the ML approach provides usually

better estimates with respect to the variance compared to estimates obtained from separate optimization of the likelihood functions [1].

A new symbol timing recovery technique based on polynomial approximation for the log-likelihood function (LLF) has been developed in [2]-[3]. In this paper, an extension of this polynomial-based log-likelihood function for jointly estimating the timing and carrier phase is derived. In addition, simulation results for different types of modulations are provided and compared with the theoretical case. The results show that the interpolator optimized in the frequency domain [6] performs much better compared to the Lagrange interpolator [8]-[9].

The feedforward architecture we are considering provides rapid acquisition characteristics, which are very important especially in the mobile communication systems where the channel characteristics are rapidly changing, and in the case of TDMA systems, also the transmission is bursty.

2. TIMING AND PHASE ADJUSTMENT USING INTERPOLATION

The block diagram of the digital receiver with non-synchronized sampling is shown in Fig. 1. The sampling of the received signal $r(t)$ is performed by a fixed sampling clock, and thus, the timing adjustment must be done after the sampling using interpolation. Consequently, the estimated symbol timing is then used for the carrier phase recovery. The interpolation filter in Fig. 1 can be used for both up-sampling and down-sampling, and furthermore, the output is not synchronized to the input. We should think interpolation from the mathematical point of view and recall how to interpolate data using polynomials.

The function of the interpolation filter is to calculate one output sample $y(nT_i)$ at a time using a set of adjacent input samples $m(kT_s)$, within a timing error estimate (μ) and a phase error estimate (θ) obtained from the synchronization control unit. In the ideal case, these output samples are the same sample values that

This work was carried out in the project "Analog and Digital Signal Processing Techniques for Highly Integrated Transceivers" supported by the Academy of Finland.

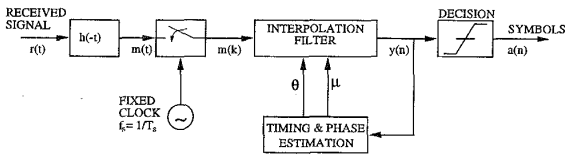


Figure 1: Digital Receiver with non-synchronized sampling.

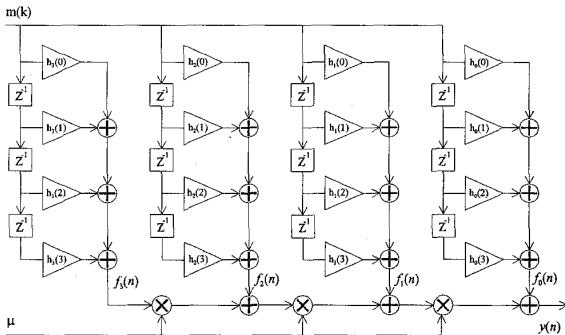


Figure 2: Farrow structure for the cubic ($L = 3$) interpolator.

would occur if the original sampling had been synchronized to the received symbols. The fractional interval μ determines the time instant $t = nT_i$ where the original continuous-time received signal $r(t)$ is approximated. This relation is given by

$$nT_i = (\mu + k)T_s, \quad (1)$$

where $\mu \in [0, 1)$ is the fractional interval, T_s is the sampling interval, and T_i is the output interval, whereas k is the largest integer for which $kT_s \leq nT_i$. In this paper, we assume that the original sampling rate is twice the symbol rate, $T = 2T_s$. Also, we use τ and μ to denote the timing error with respect to the symbol and sampling interval, respectively. In addition, the error in the carrier phase ($e^{-j\theta}$) is corrected using the phase error estimate denoted by θ as shown in Fig. 1.

The polynomial-based interpolation filters are very easily implemented using the Farrow structure [5]. This structure is characterized by the fixed values of all the filter coefficients and by only one changeable parameter which is the fractional interval μ . In the general case, the Farrow structure shown in Fig. 2 consists of $L + 1$ FIR filter branches and the length of each branch filter is N , where L is the degree of the interpolation and N is the length of the impulse response.

Timing adjustment in digital receivers using Lagrange interpolation was first introduced by Erup et al [8]. Lagrange interpolation represents the conventional time domain approach to the interpolation problems. A new synthesis technique for polynomial-based interpolation filters is proposed in [6]. In this synthe-

sis technique, the design parameters are edge frequencies for passbands and stopbands, desired amplitude and weight for every band, the length of the filter, and the degree of the interpolation. After giving these parameters, the filter coefficients of the Farrow structure are optimized in the frequency domain in the minimax sense. The new designs have been shown to provide clearly lower complexity or much better performance with the same complexity as the Lagrange designs [10].

3. JOINT MAXIMUM LIKELIHOOD ESTIMATION OF SYMBOL TIMING AND CARRIER PHASE

For decision directed (DD) maximum likelihood estimation of symbol timing (τ) and carrier phase (θ), the log-likelihood function for these two parameters is approximated by [1]-[4];

$$\Lambda(\tilde{\tau}, \tilde{\theta}) = \text{Re} \left[e^{j\tilde{\theta}} \sum_{n=1}^N \hat{a}^*(n) m(n, \tilde{\tau}) \right], \quad (2)$$

where $\hat{a}(n)$ and $m(n, \tilde{\tau})$ are the correct symbol values and samples from the output of the matched filter (one sample per symbol). $\tilde{\tau} \in [0, T)$ and $\tilde{\theta} \in [0, 2\pi]$ are the timing and phase error trials, respectively. N is the number of symbols used in the calculation and T is the symbol interval.

Synchronization algorithms for digital receivers estimating jointly the timing and phase are based on maximum likelihood estimation (MLE) theory as mentioned earlier. These algorithms are trying to find the timing and the phase error estimates ($\hat{\tau}, \hat{\theta}$) which maximize Eq. (2). Because this function includes the actual data values, this formula can be used as a basis for decision-directed (DD) or data-aided (DA) timing recovery schemes. By means of the above log-likelihood function, the following algorithm for jointly estimating ($\hat{\tau}, \hat{\theta}$) has been established [4]:

$$\hat{\tau} = \arg \max_{\tilde{\tau}} \left| \sum_{n=1}^N \hat{a}_n^* m(n, \tilde{\tau}) \right|, \quad (3)$$

$$\hat{\theta} = \arg \left[\sum_{n=1}^N \hat{a}_n^* m(n, \hat{\tau}) \right]. \quad (4)$$

An important feature here is that the ML-estimate of the timing is independent of the carrier phase. We consider here a block processing scheme which takes the data samples and the decided/known symbol values for a block of N symbols. The main idea here is to form a polynomial approximation for the log-likelihood function by using the Farrow structure, then different schemes for finding the maximum of this polynomial can be devised.

4. POLYNOMIAL APPROXIMATION OF THE LOG-LIKELIHOOD FUNCTION FOR TIMING AND CARRIER PHASE ESTIMATION

A new polynomial approximation technique for the log-likelihood function (LLF) was developed in [2]-[3] for symbol timing recovery. In this section, we will extend this polynomial-based log-likelihood function for jointly estimating the symbol timing and carrier phase based on Eqs. (3) and (4).

Here we assume that the original sampling rate is twice the symbol rate $T = 2T_s$ and cubic interpolation filter ($L = 3$) is used. Because the symbol interval is divided into two parts (two samples per one symbol), there are two different polynomial approximations for the log-likelihood function as shown in [2]-[3]. Consequently, from expression (3) the symbol timing is estimated by

$$\hat{\tau} = \arg \max_{\tilde{\tau}} \begin{cases} \Lambda_1(2\tilde{\tau}) & 0 \leq \tilde{\tau} < 0.5 \\ \Lambda_2(2\tilde{\tau} - 1) & 0.5 \leq \tilde{\tau} < 1 \end{cases} \quad (5)$$

where

$$\Lambda_1(2\tilde{\tau}) = \sum_{n=1}^N \hat{a}^*(n) m(2n - 1, 2\tilde{\tau}),$$

and

$$\Lambda_2(2\tilde{\tau} - 1) = \sum_{n=1}^N \hat{a}^*(n) m(2n, 2\tilde{\tau} - 1).$$

Also, by using the above timing estimate $\hat{\tau}$, the carrier phase estimate is given by

$$\hat{\theta} = \arg \begin{cases} \Lambda_1(2\hat{\tau}) & 0 \leq \hat{\tau} < 0.5 \\ \Lambda_2(2\hat{\tau} - 1) & 0.5 \leq \hat{\tau} < 1. \end{cases} \quad (6)$$

The value of $m(n, \tilde{\tau})$ can be interpolated for different values of $\tilde{\tau}$ by utilizing the cubic Farrow structure and the original samples $m(k)$.

Equations (5) and (6) can be expressed also as a function of the fractional interval $\tilde{\mu} \in [0, 1)$, and the output samples of the FIR filter branches in the Farrow structure $f_i(n)$, as follows:

If $\max[\Lambda_1(\tilde{\mu})] > \max[\Lambda_2(\tilde{\mu})]$ then

$$\hat{\mu} = \arg \max_{\tilde{\mu}} [\Lambda_1(\tilde{\mu})],$$

else

$$\hat{\mu} = \arg \max_{\tilde{\mu}} [\Lambda_2(\tilde{\mu})].$$

Where

$$\Lambda_1(\tilde{\mu}) = \sum_{i=0}^3 \tilde{\mu}^i \sum_{n=1}^N \overbrace{\hat{a}^*(n) f_i(2n-1)}^{X_{i1}},$$

and

$$\Lambda_2(\tilde{\mu}) = \sum_{i=0}^3 \tilde{\mu}^i \sum_{n=1}^N \overbrace{\hat{a}^*(n) f_i(2n)}^{X_{i2}}.$$

Finally, by using the above timing estimate, the phase estimate is determined by;

If $\max[\Lambda_1(\tilde{\mu})] > \max[\Lambda_2(\tilde{\mu})]$ then

$$\hat{\theta} = \arg[\Lambda_1(\hat{\mu})],$$

else

$$\hat{\theta} = \arg[\Lambda_2(\hat{\mu})].$$

In the case of a cubic interpolation filter, the overall scheme for our proposed block-based symbol timing and phase recovery is illustrated in Fig. 3. After the parameters $\hat{\mu}$ and $\hat{\theta}$ are estimated, timing adjustment is performed by evaluating the value of the polynomial at the given value of μ . At the same time, sampling rate is decreased by two. Here, even samples are discarded if $\max[\Lambda_1(\tilde{\mu})] > \max[\Lambda_2(\tilde{\mu})]$, and odd samples otherwise. Subsequently, the carrier phase is corrected by the factor $e^{-j\hat{\theta}}$.

This procedure can be used as such in the data-aided (DA) systems where the symbol values are known in advance. For example, GSM does have a known synchronization symbol sequence. In case of decision-directed (DD) systems, a reasonably good initial estimate for the sampling phase must be known. The scheme can also be utilized in non-data-aided (NDA) systems with some modifications.

5. SIMULATIONS

The proposed algorithm was simulated using QPSK, 16-QAM, and 64-QAM constellations for different block lengths. The transmitter and receiver pulse-shaping filters are square root raised cosine filters with excess bandwidth of 35%. Two interpolation filters, cubic Lagrange and third order interpolation filter of length 8 designed by the new synthesis technique [6] are compared in the simulations. The length of the FIR filters in the Farrow structure for the optimized interpolator is twice as long as for the Lagrange interpolator. However, the filter coefficients are symmetrical for this new design. The number of the FIR filter branches is four for both interpolators.

The simulations are done using the worst-case timing offset and some selected values of the phase error.

Variance and mean of the timing jitter, and symbol error probability (SEP) for the interpolation filters are shown in Fig. 4. These simulations have been realized by using 64-QAM signal when the signal-to-noise-ratio $E_b/N_0 = 15$ dB, and the block size $N = 64$.

Figure 5 illustrate the behaviour of the SEP as a function of the phase error for 16-QAM signal when $E_b/N_0 = 13$ dB, $N = 16$.

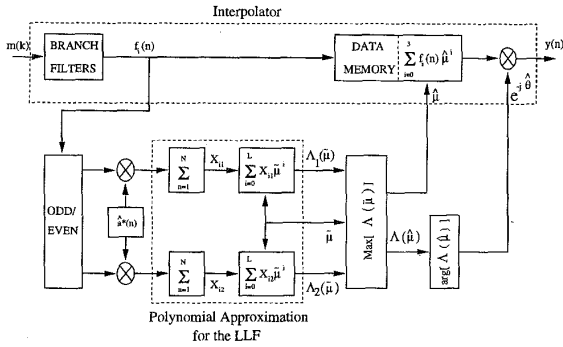


Figure 3: Phase estimation and symbol timing recovery scheme.

We noticed a dramatic difference in performance between the conventional Lagrange and the new interpolator when using 16-QAM and 64-QAM-type of modulations (see Figs. 6 & 7). Also, with QPSK an improvement of about 0.5 dB is obtained when utilizing the new interpolator (see Fig. 8).

Another type of simulations calculating the SEP as a function of E_b/N_0 for different phase errors using the same block length $N = 16$, have shown a slight difference of about 0.1 dB.

6. CONCLUSIONS

An extension of the polynomial-based maximum likelihood technique for jointly estimating the symbol timing and carrier phase of digital receivers for the data-aided case was established. Simulations for different types of modulations using the Lagrange and a new interpolator are also performed and compared with the theoretical case. The results exhibit the high performance of the new interpolator compared to the Lagrange interpolator.

It remains as a topic for future work to perform this polynomial approximation of the log-likelihood for symbol timing and carrier phase adjustment for the non-data-aided systems.

7. REFERENCES

- [1] J. G. Proakis, *Digital Communication*. McGraw-Hill, 1989.
- [2] J. Vesma, V. Tuukkanen, and M. Renfors, "Maximum likelihood feedforward symbol timing recovery based on efficient digital interpolation techniques," in *Proc. 1996, IEEE Nordic Signal Processing Symposium*, Espoo, Finland, Sept. 1996, pp. 183-186.
- [3] J. Vesma, V. Tuukkanen, R. Hamila, and M. Renfors, "Block-based feedforward maximum likelihood symbol timing recovery technique," in *Proc.*

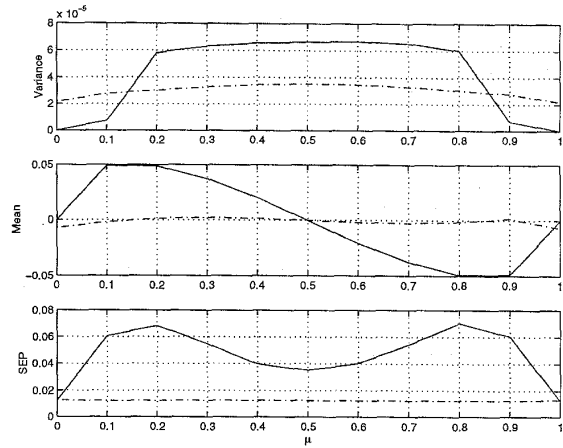


Figure 4: Variance and mean of the timing jitter, and SEP with 64-QAM for the Lagrange interpolator (solid line) and the new interpolator (dashed line), when $E_b/N_0 = 15$ dB and $N = 64$.

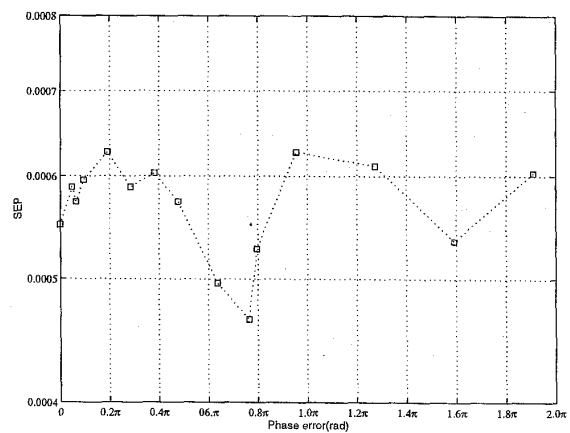


Figure 5: SEP as a function of the phase error for 16-QAM signal when $E_b/N_0 = 13$ dB and $N = 16$.

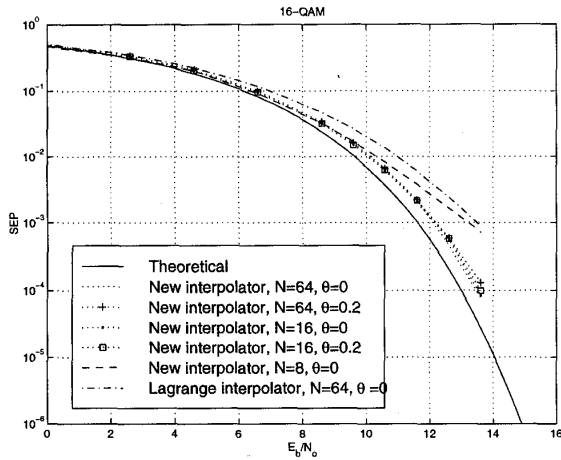


Figure 6: Worst case SEP with 16-QAM using cubic Lagrange interpolator and the new interpolator with zero phase error and different block lengths (N).

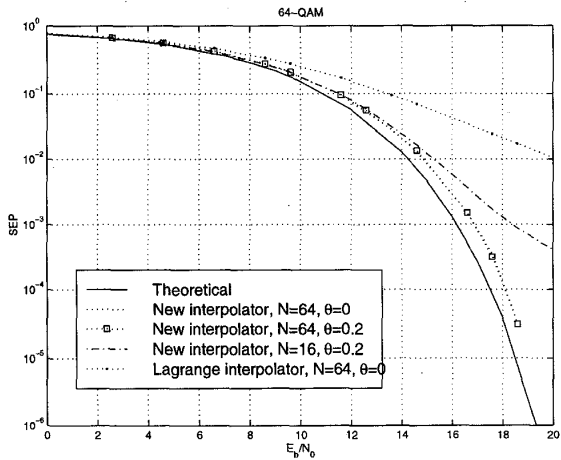


Figure 7: Worst case SEP with 64-QAM using cubic Lagrange interpolator and the new interpolator with phase error $\theta = 0.2$ rad and different block lengths (N).

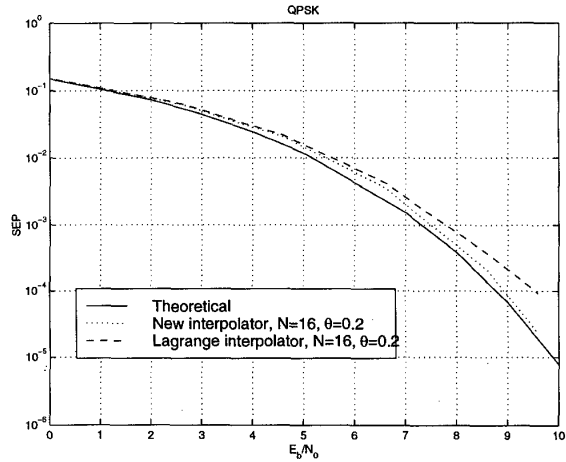


Figure 8: Worst case SEP with QPSK using cubic Lagrange interpolator and the new interpolator, with the same block length $N = 16$ and phase error $\theta = 0.2$ rad.

Communication Systems & Digital Signal Processing, Sheffield-UK, April 1998, pp. 92-95.

- [4] H. Meyr, M. Moeneclaey and S. A. Fechtel, *Digital Communication Receivers: Synchronization, Channel Estimation and Signal Processing*. John Wiley & Sons, 1998.
- [5] C. W. Farrow, "A continuously variable digital delay element," in *Proc. IEEE Int. Symp. Circuits & Syst.*, Espoo, Finland, June 1988, pp. 2641-2645.
- [6] J. Vesma and T. Saramäki, "Interpolation filters with arbitrary frequency response for all-digital receivers," in *Proc. IEEE Int. Symp. Circuits & Syst.*, Atlanta, GA, May 1996, pp. 568-571.
- [7] R. Hamila, J. Vesma, T. Saramäki and M. Renfors, "Discrete-time simulation of continuous-time systems using generalized interpolation techniques," in *Proc. 1997, the Summer Computer Simulation Conference*, Arlington, Virginia, USA, July 1997, pp. 914-919.
- [8] L. Erup, F. M. Gardner, and R. A. Harris, "Interpolation in digital modems - Part II: Implementation and performance," *IEEE Trans. Commun.*, vol. 41, pp. 998-1008, June 1993.
- [9] F. M. Gardner, "Demodulator reference recovery techniques suited for digital implementation," *ESA Final Report*, Aug. 1988.
- [10] J. Vesma, M. Renfors, and J. Rinne, "Comparison of efficient interpolation techniques for symbol timing recovery," in *Proc. IEEE Globecom 96*, London, UK, Nov. 1996, pp. 953-957.

Publication 3

R. Hamila, J. Vesma, H. Vuolle, and M. Renfors, "NDA Maximum Likelihood Approach for Timing and Phase Adjustment by Polynomial-Based Interpolation," *in Proc. 6th IEEE International Workshop on Intelligent Signal Processing and Communication Systems, ISPACS'98*, Melbourne, Australia, Nov. 1998, pp. 248–252.

Copyright ©1998 IEEE. Reprinted, with permission, from the proceedings of ISPACS'98.



The 6th IEEE International Workshop on Intelligent Signal Processing and Communication Systems

Proceedings

Volume 2

**5-6 November 1998
Melbourne, Australia**



Editors H R Wu, K N Ngan, B Qiu, S Suthakaran



**Cooperative Research Centre
Broadband Telecommunications and Networking**

NDA MAXIMUM LIKELIHOOD APPROACH FOR TIMING AND PHASE ADJUSTMENT BY POLYNOMIAL-BASED INTERPOLATION

Ridha Hamila, Jussi Vesma, Hannu Vuolle, and Markku Renfors

Telecommunications Laboratory
Tampere University of Technology
P.O Box 553, FIN-33101 Tampere, Finland
e-mail: ridha@cs.tut.fi

ABSTRACT

In this contribution, we extend the polynomial-based ML approach derived earlier for synchronization purposes to the non-data-aided (NDA) case. We propose a fully digitally implemented synchronization concept using interpolation for jointly estimating the timing and phase. The interpolation methods used in this context can be implemented using the so-called Farrow structure. The ML function is also expressed in terms of the polynomial-based interpolator filter branches. Simulation results for both NDA and DA synchronization principles using two types of interpolators are provided and compared with the theoretical case. We notice that the optimized interpolator performs much better compared to the Lagrange interpolator.

1. INTRODUCTION

In conventional receivers, the sampling of the received signal must be synchronized to the incoming data symbols. The synchronization is performed by using a feedback or feed-forward loop. Currently, there is a trend of using digital receivers where the sampling of the received signal is not synchronized to the incoming data symbols. With this approach, there is no need for the complex PLL circuits used in the conventional receivers.

In this receiver architecture, the sampling of the received signal is performed by a fixed sampling clock and thus sampling is not synchronized to the incoming symbols. Therefore, timing adjustment and consequently phase estimation must be done by digital methods after sampling. One way to perform this is to calculate the value of the signal at the desired time instants using interpolation. Hence, a polynomial-based interpolation technique using filters for the calculation of the timing and phase error estimates is applied. The so-called Farrow structure has been used in this context because it offers an efficient and flexible realization for such an interpolation task [1]. Simulation results show that the

optimized interpolator [2] performs much better compared to the Lagrange interpolator [3]-[4].

The best synchronization algorithms for digital communication systems are based on the maximum likelihood (ML) estimation theory. Estimation of joint signal parameters using the ML approach provides usually better estimates with respect to the variance compared to estimates obtained from separate optimization of the likelihood functions [5]. The feedforward architecture we are considering provides rapid acquisition characteristics, which are very important especially in the mobile communication systems where the channel characteristics are rapidly changing, and in the case of TDMA system, also the transmission is bursty.

In this paper, we extend our previous DA approach for clock and/or carrier phase synchronization of digital receivers to the case of NDA systems. The proposed method is based on the ML function for jointly estimating the symbol timing and carrier phase using a block-based feed-forward architecture. This approach is valid for M-PSK type of modulations which are commonly used in mobile communication systems.

2. TIMING AND PHASE ADJUSTMENT USING INTERPOLATION

The block diagram of the digital receiver with non-synchronized sampling is shown in Figure 1. The sampling of the received signal $r(t)$ is performed by a fixed sampling clock, and thus, the timing adjustment and consequently the carrier phase estimation must be done after the sampling using interpolation.

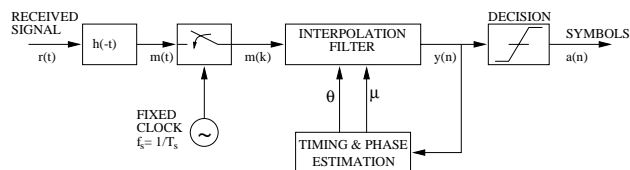


Figure 1: Digital Receiver with non-synchronized sampling.

This work was carried out in the project "Analog and Digital Signal Processing Techniques for Highly Integrated Transceivers" supported by the Academy of Finland.

Assuming an AWGN channel, the complex envelope

$r(t)$ of the received noisy M-PSK modulated signal is given by

$$r(t) = \sum_i c_i h(t - iT - \tau) e^{j\theta} + n(t), \quad (1)$$

where the couple (τ, θ) are the unknown clock and carrier phase respectively, $1/T$ is the symbol rate, $h(t)$ is the baseband pulse shape, c_i is a sequence of independent equiprobable M-PSK data symbols

$$c_i \in \{e^{\pm j\pi/M}, e^{\pm j3\pi/M}, \dots\},$$

and $n(t)$ is white Gaussian noise.

The interpolation filter in Fig. 1 can be used for both up-sampling and down-sampling, and furthermore, the output is not synchronized to the input. The function of the interpolation filter is to calculate one output sample $y(nT_i)$ at a time using a set of adjacent input samples $m(kT_s)$, within a timing error estimate (μ) and a phase error estimate (θ) obtained from the synchronization control unit. In the ideal case these output samples are the same sample values that would occur if the original sampling had been synchronized to the received symbols.

The fractional interval μ determines the time instant $t = nT_i$ where the original continuous-time received signal $r(t)$ is approximated. This relation is given by

$$nT_i = (\mu + k)T_s, \quad (2)$$

where $\mu \in [0, 1)$ is the fractional interval, T_s is the sampling interval, and T_i is the output interval, whereas k is the largest integer for which $kT_s \leq nT_i$. In this paper, we assume that the original sampling rate is twice the symbol rate $T = 2T_s$. Also, we use τ and μ to denote the timing error with respect to the symbol and sampling interval, respectively. In addition, the error in the carrier phase is corrected using the phase error estimate denoted by θ as shown in Fig. 1.

The polynomial-based interpolation filters are very easily implemented using the Farrow structure [1]. This structure is characterized by the fixed values of all the filter coefficients and by only one changeable parameter which is the fractional interval μ . In the general case, the Farrow structure shown in Fig. 2 consists of $L + 1$ FIR filter branches and the length of each branch filter is N , where L is the degree of the interpolation and N is the length of the impulse response.

Timing adjustment in digital receivers using Lagrange interpolation was first introduced by Erup et al. [3]. Lagrange interpolation represents the conventional time-domain approach to the interpolation problems. A new synthesis technique for polynomial-based interpolation filters is proposed in [2]. In this synthesis technique, the design parameters are edge frequencies for passbands and stopbands, desired amplitude and weight for every band, the length of the filter, and the degree of the interpolation. After giving these parameters, the filter coefficients of the Farrow structure

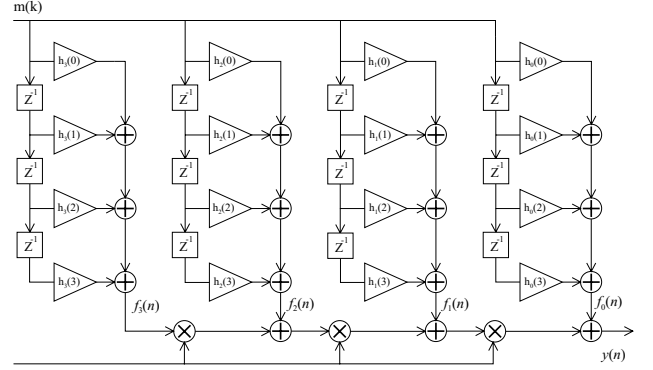


Figure 2: Farrow structure for the cubic ($L = 3$) interpolator.

are optimized in the frequency domain in the minimax sense. The new designs are shown to provide clearly lower complexity or much better performance with the same complexity as the Lagrange designs [6].

3. NDA MAXIMUM LIKELIHOOD ESTIMATION OF PHASE AND TIMING

Under the assumption that the sequence of M-PSK data symbols are independent and equiprobable, the likelihood function for NDA estimation of timing (τ) and carrier phase (θ) is given by [7];

$$\Lambda(\hat{\tau}, \hat{\theta}) = \sum_{n=1}^N |m(n, \hat{\tau})|^2 + \text{Re} \left[\sum_{n=1}^N m^2(n, \hat{\tau}) e^{-j2\hat{\theta}} \right], \quad (3)$$

where $m(n, \hat{\tau})$, $\hat{\theta} \in [-\pi, \pi]$, and $\hat{\tau} \in [0, T)$ are the samples from the output of the matched filter (one sample per symbol), carrier phase and symbol timing error trials, respectively. N is the number of symbols used in the calculation and T is the symbol interval.

The above NDA likelihood approximation is only valid for single amplitude type of modulations, e.g., M-PSK modulated signals.

Synchronization algorithms for digital receivers estimating jointly the timing and phase are based on Maximum Likelihood estimation (MLE) theory as mentioned earlier. These algorithms are trying to find the timing and the phase error estimates $(\hat{\tau}, \hat{\theta})$ which maximize Eq. (3). By means of the above likelihood function, the following algorithm for jointly estimating $(\hat{\tau}, \hat{\theta})$ can be established as follows [7]:

$$\hat{\tau} = \max_{\hat{\tau}} \sum_{n=1}^N |m(n, \hat{\tau})|^2 \quad (4)$$

$$\hat{\theta} = \frac{1}{M} \arg \left[\sum_{n=1}^N (m(n, \hat{\tau}))^M \right], \quad (5)$$

where M is the number of constellation points.

An important feature here is that the ML-estimate of the timing is independent of the carrier phase. We consider here a block processing scheme which takes the data samples for a block of N symbols.

In the following section, we will form a polynomial approximation for the above likelihood function by using the Farrow structure, then different schemes for finding the maximum of this polynomial can be devised.

4. POLYNOMIAL APPROXIMATION OF THE NDA LIKELIHOOD FUNCTION FOR TIMING AND PHASE ESTIMATION

In this section, we will extend this polynomial-based likelihood function for jointly estimating the timing and phase with respect to Eqs. (4) and (5). This procedure is derived for the non-data-aided (NDA) systems where the symbol values are not known in advance in the case of single amplitude type of modulations. In general we should expect some degradation of performance when ignoring the data values [4].

Here we assume that the original sampling rate is twice the symbol rate $T = 2T_s$ and cubic interpolation filter ($L = 3$) is used. Because the symbol interval is divided into two parts (two samples per one symbol), there are two different polynomial approximations for the log-likelihood function as in [8]-[9]-[10]. Consequently, from expression (4) the symbol timing is estimated by

$$\hat{\tau} = \arg \max_{\tilde{\tau}} \begin{cases} \Lambda_1(2\tilde{\tau}) & 0 \leq \tilde{\tau} < 0.5 \\ \Lambda_2(2\tilde{\tau} - 1) & 0.5 \leq \tilde{\tau} < 1 \end{cases} \quad (6)$$

where

$$\Lambda_1(2\tilde{\tau}) = \sum_{n=1}^N |m(2n-1, 2\tilde{\tau})|^2,$$

and

$$\Lambda_2(2\tilde{\tau} - 1) = \sum_{n=1}^N |m(2n, 2\tilde{\tau} - 1)|^2.$$

Also, by using the above timing estimate $\hat{\tau}$, the carrier phase estimate is given by

$$\hat{\theta} = \frac{1}{M} \arg \begin{cases} \sum_{n=1}^N [m(2n-1, 2\hat{\tau})]^M & \text{for } 0 \leq \hat{\tau} < 0.5 \\ \sum_{n=1}^N [m(2n, 2\hat{\tau} - 1)]^M & \text{for } 0.5 \leq \hat{\tau} < 1. \end{cases} \quad (7)$$

The value of $m(n, \hat{\tau})$ can be interpolated for different values of $\hat{\tau}$ by utilizing the cubic Farrow structure and the original samples $m(k)$. Eqs. (6) and (7) can also be expressed as a function of the fractional interval $\hat{\mu} \in [0, 1)$, and the output samples of the FIR filter branches in the Farrow structure $f_i(n)$ in the case of a cubic interpolation filter, as follows:

If $\max[\Lambda_1(\hat{\mu})] > \max[\Lambda_2(\hat{\mu})]$ then

$$\hat{\mu} = \arg \max_{\tilde{\mu}} [\Lambda_1(\tilde{\mu})],$$

else

$$\hat{\mu} = \arg \max_{\tilde{\mu}} [\Lambda_2(\tilde{\mu})].$$

Where

$$\Lambda_1(\tilde{\mu}) = \sum_{n=1}^N \left| \sum_{i=0}^3 \tilde{\mu}^i f_i(2n-1) \right|^2,$$

and

$$\Lambda_2(\tilde{\mu}) = \sum_{n=1}^N \left| \sum_{i=0}^3 \tilde{\mu}^i f_i(2n) \right|^2.$$

Finally, the above symbol timing estimate is used for computing the carrier phase estimate:

If $\max[\Lambda_1(\hat{\mu})] > \max[\Lambda_2(\hat{\mu})]$ then

$$\hat{\theta} = \frac{1}{M} \arg \sum_{n=1}^N \left[\sum_{i=0}^3 \hat{\mu}^i f_i(2n-1) \right]^M$$

else

$$\hat{\theta} = \frac{1}{M} \arg \sum_{n=1}^N \left[\sum_{i=0}^3 \hat{\mu}^i f_i(2n) \right]^M.$$

The overall scheme for our proposed block-based symbol timing and phase recovery is illustrated in Fig. 3. For the NDA feedforward (FF) phase estimator, the influence of the symbols is removed by the M^{th} power [11] (see Fig. (3)).

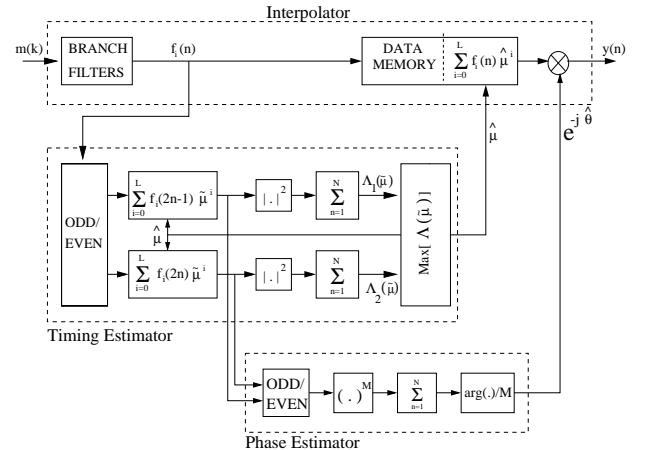


Figure 3: NDA Phase estimation and symbol timing recovery scheme.

After the parameters $\hat{\mu}$ and $\hat{\theta}$ are estimated, timing adjustment is performed by evaluating the value of the polynomial at the given value of $\hat{\mu}$. At the same time, sampling rate is decreased by two. Here, even samples are discarded if $\max[\Lambda_1(\hat{\mu})] > \max[\Lambda_2(\hat{\mu})]$, and odd samples otherwise. Subsequently, the carrier phase is corrected by the factor $e^{-j\hat{\theta}}$.

5. SIMULATIONS

The proposed algorithm is simulated using M-PSK constellations. The transmitter and receiver pulse-shaping filters are square root raised cosine filters with excess bandwidth of 35%. Two interpolation filters, cubic Lagrange and third order interpolation filter of length 8 designed by the new synthesis technique [2], are compared. The simulations are done using the worst-case timing offset and some selected values of the phase error.

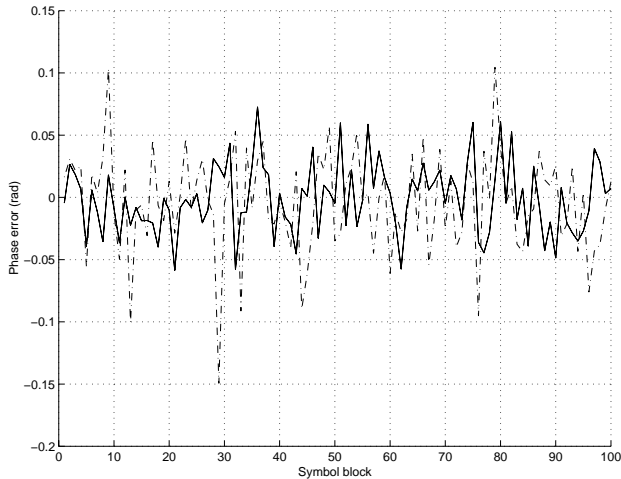


Figure 4: Phase Jitter of 4-PSK signal when $E_b/N_0 = 9$ dB, phase error $\theta = 0.6$ rad, and block length $N = 64$. The solid line shows the phase jitter of the new interpolator, and the dashed-dot line phase jitter of the Lagrange interpolator.

Figure 4 shows the phase jitter of 4-PSK signal when $E_b/N_0 = 9$ dB, phase error equal 0.6 rad, and block length $N = 64$. Variance and mean of the phase jitter for the interpolation filters are also provided in Fig. 5. Similarly, Figs. 6 & 7 illustrate the timing jitter, variance and mean of the timing jitter.

We noticed a dramatic difference in performance between the conventional Lagrange and the new interpolator when using 4-PSK-type of modulations as shown in fig. 8. The same experiments compare the SEP as a function of the signal-to-noise-ratio E_b/N_0 of the DA and NDA systems with the theoretical expectations. The performance of the scheme was found to be close to ideal for the DA systems even with short block lengths [10], thus having a rapid acquisition time. Similarly, by using a longer block length, the NDA systems perform fairly well.

Binary and M-PSK -type of modulations are generally used in mobile telecommunications systems. These modulations types do not have very demanding requirements for the interpolator. However, linear or cubic Lagrange interpolator may not be sufficient for the new synchronization scheme. Fortunately, better interpolation filters than the cubic Lagrange which are not more

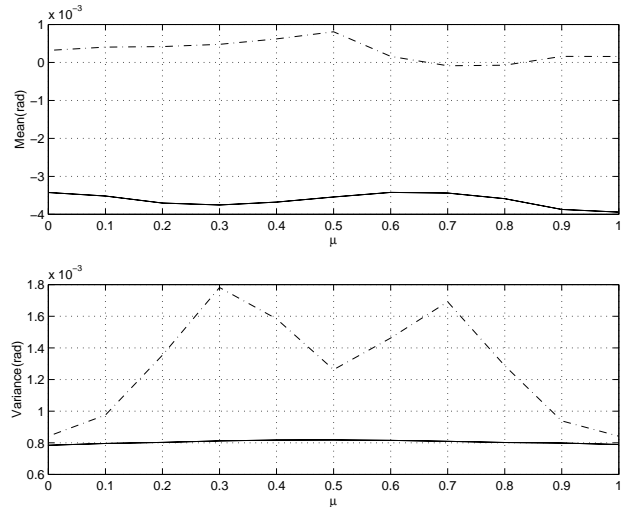


Figure 5: Variance and mean of the phase jitter of 4-PSK signal for the Lagrange interpolator (dashed-dot line) and new interpolator (solid line).

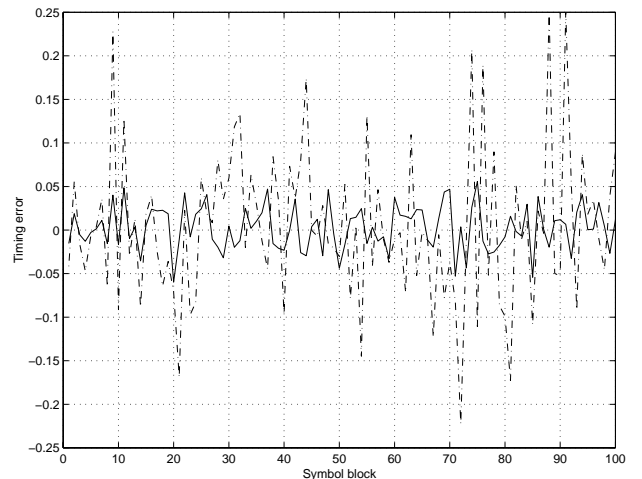


Figure 6: Timing jitter of 4-PSK signal when $E_b/N_0 = 9$ dB, phase error $\theta = 0.6$ rad, and block length $N = 64$. The solid line shows the timing jitter of the new interpolator, and the dashed-dot line the timing jitter of the Lagrange interpolator.

complicated to implement are derived in [6].

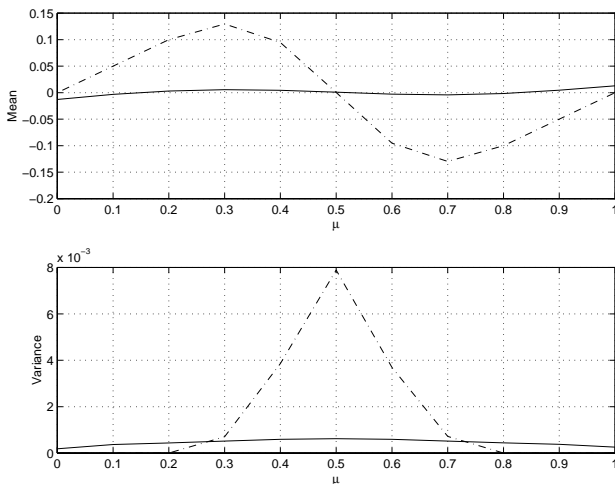


Figure 7: Variance and mean of the timing jitter of 4-PSK signal for the Lagrange interpolator (dashed-dot line) and new interpolator (solid line).

6. CONCLUSIONS

An extension of the polynomial-based maximum likelihood technique for jointly estimating the symbol timing and carrier phase of NDA systems is established. Different simulations using the Lagrange and the new interpolator are also performed for both DA and NDA systems and compared with the theoretical case. The results show the high performance of the new interpolator compared to the Lagrange interpolator. However, the NDA approach requires more computation than the DA approach for estimating the polynomial-based likelihood function. Therefore, further studies considering the computation complexity of this new NDA technique will be carried out. Normally, by omitting decision operations one may reduce equipment complexity and obtain fast acquisition. Besides, in some circumstances NDA systems may perform better than DD specially for poor quality data decisions.

7. REFERENCES

- [1] C. W. Farrow, "A continuously variable digital delay element," in *Proc. IEEE Int. Symp. Circuits & Syst.*, Espoo, Finland, June 1988, pp. 2641-2645.
- [2] J. Vesma and T. Saramäki, "Interpolation filters with arbitrary frequency response for all-digital receivers," in *Proc. IEEE Int. Symp. Circuits & Syst.*, Atlanta, GA, May 1996, pp. 568-571.
- [3] L. Erup, F. M. Gardner, and R. A. Harris, "Interpolation in digital modems - Part II: Implementation and performance," *IEEE Trans. Commun.*, vol. 41, pp. 998-1008, June 1993.

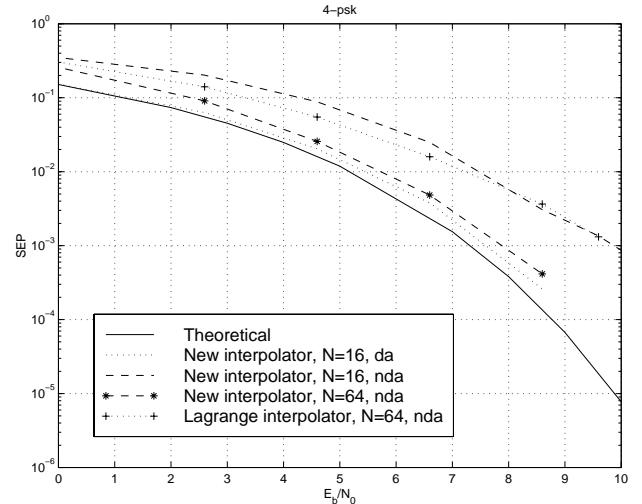


Figure 8: Worst case SEP with 4-PSK using cubic Lagrange and the new interpolator, with different block length N and phase error $\theta = 0.6$ rad.

- [4] F. M. Gardner, "Demodulator reference recovery techniques suited for digital implementation," *ESA Final Report*, Aug. 1988.
- [5] J. G. Proakis, *Digital Communication*. McGraw-Hill, 1989.
- [6] J. Vesma, M. Renfors, and J. Rinne, "Comparison of efficient interpolation techniques for symbol timing recovery," in *Proc. IEEE Globecom 96*, London, UK, Nov. 1996, pp. 953-957.
- [7] H. Meyr, M. Moeneclaey, and S. A. Fechtel, *Digital Communication Receivers: Synchronization, Channel Estimation and Signal Processing*. John Wiley & Sons, 1998.
- [8] J. Vesma, V. Tuukkanen, and M. Renfors, "Maximum likelihood feedforward symbol timing recovery based on efficient digital interpolation techniques," in *Proc. 1996, IEEE Nordic Signal Processing Symposium*, Espoo, Finland, Sept. 1996, pp. 183-186.
- [9] J. Vesma, V. Tuukkanen, R. Hamila, and M. Renfors, "Block-based feedforward maximum likelihood symbol timing recovery technique," in *Proc. Communication Systems & Digital Signal Processing*, Sheffield-UK, April 1998, pp. 92-95.
- [10] R. Hamila, J. Vesma, H. Vuolle, and M. Renfors, "Joint estimation of phase and timing using polynomial-based ML technique," to be presented in *IEEE 1998 International Conference on Universal Personal Communications*, Florence, Italy, 5-9 October, 1998.
- [11] Geert De Jonghe and Marc Moeneclaey "Asymptotic cycle slip probability expression for the NDA feedforward carrier synchronization for M-PSK," in *Proc. ICC'93*, Geneva, Switzerland, pp. 502-506.

Publication 4

R. Hamila, J. Vesma, H. Vuolle, and M. Renfors, "Effect of Frequency Offset on Carrier Phase and Symbol Timing Recovery in Digital Receivers," *in Proc. 1998 URSI International Symposium on Signals, Systems, and Electronics, ISSSE'98, Pisa, Italy, September 1998*, pp. 247–252.

Copyright ©1998 IEEE. Reprinted, with permission, from the proceedings of ISSSE'98.



Co-Design of Radiocommunication Terminals
from **WAVES** to **SILICON** through **DSP**

**CONFERENCE
PROCEEDINGS**



**1998 URSI International Symposium on
Signals, Systems, and Electronics**

29 SEPTEMBER - 2 OCTOBER, 1998
PALAZZO DEI CONGRESSI
PISA, ITALY



EFFECT OF FREQUENCY OFFSET ON CARRIER PHASE AND SYMBOL TIMING RECOVERY IN DIGITAL RECEIVERS

Ridha Hamila, Jussi Vesma, Hannu Vuolle, and Markku Renfors

Telecommunications Laboratory - Tampere University of Technology

P.O. Box 553, FIN-33101 Tampere - Finland

Ph.: +358 3 365 3910, Fax: +358 3 365 3808, e-mail: ridha@cs.tut.fi

ABSTRACT

Recently, a new all-digital technique for clock and carrier phase synchronization of digital receivers was introduced by the authors. This technique is based on a polynomial approximation of the likelihood function and utilizes the Farrow structure for symbol interpolation. In this contribution, we analyze the effect of frequency offset or Doppler shift on the performance of the receiver while adjusting jointly the symbol timing and the carrier phase. Simulation results for the data-aided synchronization principle using two types of interpolators are provided and compared with the theoretical case. We notice that our optimized interpolator performs clearly better compared to the traditional Lagrange interpolator.

1. INTRODUCTION

In conventional receivers, the sampling of the received signal must be synchronized to the incoming data symbols. The synchronization is performed by using a feedback or feed-forward loop. Currently, there is a trend of using digital receivers where the sampling of the received signal is not synchronized to the incoming data symbols. With this approach, there is no need for the complex PLL circuits used in the conventional receivers.

In this receiver architecture, the sampling of the received signal is performed by a fixed sampling clock and thus sampling is not synchronized to the incoming symbols. Therefore, timing adjustment and consequently phase estimation must be done by digital methods after sampling. One way to perform this is to calculate the value of the signal at the desired time instants using interpolation. Hence, a polynomial-based interpolation technique using filters for the calculation of the timing and phase error estimates is applied. This interpolation method is the so-called Farrow structure. It is characterized by its efficiency and flexible realization [1]-[2]-[3]-[4].

The best synchronization algorithms for digital communication systems are based on the maximum likelihood (ML) estimation theory. Estimation of

the carrier phase and the symbol timing can be performed separately or jointly. However, estimates obtained from joint optimization of the likelihood function are usually better [5].

Recently, a new technique for clock and carrier phase synchronization of digital receivers, using a block-based feedforward architecture, has been introduced in [6]-[7]-[8]. This technique is a practical fully digitally implemented synchronization concept using interpolation for jointly estimating the symbol timing and the carrier phase, where the ML function is expressed in terms of the polynomial-based interpolator filter branches. The feed-forward architecture we are considering provides rapid acquisition characteristics, which are very important especially in the mobile communication systems where the channel characteristics are rapidly changing, and in the case of TDMA system, also the transmission is bursty.

In this paper, we analyze the effect of the frequency error or Doppler shift on the receiver performance while adjusting jointly the estimated symbol timing and the carrier phase. Simulation results for the data-aided (DA) synchronization principle using two types of interpolators are provided and compared with the theoretical case. We notice that our optimized interpolator performs clearly better compared to the Lagrange interpolator.

2. SIGNAL AND TRANSMISSION MODEL

Here we consider the timing and the carrier phase recovery for digital data transmission by linear modulation schemes (PAM, QAM, M-PSK) when a small frequency error is introduced. After down conversion the received signal (e.g., QAM) can be written as

$$r(t) = \sum_i a_i g(t - iT - \tau) e^{j(2\pi F_d t + \theta)} + n(t), \quad (1)$$

with

$$g(t) = g_T(t) * c(t).$$

Here, $\{a_i\}$ are the complex valued transmitted symbols, $g(t)$ represents the impulse response of the pulse-shaping filter $g_T(t)$ convolved with the channel $c(t)$, T is the symbol duration, and $n(t)$ is the channel noise which is assumed to be white and Gaussian

This work was carried out in the project "Analog and Digital Signal Processing Techniques for Highly Integrated Transceivers" supported by the Academy of Finland.

with power density N_0 . The parameters $\{\tau, \theta, F_d\}$ denote the time-delay, the carrier phase, and the frequency offset, respectively.

The received signal $r(t)$ is then convolved with the matched filter $g_{MF}(t)$ (see Fig. (1)), and we obtain the signal $m(t) = r(t) * g_{MF}(t)$ which is afterward sampled by a free running clock. we assume here that the baseband pulse $q(t)$ which is defined by

$$q(t) = g(t) * g_{MF}(t) \quad (2)$$

satisfies the first Nyquist criterion

$$q(iT) \begin{cases} 1 & \text{for } i = 0 \\ 0 & \text{for } i \neq 0. \end{cases} \quad (3)$$

Also, we assume that the frequency response of the channel is flat within the frequency range

$$|\omega| \leq 2\pi(B + F_{max}), \quad (4)$$

where B is the bandwidth of the linearly modulated signal in the baseband, and $\pm F_{max}$ represents the maximum frequency uncertainty. Generally, the frequency estimator algorithms fulfill the above assumption in order to produce an un-biased estimate [1].

Below we consider the effect of a small frequency offset on a special type of symbol timing and carrier phase estimators which are particularly suited for digital realization. Only under the condition that the frequency offset F_d is restricted to small values ($F_d T \ll 1$) then the timing and the carrier phase information can be recovered prior to the frequency compensation [1]. Normally, when a receiver is operating on a steady-state condition, the frequency offset F_d is much smaller than the symbol rate $1/T$. However, if the frequency offset is on the order of the symbol rate, frequency error correction or reduction has to be performed before other synchronization functions.

In fact, due to un-compensated frequency errors, the carrier phase changes across a data segment N and achieves the value [12]

$$\Delta\phi = 2\pi F_d N T \quad (5)$$

at the end of the segment. Therefore, a non-negligible phase variation $\Delta\phi$ degrades the symbol error probability (SEP).

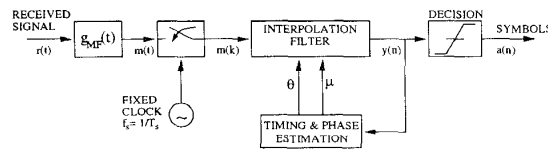


Figure 1: Digital Receiver with non-synchronized sampling.

3. TIMING AND PHASE ADJUSTMENT USING INTERPOLATION

The block diagram of the digital receiver with non-synchronized sampling is shown in Figure 1. The

sampling of the received signal $r(t)$ is performed by a fixed sampling clock, and thus, the timing adjustment and consequently the carrier phase estimation must be done after the sampling using interpolation. The interpolation filter in Fig. 1 can be used for both up-sampling and down-sampling, and furthermore, the output is not synchronized to the input. We should think interpolation from the mathematical point of view and recall how to interpolate data using polynomials.

The function of the interpolation filter is to calculate one output sample $y(nT_i)$ at a time using a set of adjacent input samples $m(kT_s)$, within a timing error estimate (μ) and a phase error estimate (θ) obtained from the synchronization control unit. In the ideal case these output samples are the same sample values that would occur if the original sampling had been synchronized to the received symbols.

The fractional interval μ determines the time instant $t = nT_i$ where the original continuous-time received signal $r(t)$ is approximated. This relation is given by

$$nT_i = (\mu + k)T_s, \quad (6)$$

where $\mu \in [0, 1)$ is the fractional interval, T_s is the sampling interval, and T_i is the output interval, whereas k is the largest integer for which $kT_s \leq nT_i$. In

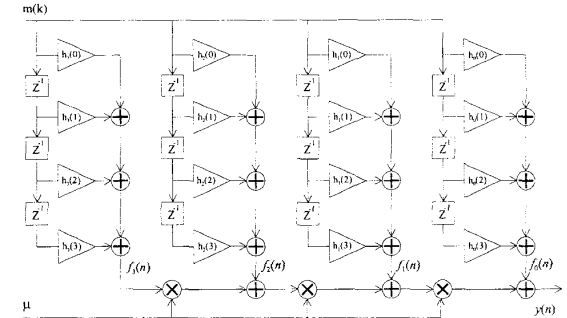


Figure 2: Farrow structure for the cubic interpolator with $L = 3$.

this paper, we assume that the original sampling rate is twice the symbol rate, $T = 2T_s$. Also, we use μ to denote the timing error with respect to the sampling interval. In addition, the error in the carrier phase is corrected using the phase error estimate denoted by θ as shown in Fig. 1.

The polynomial-based interpolation filters are very easily implemented using the Farrow structure [2]. This structure is characterized by the fixed values of all the filter coefficients and by only one changeable parameter which is the fractional interval μ .

In the general case, the Farrow structure (shown in Fig. 2) consists of $L + 1$ FIR filter branches and the length of each branch filter is N , where L is the degree of the interpolation and N is the length of the impulse response.

Timing adjustment in digital receivers using Lagrange interpolation was first introduced by Erup et.

al. [4]. Lagrange interpolation represents the conventional time-domain approach to the interpolation problems. A new synthesis technique for polynomial-based interpolation filters is proposed in [9]-[10]. In this synthesis technique, the design parameters are edge frequencies for passbands and stopbands, desired amplitude and weight for every band, the length of the filter, and the degree of the interpolation. After giving these parameters, the filter coefficients of the Farrow structure are optimized in the frequency domain in the minimax sense. The new designs are shown to provide clearly lower complexity or much better performance with the same complexity as the Lagrange designs [11].

4. POLYNOMIAL APPROXIMATION OF THE LOG-LIKELIHOOD FUNCTION FOR TIMING AND CARRIER PHASE ESTIMATION

Synchronization algorithms for digital receivers estimating jointly the timing and the carrier phase are based on maximum likelihood estimation (MLE) theory as mention earlier. These algorithms are trying to find the timing and the phase error estimates $(\hat{\mu}, \hat{\theta})$ which maximize the log-likelihood function.

A new technique of polynomial approximation for the log-likelihood function (LLF) used for symbol timing and carrier phase recovery has been developed by the co-authors in [6]-[8]. The main idea was to form a polynomial approximation for the log-likelihood function by using the Farrow structure, then different schemes for finding the maximum of this polynomial can be devised.

Considering a block processing scheme which takes the data samples and the decided/known symbol values for a block of N symbols. Also, assuming that the original sampling rate is twice the symbol rate $T = 2T_s$ and a cubic interpolation filter ($L = 3$) is used. Because the symbol interval is divided into two parts (two samples per one symbol), there are two different polynomial approximations for the log-likelihood function as shown in [6]-[7]-[8]. Consequently, the symbol timing expressed as a function of the fractional interval $\tilde{\mu} \in [0, 1)$, and the output samples of the FIR filter branches in the Farrow structure $f_i(n)$, is given by;

$$\text{If } \max[\Lambda_1(\tilde{\mu})] > \max[\Lambda_2(\tilde{\mu})] \text{ then}$$

$$\hat{\mu} = \arg \max_{\tilde{\mu}} [|\Lambda_1(\tilde{\mu})|], \quad (7)$$

else

$$\hat{\mu} = \arg \max_{\tilde{\mu}} [|\Lambda_2(\tilde{\mu})|].$$

Here

$$\Lambda_1(\tilde{\mu}) = \sum_{i=0}^3 \tilde{\mu}^i \sum_{n=1}^N \overbrace{\hat{a}^*(n) f_i(2n-1)}^{X_{i,1}}, \quad (8)$$

and

$$\Lambda_2(\tilde{\mu}) = \sum_{i=0}^3 \tilde{\mu}^i \sum_{n=1}^N \overbrace{\hat{a}^*(n) f_i(2n)}^{X_{i,2}}. \quad (9)$$

Also, by using the above timing estimate $\hat{\mu}$, the carrier phase estimate is given by

If $\max[\Lambda_1(\hat{\mu})] > \max[\Lambda_2(\hat{\mu})]$ then

$$\hat{\theta} = \arg[\Lambda_1(\hat{\mu})], \quad (10)$$

else

$$\hat{\theta} = \arg[\Lambda_2(\hat{\mu})].$$

In the case of a cubic interpolation filter, the overall scheme for our proposed block-based symbol timing and phase recovery is illustrated in Fig. 3. This pro-

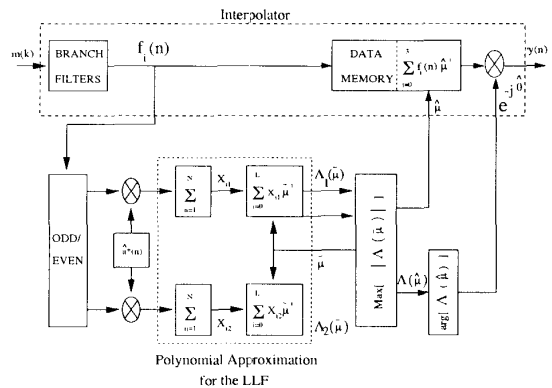


Figure 3: Phase estimation and symbol timing recovery scheme.

cedure can be used as such in the data-aided (DA) systems where the symbol values are known in advance. For example GSM does have a known synchronization symbol sequence. In case of decision-directed systems, a reasonably good initial estimate for the sampling phase must be known. The scheme can also be utilized in non-data-aided systems with some variations.

5. SIMULATIONS

The performance of this synchronization technique is analyzed in the presence of a frequency offset or Doppler shift (F_d) on the carrier (F_c). The introduced frequency offset satisfies the condition that F_d is much smaller than the symbol rate $1/T$. Therefore, symbol timing and carrier phase recovery can be done prior to the frequency error correction. The frequency offset values are controlled to keep the receiver performance close to the theoretical with respect to the SEP. The simulation are performed using 64-QAM constellations. The transmitter and the receiver pulse-shaping filters are square root raised cosine filters with excess bandwidth of 35%. Two interpolation filters, cubic Lagrange and third order interpolation filter of length 8 designed by the new

synthesis technique [9], are compared in the simulations.

Figure 4 compares the timing jitter of the Lagrange and the new interpolator using 64-QAM signal, when the signal-to noise-ratio $E_b/N_0 = 15$ dB and the block length $N = 32$. The introduced frequency offset (F_d) times the symbol period (T_{sym}) is constant for both interpolators, similarly for the introduced phase error (θ).

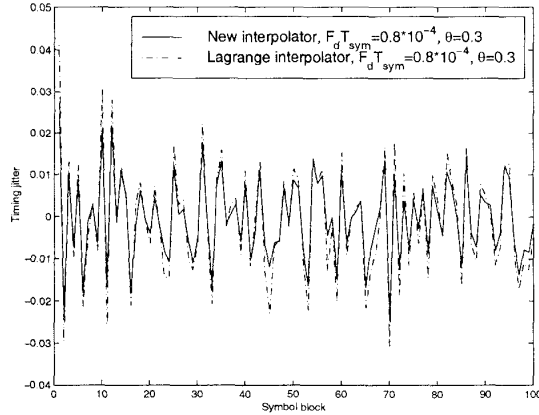


Figure 4: Timing jitter of 64-QAM signal for the Lagrange interpolator and the new interpolator, when $E_b/N_0 = 15$ dB and $N = 32$.

Mean and variance of the timing jitter, and symbol error probability (SEP) for the interpolation filters are also shown in Figs. 5, 6 and 7 respectively. These simulations have been realized by using 64-QAM signal when $E_b/N_0 = 15$ dB, block size $N = 32$, and with different frequency offsets and phase errors.

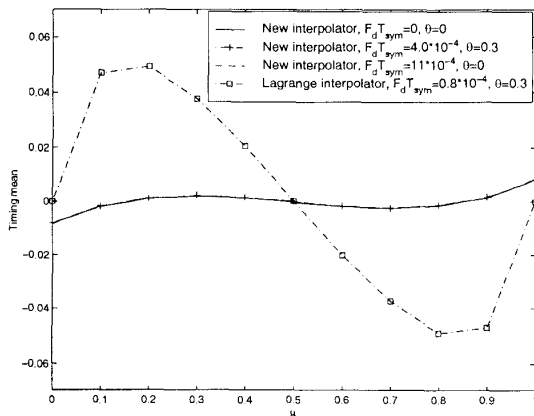


Figure 5: Mean of the timing jitter with 64-QAM for the Lagrange interpolator and the new interpolator, when $E_b/N_0 = 15$ dB and $N = 32$.

Figure 8 shows the SEP as a function of the frequency offset times the symbol period ($F_d T_{sym}$), using different block lengths. We observe that with relative big values of frequency offsets the SEP becomes

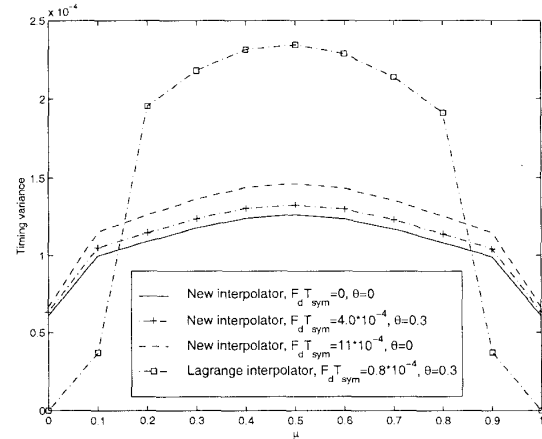


Figure 6: Variance of the timing jitter with 64-QAM for the Lagrange interpolator and the new interpolator, when $E_b/N_0 = 15$ dB and $N = 32$.

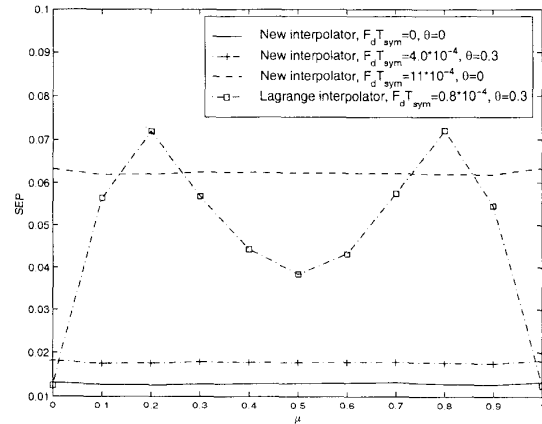


Figure 7: SEP with 64-QAM for the Lagrange interpolator and the new interpolator, when $E_b/N_0 = 15$ dB and $N = 32$.

worse by increasing the block length. However, with small values of frequency offsets the performance improves by increasing the block length.

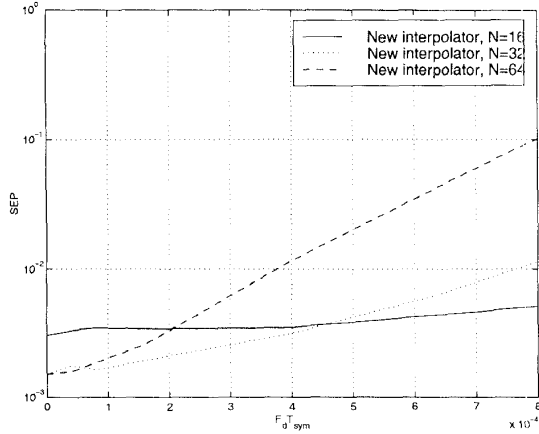


Figure 8: SEP with 64-QAM as a function of $F_d T_{sym}$ when $E_b/N_0 = 16.6$ dB and for different block lengths (N).

Finally, Figs. 9 and 10 show the SEP as a function of the signal-to noise-ratio for the Lagrange and the new interpolator, using 64-QAM constellations and a block size $N = 32$. The simulation are performed using the worst-case timing offset and for some selected values of the frequency offset and the phase error.

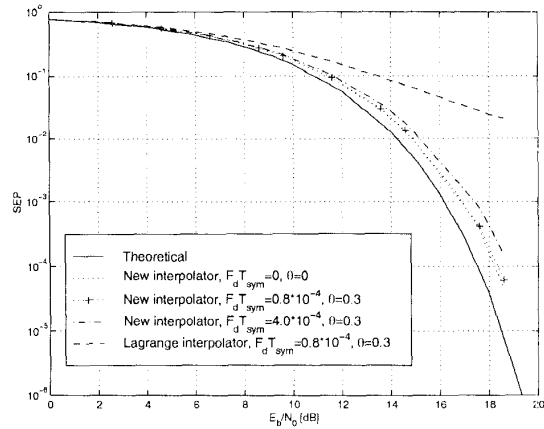


Figure 9: Worst case SEP with 64-QAM using cubic Lagrange and the new interpolator for different phase error θ (rad), and frequency offset F_d times the symbol period (T_{sym}). The block length is $N = 32$.

6. CONCLUSIONS

We analyzed the effect of the frequency offset or Doppler shift on the performance of the digital receiver while adjusting the symbol timing and the carrier phase. This effect is analyzed under the assump-

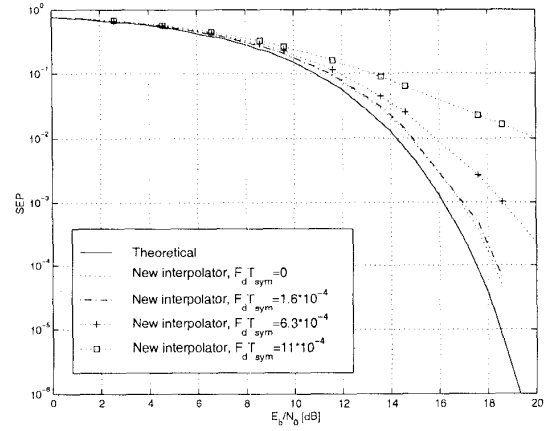


Figure 10: Worst case SEP with 64-QAM using the new interpolator, for different frequency offset times the symbol period $F_d T_{sym}$ when the phase error $\theta = 0$ rad and the block length $N = 32$.

tion that the frequency offset is much smaller than the symbol period. Simulation results for the DA synchronization principle using two types of interpolators are provided and compared with the theoretical case. We noticed that our optimized interpolator performs clearly better compared to the Lagrange interpolator when using 64-QAM-type of modulations. Also, we demonstrated that our symbol timing and carrier phase recovery scheme performs quite well within a relatively small frequency offset values with respect to the symbol period.

7. REFERENCES

- [1] H. Meyr, M. Moeneclaey, and S. A. Fechtel, *Digital Communication Receivers: Synchronization, Channel Estimation and Signal Processing*. John Wiley & Sons, 1998.
- [2] C. W. Farrow, "A continuously variable digital delay element," in *Proc. IEEE Int. Symp. Circuits & Syst.*, Espoo, Finland, June 1988, pp. 2641-2645.
- [3] F. M. Gardner, "Demodulator reference recovery techniques suited for digital implementation," *ESA Final Report*, Aug. 1988.
- [4] L. Erup, F. M. Gardner, and R. A. Harris, "Interpolation in digital modems - Part II: Implementation and performance," *IEEE Trans. Commun.*, vol. 41, pp. 998-1008, June 1993.
- [5] J. G. Proakis, *Digital Communication*. McGraw-Hill, 1989.
- [6] J. Vesma, V. Tuukkanen, and M. Renfors, "Maximum Likelihood Feedforward Symbol Timing Recovery Based on Efficient Digital Interpolation Techniques," in *Proc. 1996, IEEE*

Nordic Signal Processing Symposium, Espoo, Finland, Sept. 1996, pp. 183-186.

- [7] J. Vesma, V. Tuukkanen, R. Hamila, and M. Renfors, "Block-Based Feedforward Maximum Likelihood Symbol Timing Recovery Technique," in *Proc. of Communication Systems & Digital Signal Processing*, Sheffield-UK, April, 1998, pp. 92-95.
- [8] R. Hamila, J. Vesma, H. Vuolle, and M. Renfors, "Joint estimation of phase and timing using polynomial-based maximum likelihood technique," to be presented in *ICUPC'98*.
- [9] J. Vesma and T. Saramäki, "Interpolation filters with arbitrary frequency response for all-digital receivers," in *Proc. IEEE Int. Symp. Circuits & Syst.*, Atlanta, GA, May 1996, pp. 568-571.
- [10] R. Hamila, J. Vesma, T. Saramäki and M. Renfors, "Discrete-Time Simulation of Continuous-Time Systems Using Generalized Interpolation Techniques," in *Proc. 1997, the Summer Computer Simulation Conference*, Arlington, Virginia, USA, July 1997, pp. 914-919.
- [11] J. Vesma, M. Renfors, and J. Rinne, "Comparison of efficient interpolation techniques for symbol timing recovery," in *Proc. IEEE Globecom 96*, London, UK, Nov. 1996, pp. 953-957.
- [12] U. Mengali and A. N. D'Andrea, *Synchronization Techniques for Digital Receivers*. Plenum Press, 1997.

Publication 5

R. Hamila, M. Renfors, "New Maximum Likelihood Based Frequency Estimator for Digital Receivers," in *Proc. IEEE Wireless Communications and Networking Conference, WCNC'99*, New Orleans, USA, Sept. 1999, pp. 206–210.

Copyright ©1999 IEEE. Reprinted, with permission, from the proceedings of WCNC'99.

WCNC

*1999 IEEE Wireless Communications and
Networking Conference*

Sponsors:

Platinum

 **BELLSOUTH** *Mobility*

ERICSSON 

NORTEL
NETWORKS


WFI
the global leader
IN TELECOM OUTSOURCING

Gold

QUALCOMM[®]

NEW MAXIMUM LIKELIHOOD BASED FREQUENCY ESTIMATOR FOR DIGITAL RECEIVERS

Ridha Hamila and Markku Renfors

Telecommunications Laboratory - Tampere University of Technology
P.O. Box 553, FIN-33101 Tampere, Finland
Tel: +358 3 365 3910, Fax: +358 3 365 3808, E-mail: ridha@cs.tut.fi

ABSTRACT

Recently, a new all-digital technique for symbol timing and carrier phase synchronization of digital receivers was introduced by the authors. This technique is based on a polynomial approximation of the likelihood function by using the Farrow structure. In this contribution, we propose a new Tretter-based frequency estimator that is directly derived from the carrier phase estimate. The proposed estimator is simple to implement and is particularly suited for digital receiver architectures. This new Tretter-based estimator performs fairly well when compared with the Fitz and the Luise-Reggiannini frequency estimators, in the presence of substantial carrier frequency offset.

1. INTRODUCTION

In conventional receivers, the sampling of the received signal is synchronized to the incoming data symbols by using an analog or hybrid recovery scheme. Currently, there is a trend of using all-digital synchronization techniques where the initial sampling of the baseband signal is not synchronized to the incoming data symbols, in order to reduce the receiver analog components and perform most of the functions digitally [1],[2]. In this receiver architecture, timing adjustment and in practice also phase estimation must be done by digital methods after sampling. One way to perform this is to calculate the value of the signal at the desired time instants using interpolation, and then rotate by a complex multiplier to correct the phase error.

This work was carried out in the project "Analog and Digital Signal Processing Techniques for Highly Integrated Transceivers" supported by the Academy of Finland. This work is also supported by Tampere Graduate School in Information Science and Engineering (TISE).

Recently, a new technique for sampling clock and carrier phase synchronization of digital receivers, using a block based feedforward architecture, has been introduced in [3]-[5]. This technique is a practical, fully digitally implemented synchronization concept using the Farrow-based interpolator and maximum likelihood (ML) based joint estimation of the symbol timing and the carrier phase. Here the likelihood function is expressed in terms of the polynomial-based interpolator filter branch signals [3]. Also, the feedforward architecture we are considering provides rapid acquisition characteristics, which are very important especially in the mobile communication systems where the channel characteristics are rapidly changing, and in the case of TDMA system, also the transmission is bursty.

In this paper, we propose a new all-digital Tretter-based [6] frequency estimator algorithm for the m-PSK signaling which is directly derived from the polynomial based ML technique for jointly estimating the symbol timing and the carrier phase [4],[7]. This new estimator is particularly suited for digital receivers since it is directly deduced from the slope of the carrier phase estimate, and the algorithm can be easily integrated with the symbol timing and carrier phase recovery methods described above. However, this estimator is valid only under the condition that the frequency offset F_d is much smaller than the symbol rate $1/T$ ($F_d T \ll 1$) in which case the timing and the carrier phase information can be recovered prior to the frequency compensation [8]. Normally, when a receiver is operating on a steady-state condition, the frequency offset is much smaller than the symbol rate. However, if the frequency offset is in the order of the symbol rate, coarse frequency error correction or reduction has to be performed before other synchronization functions. The performance of the new frequency

estimator is compared with the Fitz frequency estimator [9] and Luise-Reggiannini frequency estimator [10].

2. SIGNAL AND TRANSMISSION MODEL

Here we consider the symbol timing and carrier phase recovery for digital data transmission for m-PSK modulation schemes when a frequency error is introduced. After down conversion, the received signal can be written as

$$r(t) = \sum_i a_i g(t - iT - \tau) e^{j(2\pi F_d t + \theta_0)} + n(t), \quad (1)$$

with

$$g(t) = g_T(t) * c(t).$$

Here, $\{a_i\}$ are the complex valued transmitted symbols from the m-PSK alphabet

$$\{e^{j2\pi m/M}, m = 0, 1, \dots, M-1\},$$

$g(t)$ represents the impulse response of the pulse shaping filter $g_T(t)$ convolved with the channel $c(t)$, T is the symbol duration, and $n(t)$ is the channel noise which is assumed to be white and Gaussian with power spectral density N_0 . The parameters $\{\tau, \theta_0, F_d\}$ denote the time-delay, the initial phase shift, and the frequency offset, respectively.

The received signal $r(t)$ is then convolved with the matched filter $g_{MF}(t)$ (see Fig. (1)), and we obtain the signal $m(t) = r(t) * g_{MF}(t)$ which is afterwards sampled by a free running clock. We assume here that the baseband pulse $q(t)$ which is defined by

$$q(t) = g(t) * g_{MF}(t) \quad (2)$$

satisfies the first Nyquist criterion

$$q(iT) = \begin{cases} 1 & \text{for } i = 0 \\ 0 & \text{for } i \neq 0. \end{cases} \quad (3)$$

Also, we assume that the frequency response of the channel is flat within the frequency range

$$|\omega| \leq 2\pi(B + F_{max}), \quad (4)$$

where B is the bandwidth of the linearly modulated signal in the baseband, and $\pm F_{max}$ represents the maximum frequency uncertainty. Generally, the frequency estimator algorithms fulfill the above assumption in order to produce an un-biased estimate [8].

3. FREQUENCY ESTIMATORS

3.1. Fitz and Luise-Reggiannini Estimators

Under the above assumptions and ideal clock recovery, samples from the matched filter output are given by [10]

$$m(k) = a_i e^{j[2\pi F_d k T + \theta_0]} + \text{noise}. \quad (5)$$

For the data-aided (DA) case, using the property of m-PSK that $a_i a_i^* = 1$, the modulation can be removed, as follows

$$z_{DA}(k) = a_i^* m(k) = e^{j[2\pi F_d k T + \theta_0]} + \text{noise}. \quad (6)$$

On the other hand, for the NDA case, the influence of the data symbols can be completely removed by an m^{th} power nonlinearity

$$z_{NDA}(k) = e^{jM \arg[m(k)]}. \quad (7)$$

The Fitz frequency estimator is given by [9]

$$\hat{F}_d = \frac{1}{2\pi MT} \sum_{i=1}^N \frac{6i}{N(N+1)(2N+1)} \arg[R(i)], \quad (8)$$

where $R(i)$ is the autocorrelation of $z(k)$ defined as

$$R(i) \triangleq \frac{1}{l_0 - i} \sum_{k=i}^{l_0-1} z(k) z^*(k-i). \quad (9)$$

Here, the choice of $z(k)$ depends on the use of the DA operation (Eq. (6)) or NDA operation (Eq. (7)). In (8) $M = 1$ for the DA case or equal to the number of constellation points for the NDA case. l_0 represents the observation length in symbol intervals, and N is a design parameter.

Similarly, the frequency estimator proposed by Luise and Reggiannini [10] is defined by

$$\hat{F}_d = \frac{1}{\pi MT(N+1)} \arg \left[\sum_{i=1}^N R(i) \right]. \quad (10)$$

These two frequency estimators belong to the class of autocorrelation-based estimators [10].

3.2. Tretter Estimator

Under the same conditions and for ideal timing recovery, another estimator which belongs to the class of least-squares-based estimators is called Tretter frequency estimator [6], defined by

$$\hat{F}_d = \frac{1}{2\pi MT} \sum_{k=0}^{l_0-1} \frac{6(2k - l_0 + 1)}{l_0(l_0^2 - 1)} \arg[z(k)], \quad (11)$$

where $\arg[z(k)]$ can be approximated from Eq. (6) or (7) as follows

$$\arg[z(k)] = \{M2\pi k F_d T + \theta_0 + \text{noise}\}_{-\pi}^{\pi}. \quad (12)$$

Here, $\{x\}_{-\pi}^{\pi}$ denotes the modulo 2π operation of x .

In fact, due to un-compensated frequency errors, the carrier phase changes across the data segment l_0 . Along the trajectory of $\arg[z(k)]$, we obtain jumps of 2π when the value of $\arg[z(k)]$ crosses odd multiples of π . In order to eliminate the jump ambiguity, the provisional phase estimate $\arg[z(k)]$ is unwrapped by a post-processing unit, yielding

$$\phi(k) = \phi(k-1) + \{\arg[z(k)] - \arg[z(k-1)]\}_{-\pi}^{\pi}. \quad (13)$$

Finally, the Tretter estimator is stated as

$$\hat{F}_d = \frac{1}{2\pi MT} \sum_{k=0}^{l_0-1} \frac{6(2k-l_0+1)}{l_0(l_0^2-1)} \phi(k). \quad (14)$$

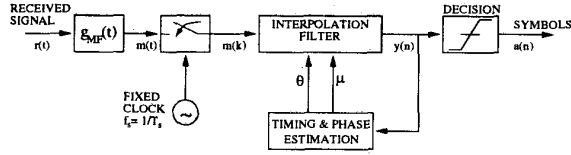


Figure 1: Digital Receiver with non-synchronized sampling.

4. TIMING AND PHASE ADJUSTMENT IN DIGITAL RECEIVERS

4.1. Digital Receiver with Non-Synchronized Sampling

The block diagram of the digital receiver with non-synchronized sampling is shown in Figure 1. The sampling of the received signal $r(t)$ is performed by a fixed sampling clock, and thus, the timing adjustment and consequently the carrier phase estimation must be done after the sampling using interpolation.

The function of the interpolation filter is to calculate one output sample $y(nT_i)$ at a time using a set of adjacent input samples $m(kT_s)$, with a timing error estimate (μ) and a phase error estimate (θ) obtained from the synchronization control unit. In the ideal case these output samples are the same sample values that would occur if the original sampling and the local

oscillator phase had been synchronized to the received signal.

The fractional interval μ determines the time instant $t = nT_i$ where the original continuous-time received signal $r(t)$ is approximated. This relation is given by

$$nT_i = (\mu + k)T_s, \quad (15)$$

where $\mu \in [0, 1)$ is the fractional interval, T_s is the sampling interval, and T_i is the output interval, whereas k is the largest integer for which $kT_s \leq nT_i$.

The polynomial-based interpolation filters are very easily implemented using the Farrow structure [11]. This structure is characterized by the fixed values of all the filter coefficients and by only one changeable parameter which is the fractional interval μ .

4.2. Polynomial Approximation of the Log Likelihood Function

Synchronization algorithms for digital receivers estimating jointly the timing and the carrier phase are based on maximum likelihood estimation (MLE) theory. These algorithms are trying to find the timing and the phase error estimates ($\hat{\mu}, \hat{\theta}$) which maximize the log-likelihood function [1],[8],[10].

A new technique of polynomial approximation for the log-likelihood function used for symbol timing and carrier phase recovery has been developed by the authors in [4],[5]. The main idea was to form a polynomial approximation for the log-likelihood function by using the Farrow structure, then different schemes for finding the maximum of this polynomial can be devised.

We consider a block processing scheme which takes the data samples and the unknown/decided/known symbol values for a block of N symbols. Also, we assume that the original sampling rate is twice the symbol rate, $T = 2T_s$, and a cubic interpolation filter is used. Because the symbol interval is divided into two parts (two samples per one symbol), there are two different polynomial approximations for the log-likelihood function as shown in [4],[5]. Consequently, the symbol timing expressed as a function of the fractional interval $\tilde{\mu} \in [0, 1)$, and the output samples of the FIR filter branches in the Farrow structure $f_i(n)$, are given by;

If $\max[\Lambda_1(\tilde{\mu})] > \max[\Lambda_2(\tilde{\mu})]$ then

$$\hat{\mu} = \arg \max_{\tilde{\mu}} [|\Lambda_1(\tilde{\mu})|], \quad (16)$$

else

$$\hat{\mu} = \arg \max_{\tilde{\mu}} [|\Lambda_2(\tilde{\mu})|].$$

Where, for the DA operation $\Lambda_1(\hat{\mu})$ and $\Lambda_2(\hat{\mu})$ are given by

$$\Lambda_1(\hat{\mu}) = \sum_{i=0}^3 \tilde{\mu}^i \sum_{n=1}^N \hat{a}^*(n) f_i(2n-1), \quad (17)$$

and

$$\Lambda_2(\hat{\mu}) = \sum_{i=0}^3 \tilde{\mu}^i \sum_{n=1}^N \hat{a}^*(n) f_i(2n). \quad (18)$$

Similar expressions for $\Lambda_1(\hat{\mu})$ and $\Lambda_2(\hat{\mu})$ are also derived for the NDA case in [4].

Also, by using the above timing estimate $\hat{\mu}$, the carrier phase estimate for the DA operation is given by

If $\max[\Lambda_1(\hat{\mu})] > \max[\Lambda_2(\hat{\mu})]$ then

$$\hat{\theta} = \arg[\Lambda_1(\hat{\mu})], \quad (19)$$

else

$$\hat{\theta} = \arg[\Lambda_2(\hat{\mu})].$$

Similarly, the carrier phase estimate for the NDA operation is given by

If $\max[\Lambda_1(\hat{\mu})] > \max[\Lambda_2(\hat{\mu})]$ then

$$\hat{\theta} = \frac{1}{M} \arg \sum_{n=1}^N \left[\sum_{i=0}^3 \hat{\mu}^i f_i(2n-1) \right]^M \quad (20)$$

else

$$\hat{\theta} = \frac{1}{M} \arg \sum_{n=1}^N \left[\sum_{i=0}^3 \hat{\mu}^i f_i(2n) \right]^M.$$

5. TRETTER-BASED FREQUENCY ESTIMATOR

All the estimators shown previously are using directly the samples from the output of the matched filter, and they are functional under ideal clock recovery. By analyzing Eq. (12) of the Tretter estimator, we remark that the right hand side of this equation can be viewed as a straight line with initial phase offset θ_0 , and with a slope equal $2\pi F_d T$. Since the carrier phase estimate $\hat{\theta}$ that we derived for both DA and NDA operations (Eqs. (19) & (20)) is performed for ideal timing recovery, similar concept to the Tretter estimator can be applied for this carrier phase estimate. Therefore,

the frequency offset can be directly calculated by using the filter branches in the Farrow structure and the fractional interval $\hat{\mu}$ providing the correct timing. The Tretter-based frequency estimator is then defined by

$$\hat{\theta}(k) = \{2\pi F_d(\hat{\mu} + k)T_s + \theta_0\}_{-\pi}^{\pi}. \quad (21)$$

Similar to Tretter estimator, the post-processing unit or unwrapping algorithm is applied to the above equation (21) in order to eliminate equivocation. Also, the above algorithm is valid for both DA and NDA operations.

6. SIMULATIONS AND CONCLUSIONS

The performance of this synchronization technique is analyzed in the presence of a frequency offset (Doppler shift F_d) on the carrier (F_c). The introduced frequency offset satisfies the condition that F_d is much smaller than the symbol rate $1/T$. Therefore, symbol timing and carrier phase recovery can be done prior to the frequency error correction. The frequency offset values are controlled to keep the receiver performance close to the theoretical with respect to the SEP. The simulations are performed using 4-PSK constellations, a block length size $N = 32$ symbols, and a third order interpolation filter. The transmitter and the receiver pulse-shaping filters are square root raised cosine filters with excess bandwidth of 35%.

Figures 2 and 3 illustrate the direct carrier phase estimate output (Eqs. (19) & (20)) and the unwrapped carrier phase, for different values of frequency and initial phase offsets.

Figure 4 compares the results of the three frequency estimators described in this paper. These results prove that the new frequency estimator performs fairly well when compared with the Fitz and Luise-Regiannini estimators. Besides, this new estimator is easily implemented, since it is directly integrated with the symbol timing and carrier phase recovery approach. Consequently, the receiver complexity can be reduced by avoiding the implementation of an additional frequency estimator block.

The size of the block length has a strong effect on the timing jitter in the presence of noise, and consequently on the frequency offset estimation. By increasing the number of symbols in the block length, timing jitter reduces. It remains a topic for future work to study the effect of the block length size on the frequency offset estimation.

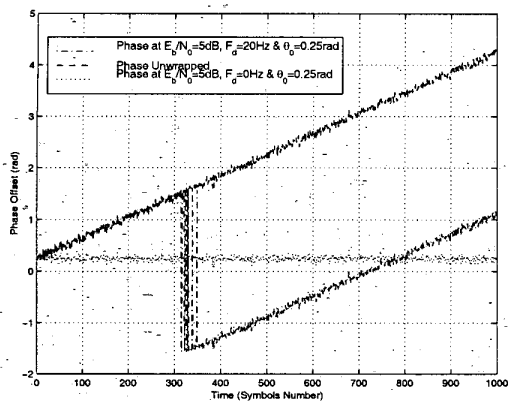


Figure 2: Carrier phase output (Eq. 21) with and without unwrapping.

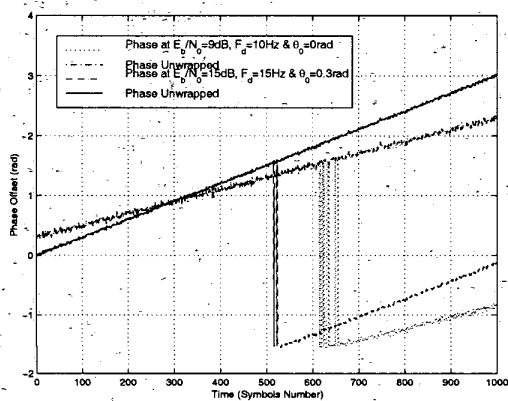


Figure 3: Carrier phase output (Eq. 21) with and without unwrapping.

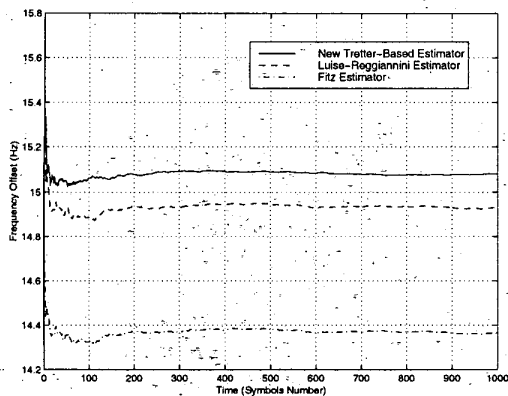


Figure 4: Frequency error estimation for $E_b/N_0 = 9\text{dB}$ and $F_d = 15\text{Hz}$.

7. REFERENCES

- [1] F. M. Gardner, "Demodulator reference recovery techniques suited for digital implementation," *ESA Final Report*, Aug. 1988.
- [2] L. Erup, F. M. Gardner, and R. A. Harris, "Interpolation in digital modems - Part II: Implementation and performance," *IEEE Trans. Commun.*, Vol. 41, pp. 998-1008, June 1993.
- [3] V. Tuukkanen, J. Vesma, and M. Renfors, "Efficient near optimal maximum likelihood symbol timing recovery in digital modems," *Proc. IEEE Int. Symp. on Personal, Indoor and Mobile Radio Communications*, Helsinki, Finland, Sep. 1997, pp. 825-829.
- [4] R. Hamila, J. Vesma, H. Vuolle, and M. Renfors, "NDA maximum likelihood approach for timing and phase adjustment by polynomial-based interpolation," *Proc. 6th IEEE International Workshop on Intelligent Signal Processing and Communications Systems*, Melbourne, Australia, Nov. 1998, pp. 248-252.
- [5] R. Hamila, J. Vesma, H. Vuolle, and M. Renfors, "Joint estimation of phase and timing using polynomial-based maximum likelihood technique," *Proc. IEEE 1998 International Conference on Universal Personal Communications*, Florence, Italy, Oct. 1998, pp. 369-373.
- [6] S. A. Tretter, "Estimating the Frequency of a noisy sinusoid by linear regression," *IEEE Trans. Inf. Theory*, Vol. IT-31, Nov. 1985, pp. 832-835.
- [7] R. Hamila, J. Vesma, H. Vuolle, and M. Renfors, "Effect of frequency offset on carrier phase and symbol timing recovery in digital receivers," *Proc. 1998 URSI International Symposium on Signals, Systems, and Electronics*, Pisa, Italy, Sep. 1998, pp. 247-252.
- [8] H. Meyr, M. Moeneclaey, and S. A. Fechtel, *Digital Communication Receivers: Synchronization, Channel Estimation and Signal Processing*. John Wiley & Sons, 1998.
- [9] M.P. Fitz, "Further results in the fast estimation of a single frequency," *IEEE Trans. Commun.*, Vol. 42, pp. 862-864, March 1994.
- [10] U. Mengali and A. N. D'Andrea, *Synchronization Techniques for Digital Receivers*. Plenum Press, 1997.
- [11] C. W. Farrow, "A continuously variable digital delay element," *Proc. IEEE Int. Symp. Circuits & Syst.*, Espoo, Finland, June 1988, pp. 2641-2645.

Publication 6

R. Hamila, S. Lohan, and M. Renfors, "Effect of Correlation Estimation on Multipath Delay Estimation Techniques in DS-CDMA Systems," *in Proc. of 4th International Symposium on Wireless Personal Multimedia Communications, WPMC'01, Aalborg, Denmark, September 2001*, pp. 331–335.

Copyright ©2001 IEEE. Reprinted, with permission, from the proceedings of WPMC'01.

CONFERENCE PROCEEDINGS



THE FOURTH INTERNATIONAL SYMPOSIUM ON
**WIRELESS PERSONAL
MULTIMEDIA COMMUNICATIONS**

SEPTEMBER 9 - 12, 2001 - AALBORG, DENMARK



Organized by
CPK, YRP R&D Committee and CRL

Local organizer:
CPK - Center for Personkommunikation
Aalborg University, Denmark

Sponsored by
Yokosuka Research Park R&D Committee, Japan
Communications Research Laboratory, Japan
Supported by
Support Center for Advanced Telecom-
munications Technology Research, Japan



Effect of Correlation Estimation on Multipath Delay Estimation Techniques in DS-CDMA Systems

Ridha Hamila, Elena-Simona Lohan and Markku Renfors

Telecommunications Laboratory, Tampere University of Technology
P.O. Box 553, FIN-33101 Tampere, Finland

{ridha, simona, mr}@cs.tut.fi, <http://www.cs.tut.fi/tlt/>

Abstract

Accurate detection and estimation of overlapping fading multipath components is vital for many communication systems. In this paper, we analyze the effect of the coherent integration and non-coherent averaging length over the correlation function for estimating correctly the delays introduced by a multipath channel. Study of correlation estimation properties paves the way to derive simple and efficient multipath delay estimation techniques with subchip resolution capability for use in direct sequence CDMA systems.

1. Introduction

Commonly, in most applications of radio communications and navigations [1], the line of sight (LOS) signal is succeeded by multipath components that arrive at the receiver within short delays, that can be smaller than the pulse shape. This causes overlapping fading multipath components and introduces significant errors in the LOS path time of arrival and gain estimation. In spread spectrum CDMA systems, such as Third generation mobile communications or Global Positioning System (GPS) receivers, it is important to achieve accurate delay estimation (or code synchronization) before despreading and data detection. Most spread spectrum systems use spreading codes with non-ideal correlation properties which result in co-channel interference, or multiuser-interference, for radio communication systems, which is also called multi-transmitter interference in radio-navigation systems [1]. Generally, the performance of radio communication systems is heavily affected by the multipath and multiuser-interference.

Generally, multipath delay estimation techniques in most DS-CDMA receivers are based on the maximum likelihood theory [1]. Different methods have been derived, considering mainly coherent and non-coherent delay lock loops (DLL) with arbitrary early and late code spacings [2],[3],[4]. These methods are just trying to track the delay of the line-of-sight path by correlating the down-converted received signal with replicas of spreading codes locally generated by the DS-SS receiver. However, phase lock loop circuits generally fail to estimate closely-spaced multipaths with less than one chip interval, besides their convergence can be quite slow [1],[2]. Several subspace-based approaches have also been derived, however, they are usually

This work was carried out in the project "Advanced Transceiver Architectures and Implementations for Wireless Communications" supported by the Academy of Finland. This work is also supported by Tampere Graduate School in Information Science and Engineering (TISE), and Graduate School in Electronics, Telecommunications and Automation (GETA).

too complex for practical purposes, and suitable only for systems employing short codes [5],[6].

The paper is organized as follows. In Section 2, we briefly review the correlation estimation principles over short and infinite time observations. In Section 3, we analyze multipath delay estimation techniques based on the maximum likelihood theory, and we demonstrate with simulations the impact of the coherent and the non-coherent averaging length of the correlation function on multipath delay estimation. Finally, Concluding remarks are drawn in Section 4.

2. Correlation Estimation Principles

Consider that the autocorrelation function of a stationary process $C(t)$ is expressed as

$$R(\tau) = E\{\rho(t, \tau)\} = E\{C(t)C(t - \tau)\}. \quad (1)$$

The time average of the process $\rho(t, \tau)$ is defined by

$$R_c(\tau) = \frac{1}{T_D} \int_{T_D} \rho(t, \tau) dt. \quad (2)$$

The stationary process $C(t)$ is called ergodic in the autocorrelation function if it satisfies the following two conditions. First, the time average approaches the ensemble average in the limit as the observation interval T_D approaches infinity,

$$\lim_{T_D \rightarrow \infty} R_c(\tau) = E\{\rho(t, \tau)\} = R(\tau), \quad (3)$$

and then the variance of the time average approaches zero in the limit as the observation interval T_D approaches infinity [Papoulis, Chap. 11],

$$\lim_{T_D \rightarrow \infty} \sigma_c^2 = \lim_{T_D \rightarrow \infty} \frac{1}{T_D} \int_{2T_D} [R^2(\alpha) + R(\tau + \alpha)R(\tau - \alpha)] \left(1 - \frac{|\alpha|}{T_D}\right) d\alpha = 0. \quad (4)$$

Thus, provided that the observation time interval T_D is sufficiently large, the time average $R_c(\tau)$ is an unbiased estimator and can be used to estimate $R(\tau)$.

However, if we are averaging over a finite short-time interval, we shall consider the following biased estimator

$$R_{T_D}(\tau) = \begin{cases} \frac{1}{T_D} \int_{T_D} C(t)C(t - \tau) dt & \text{for } |\tau| < T_D \\ 0 & \text{otherwise} \end{cases}$$

whose expected value or mean is given by [Papoulis, Chap. 11]

$$E\{R_{T_D}\} = R(\tau) \left(1 - \frac{|\tau|}{T_D}\right) = R(\tau)\Lambda(\tau, T_D), \quad (5)$$

and its variance is expressed as follows

$$\sigma_{R_{T_D}}^2 = \frac{1}{T_D} \int_{2T_D} [R^2(\alpha) + R(\alpha + \tau)R(\alpha - \tau)] \left(1 - \frac{|\tau| + |\alpha|}{T_D}\right) d\alpha. \quad (6)$$

Here, $\Lambda(\tau, T_D)$ denotes a triangular function defined as follows

$$\Lambda(\tau, T_D) = \begin{cases} 1 - |\tau|/T_D & |\tau| \leq T_D \\ 0 & \text{otherwise.} \end{cases} \quad (7)$$

By computing the mean of the power spectrum of each of the above estimators, we obtain

$$E\{S_c(\omega)\} = \int_{2T_D} R(\tau)e^{-j\omega\tau} d\tau = S(\omega) * \frac{\sin T_D\omega}{\pi\omega} \quad (8)$$

$$\begin{aligned} E\{S_{T_D}(\omega)\} &= \int_{2T_D} R(\tau)\Lambda(\tau)e^{-j\omega\tau} d\tau \\ &= S(\omega) * \frac{\sin^2 T_D\omega/2}{\pi T_D\omega^2/2}, \end{aligned} \quad (9)$$

where $S_c(\omega)$, $S_{T_D}(\omega)$, and $S(\omega)$ represent the power spectra corresponding to the functions $R_c(\tau)$, $R_{T_D}(\tau)$ and $C(t)$, respectively, defined over the finite observation interval T_D .

Notice that both estimators are biased if we are considering finite time observation. However, if the observation interval tends to infinity, both of the kernel windows $\sin(T_D\omega)/(\pi\omega)$ and $\sin^2(T_D\omega/2)/(\pi T_D\omega^2/2)$ tend to one. Consequently, both estimators become unbiased.

3. Timing Estimation for a Multipath Signal Based on the Correlation Estimation Principles

After down-conversion of the received signal to baseband through mixing and filtering, the received DS-SS signal in the presence of M -path channel is modeled as [1],[4]

$$\begin{aligned} r(t) &= x(t) + n(t) \\ &= \sum_{k=0}^{N_{sym}} b_k \sum_{i=0}^{M-1} a_{i,k} C(t - \tau_{i,k} - kT_{sym}) e^{j\theta_{i,k}} \\ &\quad + n(t), \end{aligned} \quad (10)$$

where $C(t)$ is the spread-spectrum code, and $n(t)$ is additive white Gaussian noise with power spectral density $N_0/2$, T_{sym} is the symbol interval, and b_k is the k^{th} transmitted complex data symbol. The time-variant a_i , τ_i and θ_i represent the attenuation factor, time delay, and phase for the i^{th} path, respectively. The estimation of the set of synchronization parameters $\{a_i, \tau_i, \theta_i\}$ is very essential for locating the line-of-sight path, and consequently, for achieving accurate delay estimation (or code synchronization) before despreading and data detection.

Assuming that the down-converted signal $r(t)$ is completely defined in the time interval T_D , the conditional likelihood function of $r(t)$ for a given set of synchronization parameters $\{a, \tau, \theta\}$ is given by

$$p[r(t)|\{a, \tau, \theta\}] = \xi \exp \left\{ -\frac{1}{N_0} \int_{T_D} [r(t) - \hat{x}(t)]^2 dt \right\} \quad (11)$$

where ξ is just a positive constant independent of the synchronization parameters which can be neglected, and $\hat{x}(t)$ is the local trial signal replica generated at the receiver, modeling the estimated line-of-sight and multipath signals. Without loss of generality, we consider that the desired symbol is the zeroth symbol, the trial signal replica generated at the receiver is given by

$$\hat{x}(t) = \sum_{i=0}^{M-1} \hat{a}_{i,0} C(t - \hat{\tau}_{i,0}) e^{j\hat{\theta}_{i,0}}. \quad (12)$$

We assume that during the observation interval T_D , the channel is very slowly changing, therefore the subscript k can be ignored for convenience.

In conventional receivers, multipath delay estimation techniques are based on the maximum likelihood theory [1] which are trying to estimate the set of parameters $\{\hat{a}_i, \hat{\tau}_i, \hat{\theta}_i\}$ by minimizing the mean square error of the log-likelihood function (LLF) given by

$$L_{ML}(\hat{a}_i, \hat{\tau}_i, \hat{\theta}_i) = Re \left\{ \int_{T_D} [r(t) - \hat{x}(t)]^2 dt \right\}. \quad (13)$$

Thus, the synchronization parameters are determined by differentiating the above LLF function with respect to the synchronization parameters, then setting the partial derivatives equal to zero. The partial derivative with respect to the time-delay estimate is given by [1]

$$\begin{aligned} \frac{\partial}{\partial \tau} L_{ML}(\hat{a}_i, \tau, \hat{\theta}_i) \Big|_{\tau=\tau_i} &= 2 \frac{\partial}{\partial \tau} \left[Re \left\{ \left[R_{rc}(\tau) \right. \right. \right. \\ &\quad \left. \left. \left. - \sum_{l=0, l \neq i}^{M-1} \hat{a}_l R_c(\tau - \hat{\tau}_l) e^{j\hat{\theta}_l} \right] e^{-j\hat{\theta}_i} \right\} \right]_{\tau=\tau_i} \end{aligned} \quad (14)$$

In the above equation, $R_{rc}(\tau)$ is the in-phase/ quadrature time-average cross-correlation function over the observation time interval T_D , given by

$$R_{rc}(\tau) = \frac{1}{T_D} \int_{T_D} r(t) C(t - \tau) dt, \quad (15)$$

and $R_c(\tau)$ is the reference time-average correlation function of the spreading code, given by

$$R_c(\tau) = \frac{1}{T_D} \int_{T_D} C(t) C(t - \tau) dt. \quad (16)$$

Consequently, the desired time delay for the i^{th} path that maximizes the above expression (14) is given by

$$\begin{aligned} \hat{\tau}_i &= \arg \max_{\tau} \left[Re \left\{ \left[R_{rc}(\tau) \right. \right. \right. \\ &\quad \left. \left. \left. - \sum_{l=0, l \neq i}^{M-1} \hat{a}_l R_c(\tau - \hat{\tau}_l) e^{j\hat{\theta}_l} \right] e^{-j\hat{\theta}_i} \right\} \right]. \end{aligned} \quad (17)$$

Generally, multipath delay estimation techniques are based on the cross-correlation function (Eq. 15) of the down-converted signal de-spread with a copy of the spreading code locally generated by the DS-SS receiver. The multipath estimating DLL techniques [2] are trying to approximate the overall cross-correlation using a set of reference correlation (Eq. 16) functions with certain delays, phases and amplitudes.

When the locally generated code is locked to the received code, by substituting equation (11) into (15), the cross-correlation function is simply expressed by

$$R_{rc}(\tau) = \frac{1}{T_D} \sum_{i=0}^{M-1} a_i e^{j\theta_i} \int_{T_D} b_0 C(t - \tau_i) C(t - \tau) dt + \frac{1}{T_D} \int_{T_D} n(t) C(t - \tau) dt. \quad (18)$$

If the data symbols, $\{b_k\}$, are known in advance, then we can perform coherent integration over several symbols. Otherwise, we perform the integration over one symbol and then apply a non-coherent averaging over several symbols in order to reduce the interference.

Normally, even-though we are considering averaging over a sufficiently large observation time interval, we shall consider the previously mentioned biased estimator. Recalling the Gaussian nature of the random process as well as the mean of the biased estimator (5), the expectation of the above cross-correlation function becomes

$$E\{R_{rc}(\tau)\} = \sum_{i=0}^{M-1} a_i e^{j\theta_i} R_c(\tau - \tau_i) \Lambda(\tau - \tau_i, T_D). \quad (19)$$

Notice that the expected value of the cross-correlation function is expressed simply as a weighted sum of delayed correlation functions times triangular windows with certain amplitude and phase specific to each signal path. Thus, the correlation effectively amplifies the underlying data signal, with an amplification factor equal to the length of the PRN code sequence. Figure 1 shows an example of a normalized autocorrelation function using a Gold code sequence of length 1023 weighted by a triangular window.

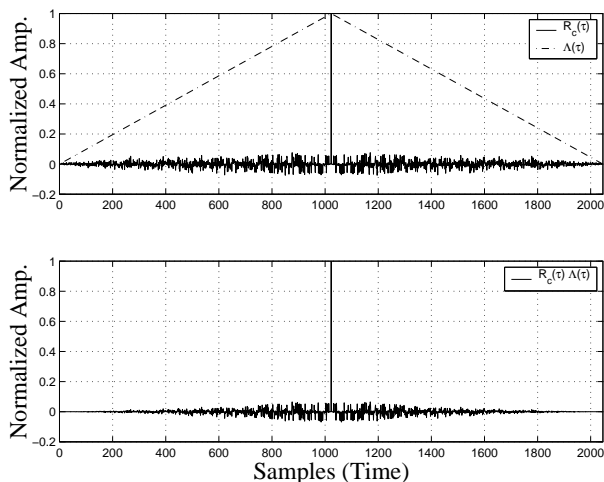


Figure 1: The upper figure shows a normalized autocorrelation function of one Gold code sequence within a triangular window. The lower curve illustrates their product.

Here, T_D can also be referred to as a coherent integration length, since the integral from Eq. (18) is performed coherently. However, if the data modulation is not known or estimated in advance, the integration length T_D is limited to one symbol interval, which is usually not sufficient to diminish the

effect of noise. Therefore, a non-coherent averaging can also be employed in such way that the decision variable becomes

$$J = \sum_{k=0}^{N_{BA}} \left| \sum_{i=0}^{M-1} a_i e^{j\theta_i} R_c(\tau - \tau_i) \Lambda(\tau - \tau_i, T_{Dk}) \right|, \quad (20)$$

where N_{BA} denotes the number of blocks used in the non-coherent block averaging, and T_{Dk} is the coherent integration interval for the k^{th} symbol.

Also, we noticed by increasing either the coherent integration length or the non-coherent averaging length, the peaks in the correlation function can be clearly distinguished and the side lobes decrease as illustrated in Figs 2 and 3. The coherent integration provides lower side lobes in the correlation function compared to the non-coherent averaging, but data decisions or pilot symbols are required for performing the coherent integration. It is clear that the more we increase the averaging length (coherent or non-coherent), the more the correlation function approaches to the ideal one (i.e., superposition of two triangular pulse shapes at the positions corresponding to the path delays).

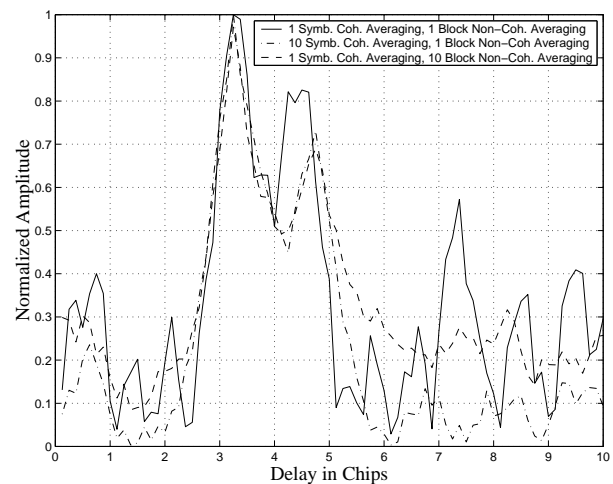


Figure 2: Correlation function with a spreading factor of 32 at $E_b/N_0 = 5$ dB, using 2-path channel, with path locations at [3.25, 4.75] chips and average path powers of [0, -3] dB.

By exploiting the above study, a new technique for multipath delay estimation using peak tracking with subtraction has been derived. This approach is analogous to the DLL techniques in the sense that it is trying to estimate the overall cross-correlation function using a set of reference functions, but with different and simpler implementation [7],[8]. Also, based on the above analysis an innovative multipath delay estimation approach based on a nonlinear quadratic Teager-Kaiser operator is introduced [9],[10]. This new technique is extremely simple and very efficient for estimating closely-spaced multipaths with much less computational complexity compared, e.g., to the subspace-based multipath delay estimation methods [5],[6].

4. Conclusions

Generally, the transmitted signal arrives at the receiver via multiple propagation paths at different delays, which can be smaller than the pulse shape duration, introducing overlapped multipath components and causing significant errors to the prompt LOS signal time and amplitude of arrival estimation. Correlation estimation properties related to DS-SS receiver signal have

been studied. We demonstrated the influence of the coherent integration and the non-coherent averaging length on multipath delay estimation, and the importance of the considered observation time interval length. This analysis paves the way to derive simple and very efficient multipath delay estimation methods with subchip resolution capability .

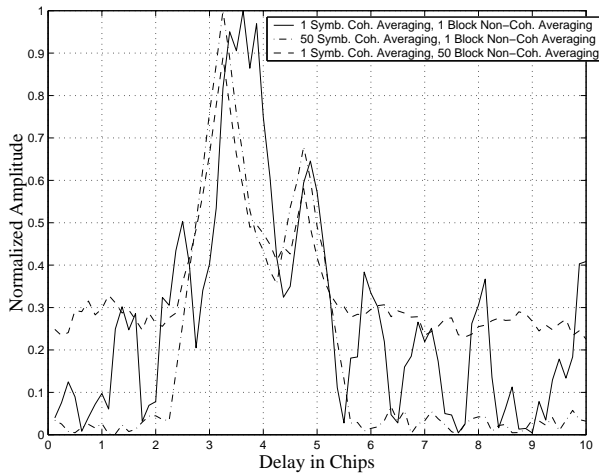


Figure 3: Correlation function with a spreading factor of 32 at $E_b/N_0 = 0$ dB, using 2-path channel, with path locations at [3.25, 4.75] chips and average path powers of [0, -3] dB.

5. References

- [1] R. Van Nee, Multipath and multi-transmitter interference in spread-spectrum communication and navigation system, *Delft University Press*, 1995.
- [2] R. Van Nee, J. Sierveld, P. Fenton, and B. Townsend, "The multipath estimating delay lock loop: Approaching theoretical accuracy limits," in *Proc. of IEEE Position, Location, and Navigation Symposium*, April 1994, pp. 246–251.
- [3] M. Braasch and A.J.V. Dierendonck, "GPS receiver architectures and measurements," *Proc. of the IEEE*, vol. 87, No. 1, January 1999, pp. 48–64.
- [4] M.C. Laxton and S.L. DeVilbis, "GPS multipath mitigation during code tracking," in *Proc. of the American Control Conference*, Albuquerque, New Mexico, pp. 1429–1433, June 1997.
- [5] P. Luukkanen, and J. Joutsensalo, "Comparison of MUSIC and matched filter delay estimators in DS-CDMA," in *Proc. of IEEE Personal, Indoor and Mobile Radio Communications*, vol. 3, 1997, pp. 830–834.
- [6] Z. Kostić, G. Pavlović, "Resolving sub-chip spaced multipath components in CDMA communication systems," in *Proc. of IEEE VTC*, vol. 1, 1993, pp. 469–472.
- [7] R. Hamila, S. Lohan and M. Renfors, "Multipath delay estimation in GPS receivers," in *Proc. of Third International Symposium on Wireless Personal Multimedia Communications*, Bangkok, Thailand, November 2000, pp. 646–649.
- [8] S. Lohan, M. Renfors, "Feedforward approach for estimating the multipath delays in CDMA systems," in *Proc.*

of Nordic Signal Processing Symposium, Kolmården, Sweden, pp. 125–128, June 2000.

- [9] R. Hamila, S. Lohan and M. Renfors, "Nonlinear operator for multipath channel estimation in GPS receivers," in *Proc. of the 7th IEEE International Conference On Electronics, Circuits & Systems*, Jounieh, Lebanon, pp. 352–356, December 2000.
- [10] R. Hamila, S. Lohan and M. Renfors, "Novel technique for multipath delay channel estimation in GPS receivers," in *Proc. of IEEE International Conference on Third Generation Wireless and Beyond*, San Francisco, USA, pp. 993–998, May 2001.

Publication 7

R. Hamila, S. Lohan, and M. Renfors, "Novel Technique for Closely-Spaced Multipath Delay Estimation in DS-CDMA Systems," *Submitted to Signal Processing*, (EURASIP).

Novel Technique for Closely-Spaced Multipath Delay Estimation in DS-CDMA Systems

Ridha Hamila, Simona Lohan and Markku Renfors *
Telecommunications Laboratory
Tampere University of Technology
P.O. Box 553 FIN-33101 Tampere, Finland

Abstract

In this paper, we introduce a novel, simple and quite efficient technique for estimating closely-spaced multipath delays in GPS receivers as well as in other spread spectrum CDMA systems. Subchip resolution is achieved via a nonlinear quadratic operator called Teager-Kaiser operator which exploits the properties of the cross-correlation between the received signal and the reference despreading code replica generated at the receiver. Simulation results using different Rayleigh fading channels show the good performance of the proposed technique, in addition to its very simple implementation compared to the earlier maximum likelihood based approaches. This new technique with subchip resolution capability can be used for improving GPS and mobile phone positioning accuracy in a cellular network using the cellular network-assisted GPS technology.

Keywords:

Global Positioning System, CDMA Channel Estimation, Code Synchronization, and DSP for Wireless Communications.

Contact Person:

Ridha Hamila

Telecommunications Laboratory, Tampere University of Technology,

P.O. Box 553 FIN-33101 Tampere, Finland

Tel:+358 3 365 3923

Fax:+358 3 365 3808

Emai:ridha.cs.tut.fi

*This work was carried out in the project "Advanced Transceiver Architectures and Implementations for Wireless Communications" supported by the Academy of Finland. This work is also supported by Tampere Graduate School in Information Science and Engineering (TISE), and Graduate School in Electronics, Telecommunications and Automation (GETA).

1 Introduction

A frequently occurring problem in most applications of radio communications and navigations [1] is multipath propagation. Generally, the transmitted signal arrives at the receiver via multiple propagation paths at different delays which may add destructively, resulting in signal fading and consequently in receiver performance degradations. In spread spectrum CDMA systems, such as Third generation mobile communications or Global Positioning System (GPS) receivers, it is important to achieve accurate delay estimation (or code synchronization) before despreading and data detection. Most spread spectrum systems use spreading codes with non-ideal correlation properties which result in co-channel interference, or multiuser-interference, for radio communication systems, which is also called multi-transmitter interference in radio-navigation systems [1]. Generally, the performance of radio communication systems is heavily affected by the multipath and multiuser-interference. In this paper, we will focus our study on the GPS case.

Usually, multipath effects have a strong impact on the precision of the Global Positioning System and differential GPS (DGPS) [2]. GPS direct-sequence spread spectrum (DS-SS) receiver tries to estimate the exact envelope delay and carrier phase of a particular satellite signal which provide information about the propagation time, and hence about the corresponding distance. However, the presence of multipath introduces certain amount of error that makes accurate estimation of delay and phase a very critical task.

Mobile phone positioning in a cellular network with reliable and rather accurate position information has become unavoidable after the Federal Communications Commission mandate, FCC-E911 docket on emergency call positioning in USA, and the coming E112 in the European Union. Various positioning technologies have been recently devised using either cellular network-based or mobile-based methods. However, the most prominent technology that has been approved by the standardization bodies is the

cellular network-assisted GPS (AGPS) [3]. Currently, AGPS positioning technique provides slightly better accuracy outdoors and in urban environment, but it is suffering heavily from reflected multipath components especially in the indoor environment.

Commonly, multipath delay estimation techniques in most GPS receivers are based on the maximum likelihood theory [1]. Different methods have been derived, considering mainly coherent and non-coherent delay lock loops (DLL) with arbitrary early and late code spacings [2, 4, 5]. These methods are just trying to track the delay of the line-of-sight path by correlating the down-converted received signal with replicas of spreading codes locally generated by the DS-SS receiver. However, phase lock loop circuits generally fail to estimate closely-spaced multipaths with less than one chip interval, besides their convergence can be quite slow [1, 2]. Several subspace-based approaches have also been derived, however, they are usually too complex for practical purposes, and suitable only for systems employing short codes [6, 7].

Another solution to resolve closely-spaced paths is the peak tracking with pulse subtraction method [8, 9]. Here, the output of the matched filter (or correlator) is approximated by the superposition of a set of reference correlation functions. Once we detect a multipath delay, its contribution is subtracted from the overall cross-correlation function, and the successive delays are searched from the residual function. The pulse subtraction method does not require heavy computations and performs reasonably well if the paths are at more than half chip spacing [9, 10].

In this contribution, we introduce a very simple innovative technique for channel estimation with a subchip resolution based on the Teager-Kaiser quadratic operator [11, 12, 13]. This operator exploits the properties of the cross-correlation function between the received signal and the despreading code replica generated at the receiver, in order to estimate accurately overlapped multipath delays independently of the delay spacing between the multipaths. The proposed technique can be used for improving the mobile phone positioning accuracy in a cellular network for the assisted GPS positioning technology.

This paper is organized as follows. Section II gives a brief review about correlation estimates for short and infinite time interval observations. The GPS signal structure, conventional maximum likelihood approach for estimating time delays introduced by a multipath channel, as well as the envelope tracking with subtraction method are established in Section III. The Teager-Kaiser operator within some of its properties related to the reference correlation function are derived in Section IV together with the proposed technique for estimating closely-spaced multipath delays. Simulation results using different Rayleigh fading channels are provided in Section V, comparing the new technique with the envelope tracking with subtraction method with respect to the probability of acquisition. Conclusions are drawn in Section VI.

2 Review of Correlation Estimation Principles

Consider that the autocorrelation function of a stationary process $C(t)$ is expressed as

$$R(\tau) = E\{\rho(t, \tau)\} = E\{C(t)C(t - \tau)\}. \quad (1)$$

The time average of the process $\rho(t, \tau)$ is defined by

$$R_c(\tau) = \frac{1}{T_D} \int_{T_D} \rho(t, \tau) dt. \quad (2)$$

The stationary process $C(t)$ is called ergodic in the autocorrelation function if it satisfies the following two conditions. First, the time average approaches the ensemble average in the limit as the observation interval T_D approaches infinity,

$$\lim_{T_D \rightarrow \infty} R_c(\tau) = E\{\rho(t, \tau)\} = R(\tau), \quad (3)$$

and then the variance of the time average approaches zero in the limit as the observation interval T_D approaches infinity [14],

$$\lim_{T_D \rightarrow \infty} \sigma_c^2 = \lim_{T_D \rightarrow \infty} \frac{1}{T_D} \int_{2T_D} [R^2(\alpha) + R(\tau + \alpha)R(\tau - \alpha)] \left(1 - \frac{|\alpha|}{T_D}\right) d\alpha = 0. \quad (4)$$

Thus, provided that the observation time interval T_D is sufficiently large, the time average $R_c(\tau)$ is an unbiased estimator and can be used to estimate $R(\tau)$.

However, if we are averaging over a finite short-time interval, we shall consider the following biased estimator

$$R_{T_D}(\tau) = \begin{cases} \frac{1}{T_D} \int_{T_D} C(t)C(t-\tau)dt & \text{for } |\tau| < T_D \\ 0 & \text{otherwise} \end{cases}$$

whose expected value or mean is given by [14]

$$E\{R_{T_D}\} = R(\tau) \left(1 - \frac{|\tau|}{T_D}\right) = R(\tau)\Lambda(\tau, T_D), \quad (5)$$

and its variance is expressed as follows

$$\sigma_{R_{T_D}}^2 = \frac{1}{T_D} \int_{2T_D} [R^2(\alpha) + R(\alpha + \tau)R(\alpha - \tau)] \left(1 - \frac{|\tau| + |\alpha|}{T_D}\right) d\alpha. \quad (6)$$

Here, $\Lambda(\tau, T_D)$ denotes a triangular function defined as follows

$$\Lambda(\tau, T_D) = \begin{cases} 1 - |\tau|/T_D & |\tau| \leq T_D \\ 0 & \text{otherwise.} \end{cases} \quad (7)$$

By computing the mean of the power spectrum of each of the above estimators, we obtain [14]

$$E\{S_c(\omega)\} = \int_{2T_D} R(\tau)e^{-j\omega\tau} d\tau = S(\omega) * \frac{\sin T_D\omega}{\pi\omega} \quad (8)$$

$$E\{S_{T_D}(\omega)\} = \int_{2T_D} R(\tau)\Lambda(\tau)e^{-j\omega\tau} d\tau = S(\omega) * \frac{\sin^2 T_D\omega/2}{\pi T_D\omega^2/2}, \quad (9)$$

where $S_c(\omega)$, $S_{T_D}(\omega)$, and $S(\omega)$ represent the power spectra corresponding to the functions $R_c(\tau)$, $R_{T_D}(\tau)$ and $C(t)$, respectively, defined over the finite observation interval T_D .

Notice that both estimators are biased if we are considering finite time observation. However, if the observation interval tends to infinity, both of the kernel windows $\sin(T_D\omega)/(\pi\omega)$ and $\sin^2(T_D\omega/2)/(\pi T_D\omega^2/2)$ tend to one. Consequently, both estimators become unbiased.

3 Received Signal Structure and Conventional Multipath Estimation Methods

In the following, we first define shortly the GPS received signal format, then we present the conventional maximum likelihood approach for estimating time delays introduced by a multipath channel.

3.1 GPS Received Signal Structure

The GPS signal format is direct sequence spread spectrum (DS-SS) [4]. The navigation data stream with input rate $1/T_D = 50$ bits/s is first modulated onto the carrier using BPSK modulation. Then, the spreading code is modulated onto the data modulated carrier with a rate of $1/T_C$ much higher than $1/T_D$.

After down-conversion of the received signal to baseband through mixing and filtering, the received GPS signal from one satellite in the presence of M -path channel is modeled as [1, 5]

$$\begin{aligned} r(t) &= x(t) + n(t) \\ &= \sum_{i=0}^{M-1} a_i C(t - \tau_i) e^{j\theta_i} + n(t), \end{aligned} \quad (10)$$

where $C(t)$ is the spread-spectrum code, and $n(t)$ is additive white Gaussian noise with power spectral density $N_0/2$. The time-variant a_i , τ_i and θ_i represent the attenuation factor, time delay, and phase for the i^{th} path, respectively. The estimation of the set of parameters $\{a_i, \tau_i, \theta_i\}$ is very essential for locating the line-of-sight path, and consequently for determining the GPS position, velocity and/or time.

The civilian portion of the GPS signal employs pseudo random-noise (PRN) Gold codes of sequence length 1023, and each satellite is assigned a unique code signature. PRN codes are simply deterministic binary sequences with specific statistical random noise-like properties [4]. The family of PRN codes is mainly characterized by the low cross-correlation between the codes, they are nearly orthogonal, and

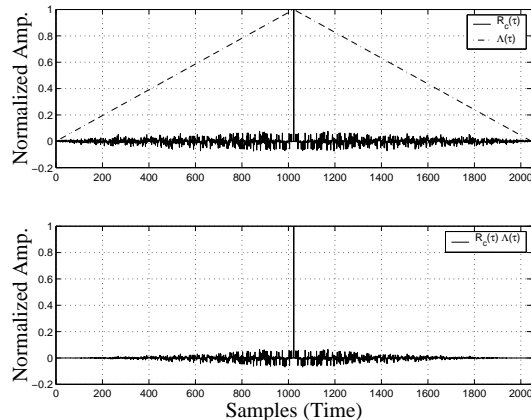


Figure 1: The upper figure shows a normalized autocorrelation function of one Gold code sequence within a triangular window. The lower curve illustrates their product.

the autocorrelation function is almost zero except at zero delay (see Fig. 1). Because all the PRN code sequences are nearly uncorrelated with respect to each other, all the satellites transmit on the same carrier frequency without incurring significant mutual interference.

3.2 ML Timing Estimation for a Multipath Signal

Assuming that the down-converted signal $r(t)$ is completely defined in the time interval T_D , the conditional likelihood function of $r(t)$ for a given set of synchronization parameters $\{a, \tau, \theta\}$ is given by

$$p[r(t)|\{a, \tau, \theta\}] = \xi \exp \left\{ -\frac{1}{N_0} \int_{T_D} [r(t) - \hat{x}(t)]^2 dt \right\} \quad (11)$$

where $\hat{x}(t)$ is the local trial signal replica generated at the receiver, modeling the estimated line-of-sight and multipath signals

$$\hat{x}(t) = \sum_{i=0}^{M-1} \hat{a}_i C(t - \hat{\tau}_i) e^{j\hat{\theta}_i}, \quad (12)$$

and ξ is just a positive constant independent of the synchronization parameters which can be neglected.

In conventional receivers, multipath delay estimation techniques are based on the maximum likelihood theory [1] which are trying to estimate the set of parameters $\{\hat{a}, \hat{\tau}, \hat{\theta}\}$ by minimizing the mean square

error of the log-likelihood function (LLF) given by

$$L_{ML}(\hat{a}, \hat{\tau}, \hat{\theta}) = Re \left\{ \int_{T_D} [r(t) - \hat{x}(t)]^2 dt \right\}. \quad (13)$$

Thus, the synchronization parameters are determined by differentiating the above LLF function with respect to the synchronization parameters, then setting the partial derivatives equal to zero. The partial derivative with respect to the time-delay estimate is given by [1]

$$\left. \frac{\partial}{\partial \tau} L_{ML}(\hat{a}_i, \tau, \hat{\theta}_i) \right|_{\tau=\tau_i} = 2 \frac{\partial}{\partial \tau} \left[Re \left\{ \left[R_{rc}(\tau) - \sum_{l=0, l \neq i}^{M-1} \hat{a}_l R_c(\tau - \hat{\tau}_l) e^{j\hat{\theta}_l} \right] e^{-j\hat{\theta}_i} \right\} \right]_{\tau=\tau_i}. \quad (14)$$

In the above equation, $R_{rc}(\tau)$ is the in-phase/quadrature time-average cross-correlation function over the observation time interval T_D , given by

$$R_{rc}(\tau) = \frac{1}{T_D} \int_{T_D} r(t) C(t - \tau) dt, \quad (15)$$

and $R_c(\tau)$ is the reference time-average correlation function of the spreading code, given by

$$R_c(\tau) = \frac{1}{T_D} \int_{T_D} C(t) C(t - \tau) dt. \quad (16)$$

Consequently, the desired time delay for the i^{th} path that maximizes the above expression (14) is given by

$$\hat{\tau}_i = \arg \max_{\tau} \left[Re \left\{ \left[R_{rc}(\tau) - \sum_{l=0, l \neq i}^{M-1} \hat{a}_l R_c(\tau - \hat{\tau}_l) e^{j\hat{\theta}_l} \right] e^{-j\hat{\theta}_i} \right\} \right]. \quad (17)$$

Similarly, by solving equation (13) for the M multipath components, the estimated carrier phase and amplitude for the i^{th} path are, respectively, given by [1]

$$\hat{\theta}_i = \arg \left[R_{rc}(\hat{\tau}_i) - \sum_{l=0, l \neq i}^{M-1} \hat{a}_l R_c(\hat{\tau}_i - \hat{\tau}_l) e^{j\hat{\theta}_l} \right] \quad (18)$$

$$\hat{a}_i = Re \left\{ \left[R_{rc}(\hat{\tau}_i) - \sum_{l=0, l \neq i}^{M-1} \hat{a}_l R_c(\hat{\tau}_i - \hat{\tau}_l) e^{j\hat{\theta}_l} \right] e^{-j\hat{\theta}_i} \right\}. \quad (19)$$

Generally, multipath delay estimation techniques are based on the cross-correlation function (Eq. 15) of the down-converted signal de-spread with a copy of the spreading code locally generated by the

DS-SS receiver. The multipath estimating DLL techniques [2] are trying to approximate the overall cross-correlation using a set of reference correlation (Eq. 16) functions with certain delays, phases and amplitudes.

When the locally generated code is locked to the received code, by substituting equation (10) into (15), the cross-correlation function is simply expressed by

$$R_{rc}(\tau) = \frac{1}{T_D} \sum_{i=0}^{M-1} a_i e^{j\theta_i} \int_{T_D} C(t - \tau_i) C(t - \tau) dt + \frac{1}{T_D} \int_{T_D} n(t) C(t - \tau) dt. \quad (20)$$

Normally, even-though we are considering averaging over a sufficiently large observation time interval, we shall consider the previously mentioned biased estimator. Recalling the Gaussian nature of the random process as well as the mean of the biased estimator (5), the expectation of the above cross-correlation function becomes

$$E\{R_{rc}(\tau)\} = \sum_{i=0}^{M-1} a_i e^{j\theta_i} R_c(\tau - \tau_i) \left(1 - \frac{|\tau - \tau_i|}{T_D}\right) = \sum_{i=0}^{M-1} a_i e^{j\theta_i} R_c(\tau - \tau_i) \Lambda(\tau - \tau_i, T_D). \quad (21)$$

Notice that the expected value of the cross-correlation function is expressed simply as a weighted sum of delayed correlation functions times triangular windows with certain amplitude and phase specific to each signal path. Thus, the correlation effectively amplifies the underlying BPSK data signal, with an amplification factor equal to the length of the PRN Gold code sequence. Figure 1 shows an example of a normalized autocorrelation function using a Gold code sequence of length 1023 weighted by a triangular window.

3.3 Multipath Delay Estimation Using Peak Tracking with Subtraction Approach

This approach for estimating the multipath delays is analogous to the DLL techniques in the sense that it is trying to estimate the overall cross-correlation function using a set of reference functions, but with different and simpler implementation. This approach is based on the search of the global maxima of the

cross-correlation function (Eq. 15). Then, the contribution of each selected maximum is reduced from the overall cross-correlation using the autocorrelation function of a rectangular pulse [9]. The proposed technique is described further by the following algorithm:

- find the global maximum $\hat{\tau}_1 = \arg \max_{\tau} [|R_{rc}(\tau)|]$
- estimate successively the next $M_{est} - 1$ maxima:

$$\hat{\tau}_k = \arg \max_{\tau} \left[\text{Re} \left\{ R_{rc}(\tau) - \sum_{l=1}^{k-1} R_{rc,l}(\hat{\tau}_l) \Lambda(\tau - \hat{\tau}_l, T_C) \right\} \right], \quad k = 2, 3, \dots, M_{est}. \quad (22)$$

Where $R_{rc,l}(\tau)$ is the residual cross-correlation function after peak subtraction, M_{est} is an estimate for the number of multipaths of the channel (it can be taken equal to the number of fingers (or correlators) similar to a Rake receiver), and $\Lambda(\tau, T_C)$ is the ideal reference correlation function of the Gold code.

By using this ideal code correlation pulse for subtracting the contribution of each channel path, we are able to detect very closely-spaced multipaths within less than one chip period ($|\tau_l - \tau_k| < T_C$) [9].

4 Multipath Delay Estimation Based on Teager-Kaiser Operator

In this section, we introduce an innovative multipath delay estimation approach based on the nonlinear quadratic Teager-Kaiser operator.

The nonlinear quadratic TK operator was first introduced for measuring the real physical energy of a system [11, 12]. The energy of a generating system of a simple oscillation signal was computed as the product of the square of the amplitude and the frequency of the signal. It was found that this nonlinear operator exhibits several attractive features such as simplicity, efficiency and ability to track instantaneously-varying spatial modulation patterns [15]. Since its introduction, several applications have been derived for one-dimensional signal processing [13, 16] and two-dimensional signal processing [17, 18].

The continuous-time TK energy operator of a complex-valued signal $x(t)$ is defined as follows [13]

$$\Psi_c[x(t)] = \dot{x}(t)\dot{x}^*(t) - \frac{1}{2}[\ddot{x}(t)x^*(t) + x(t)\ddot{x}^*(t)]. \quad (23)$$

Similarly, the discrete-time Teager operator of a complex valued signal is given by [13]

$$\Psi_d[x(n)] = x(n-1)x^*(n-1) - \frac{1}{2}[x(n-2)x^*(n) + x(n)x^*(n-2)]. \quad (24)$$

Many useful properties of this nonlinear quadratic operator have been derived, and the analogy with the discrete-time domain has also been established [19, 20]. We notice that applying the continuous-time TK operator to the ideal reference correlation function of the spreading code (Eq. 7) which is characterized by the triangular shape, we obtain

$$\Psi_c[\Lambda(t)] = \frac{\Pi(t, T_C)}{T_C^2} + \frac{\Lambda(t, T_C)\delta(t)}{T_C}, \quad (25)$$

where $\delta(t)$ is the dirac function, and $\Pi(t, T_C)$ stands for a rectangular function with unit amplitude and duration $2T_C$ centered at $t = 0$ defined as

$$\Pi(t, T_C) \triangleq \begin{cases} 1 & |t| \leq T_C \\ 0 & \text{otherwise.} \end{cases}$$

Obviously, Eq. (25) shows that the TK operator applied to a triangular function provides a clear time-aligned peak location of the triangular pulse in the presence of a certain 'noise' floor. Figure 2 shows a simple example of TK operator applied to a triangular function using the discrete-time operator.

Assuming now that the cross-correlation function is the sum of M -path triangular pulses as follows

$$R(t) = \sum_{i=0}^M a_i \Lambda(t - t_i, T_C) e^{j\theta_i}, \quad (26)$$

where a_i , t_i and θ_i denote the time-variant amplitude, delay and phase, respectively. By applying the TK operator to the above equation (26) we obtain

$$\begin{aligned} \Psi_c[R(t)] = & \frac{1}{T_C^2} \left[\left(\sum_{i=0}^M a_i \text{sign}(t - t_i) \Pi(t - t_i, T_C) \cos \theta_i \right)^2 + \left(\sum_{i=0}^M a_i \text{sign}(t - t_i) \Pi(t - t_i, T_C) \sin \theta_i \right)^2 \right] \\ & + \frac{1}{2T_C} \left[R^*(t) \left(\sum_{i=0}^M a_i \delta(t - t_i) e^{j\theta_i} \right) + R(t) \left(\sum_{i=0}^M a_i \delta(t - t_i) e^{-j\theta_i} \right) \right]. \end{aligned} \quad (27)$$

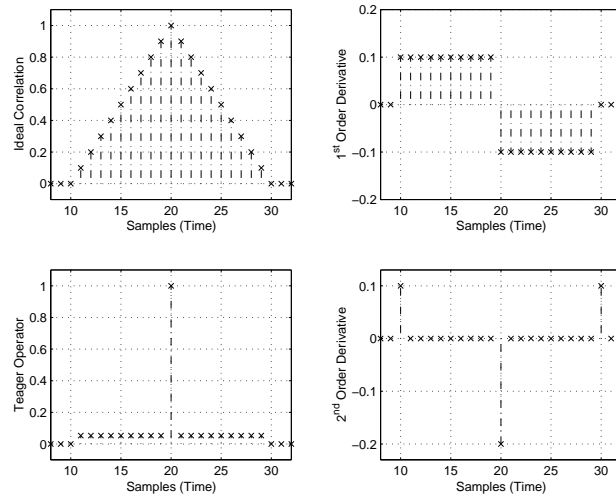


Figure 2: TK operator applied to a triangular function. 1^{st} and 2^{nd} order derivatives of the triangular function are also shown.

Notice that the above expression becomes very large if the time variable t is equal to one of the true delays t_i . Thus, equation (27) shows that the TK operator is capable of tracking very accurately the peak locations of the triangular pulses within certain 'noise' floor [21] independently of the delay spacing between the multipaths. Figures 3 and 4 show simple illustrative examples of TK operator applied to the sum of two triangular functions with different amplitudes and zero phases.

We also noticed that the above properties of TK operator hold as well for the magnitude squared cross-correlation function. Similar mathematical derivations can be easily conducted. Figures 3 and 4 illustrate examples of TK operator applied to the magnitude squared cross-correlation function.

By exploiting the above properties of the quadratic operator, we found out that by applying this nonlinear TK operator to the specific cross-correlation function (Eq. 15) of a GPS receiver, one can easily estimate the multipath delays introduced by the channel. The multipath delays are simply estimated by selecting the time location of the highest (strongest) peaks of the Teager-Kaiser operator output function. Figure 5 illustrates the proposed algorithm. The number of the selected peaks depends on the expected number

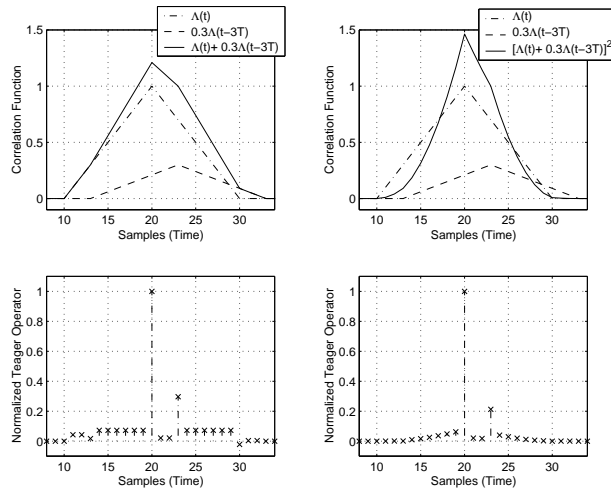


Figure 3: TK operator applied to the sum and squared sum of two triangular functions.

of paths in the channel (equal to the number of fingers in the Rake receiver).

5 Simulation Results

Simulations have been performed to analyze the performance of the proposed technique in a GPS receiver, using different Rayleigh channel profiles. An oversampling factor of 16, and the typical Gold code sequence of length 1023 are used. The delay estimation methods are compared in terms of the acquisition probability of detecting the true paths with a decision based on one symbol. The probability of acquisition is defined as the probability that all the paths are estimated within +/- one sample error. Also, we performed an averaging over 200 delay estimates for the provided simulation results.

Fig. 6 shows an example of S-curves obtained via a non-coherent DLL (NCDLL) with SNR=20 dB for half chip and two chips spaced taps. The first tap magnitude is equal to 0 dB and the second peak is equal to -3 dB. We clearly notice that NCDLL fails to detect very closely spaced multipaths.

Fig. 7 shows an example of cross-correlation function and TK operator output using a static channel profile and SNR=5 dB. We notice that this approach is capable of detecting accurately closely-spaced

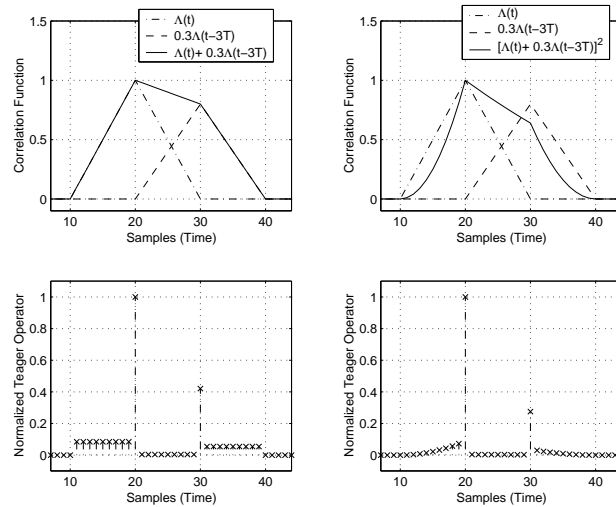


Figure 4: TK operator applied to the sum and squared sum of two triangular functions.

multipaths, within less than quarter of the chip period.

Figs. 8 till 11 show the acquisition probability of detecting the true paths at the exact locations and within one sample error for different Rayleigh channel profiles and taps spacings. The simulations are performed for the proposed TK operator technique as well as for the envelope subtraction approach.

We notice that the proposed TK technique performs clearly better than the envelope subtraction approach especially for detecting accurately very closely-spaced multipaths within less than half a chip period (see Fig. 11). The TK-based approach works even at very low signal-to-noise ratios. The results are quite remarkable taking into account the simple implementation and very low complexity compared to the traditional maximum likelihood based methods and envelope subtraction approach.

6 Conclusions

In this contribution, we introduced an innovative technique for subchip multipath delay estimation based on Teager-Kaiser quadratic operator suited for spread spectrum CDMA systems, and we focused our study to the case of GPS receivers. Some properties of this nonlinear operator were derived for the case

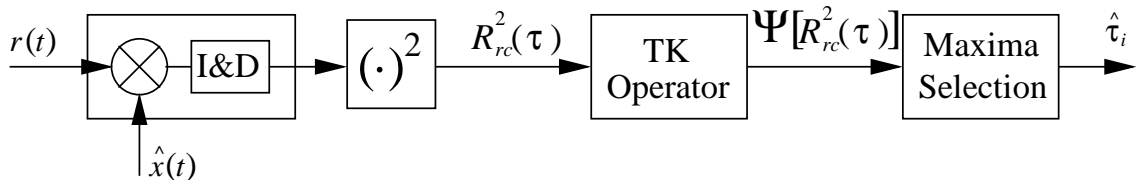


Figure 5: Teager-Kaiser approach for multipath delay estimation.

of ideal triangular reference correlation functions. Simulations results confirmed the high performance of the proposed technique compared to the peak tracking with pulse subtraction method for all cases of closely-spaced multipaths within less than half chip period. The ability of solving closely-spaced paths in the presence of overlapped multipath components comes from the exploitation of the properties of the cross-correlation function. This new technique is extremely simple and very efficient for estimating closely-spaced multipaths with much less computational complexity compared, e.g., to the subspace-based multipath delay estimation methods. The subchip resolution can be used to improve GPS and mobile phone positioning accuracy using the cellular network-assisted GPS technology.

In general, for each shape of the reference correlation function or pulse shaping filter used, there may exist a linear or nonlinear operator capable of estimating easily the multipath delays. It remains as a challenging topic for future work to derive other linear or nonlinear operator capable of tracking multipath delays in different communication systems using different pulse shaping filters than the rectangular one.

References

- [1] R. Van Nee, "Multipath and multi-transmitter interference in spread-spectrum communication and navigation system," *Delft University Press*, 1995.
- [2] R. Van Nee, J. Sierveld, P. Fenton, and B. Townsend, "The multipath estimating delay lock loop: Approaching theoretical accuracy limits," *Proc. IEEE position, Location, and Navigation Symposium*, April 1994, pp. 246–251.
- [3] J. Syrjärinne, "Studies of modern techniques for personal positioning," *Ph.D. Thesis*, Tampere University of Technology, March 2001.
- [4] M. Braasch and A.J.V. Dierendonck, "GPS receiver architectures and measurements," *Proc. of the IEEE*, vol. 87, No. 1, January 1999, pp. 48–64.
- [5] M.C. Laxton and S.L. DeVilbis, "GPS multipath mitigation during code tracking," *Proc. of the American Control Conference*, Albuquerque, New Mexico, pp. 1429–1433, June 1997.

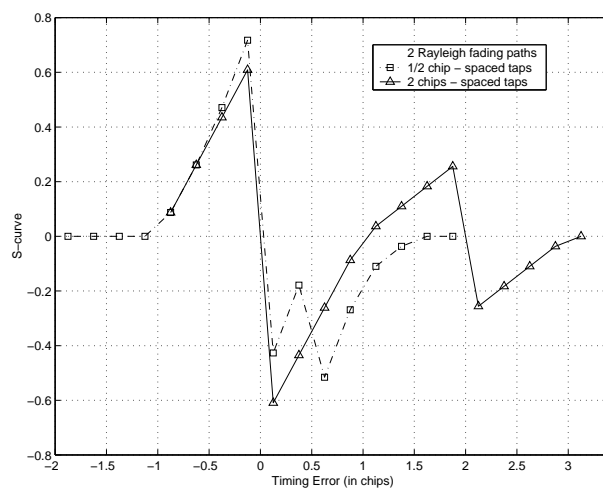


Figure 6: Non-coherent DLL S-curve with taps magnitudes equal to 0 dB and -3 dB.

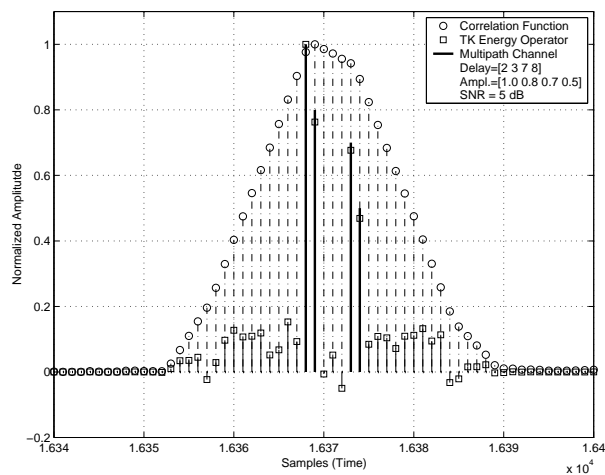


Figure 7: TK operator applied to the cross-correlation function.

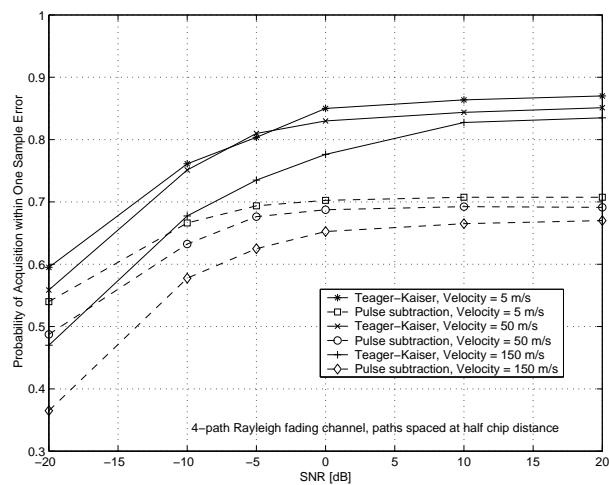


Figure 8: Probability of detecting the true paths within one sample error at half chip spaced taps using four path Rayleigh fading channel.

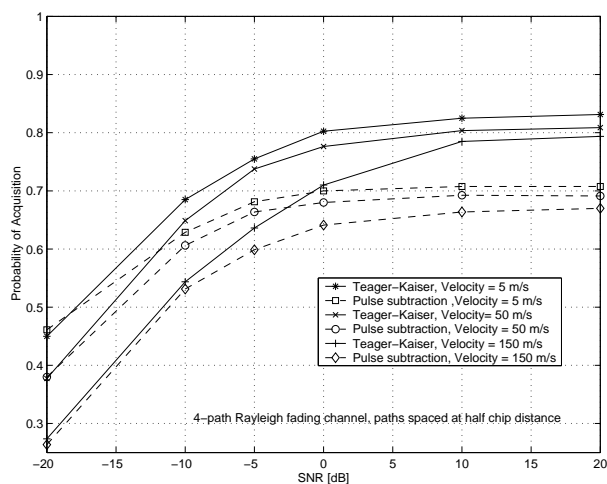


Figure 9: Probability of detecting the true paths at the exact locations at half chip spaced taps using four path Rayleigh fading channel.

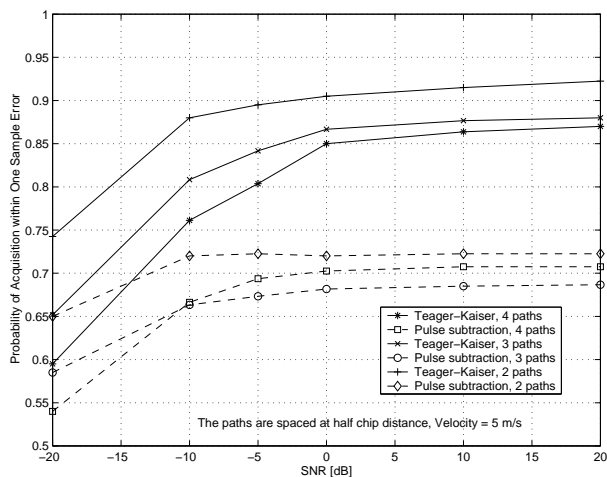


Figure 10: Probability of detecting the true paths within one sample error at half chip spaced taps using different Rayleigh fading channel profiles.

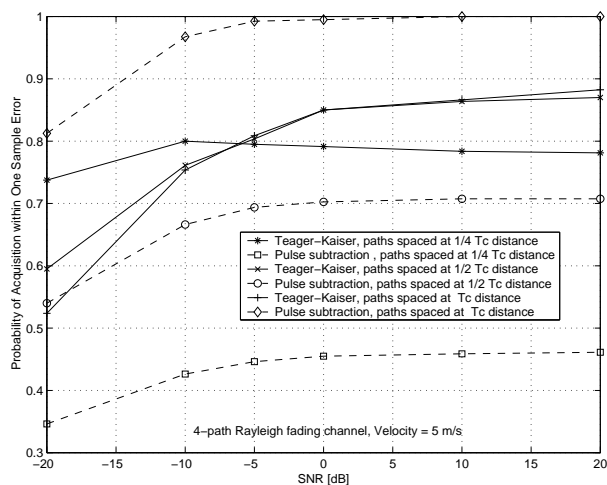


Figure 11: Probability of detecting the true paths within one sample error for different spaced taps, and using different Rayleigh fading channel profiles.

- [6] P. Luukkanen, and J. Joutsensalo, "Comparison of MUSIC and matched filter delay estimators in DS-CDMA," in *Proc. IEEE Personal, Indoor and Mobile Radio Communications*, vol. 3, 1997, pp.830-834.
- [7] Z. Kostić, G. Pavlović, "Resolving sub-chip spaced multipath components in CDMA communication systems," in *Proc. IEEE VTC*, vol. 1, 1993, pp. 469-472.
- [8] E. Sourour, G. Bottomly, And R. Ramesh, "Delay tracking for direct sequence spread spectrum systems in multipath fading channels," *IEEE 49th Vehicular Technology Conference*, vol. 1, 1999, pp. 422-426.
- [9] R. Hamila, S. Lohan and M. Renfors, "Multipath delay estimation in GPS receivers," In *Proc. Nordic Signal Processing Symposium (Norsig'2000)*, Kolmården, Sweden, pp. 417-420, June 2000.
- [10] S. Lohan, M. Renfors, "Feedforward approach for estimating the multipath delays in CDMA systems," in *Proc. Nordic Signal Processing Symposium (Norsig'2000)*, Kolmården, Sweden, pp. 125-128, June 2000.
- [11] J. F. Kaiser, "On a simple algorithm to calculate the 'energy' of a signal," *Proc. IEEE ICASSP-90*, Albuquerque, New Mexico, pp. 381-384, April 1990.
- [12] J. F. Kaiser, "On Teager's energy algorithm and its generalization to continuous signals," *Proc. 4th IEEE Digital Signal Processing Workshop*, Mohonk (New Paltz), NY, September 1990.
- [13] R. Hamila, J. Astola, F. Alaya Cheikh, M. Gabbouj, and M. Renfors, "Teager energy and the ambiguity function," *IEEE Transactions on Signal Processing*, vol. 47, no. 1, pp. 260-262, January 1999.
- [14] A. Papoulis, "Signal analysis," *McGraw-Hill*, 1988.
- [15] Petros Maragos, James F. Kaiser, and Thomas F. Quatieri, "On amplitude and frequency demodulation using energy operators," *IEEE Trans. Signal Processing*, vol. 41, pp. 1532-1550, April 1993.
- [16] P. Maragos, J. F. Kaiser, and T. F. Quatieri, "Energy Separation in Signal Modulations with Application to Speech Analysis," *IEEE Trans. Signal Processing*, vol. 41, no. 10, pp. 3024-3051, October 1993.
- [17] J. Fang and L. Atlas, "Quadratic detectors for energy estimation," *IEEE Transactions on Signal Processing*, vol. 43, no. 11, pp. 2582-2594, November 1995.
- [18] F. Alaya Cheikh, R. Hamila, M. Gabbouj and J. Astola, "Impulse Noise Removal in Highly Corrupted Color Images," *Proc. 1996 IEEE International Conference on Image Processing*, Lausanne, Switzerland, 1996.
- [19] J. F. Kaiser, "Some Useful Properties of Teager's Energy Operators," *Proc. IEEE ICASSP-93*, vol. III, pp. 149-152, April 27-30, 1993.
- [20] R. Hamila, "Teager energy operator; Theory and Applications," *Licentiate Thesis*, Tampere University of Technology, December 1998.
- [21] R. Hamila, S. Lohan and M. Renfors, "Nonlinear operator for multipath channel estimation in GPS receivers," In *The 7th IEEE International Conference On Electronics, Circuits & Systems*, Jounieh, Lebanon, pp. 352-356, December 2000.

Publication 8

S. Lohan, R. Hamila, and M. Renfors, "Performance Analysis of an Efficient Multipath Delay Estimation Approach in a CDMA Multiuser Environment," in *Proc. of 12th IEEE International Symposium on Personal, Indoor and Mobile Radio Communications, PIMRC'01*, San Diego, California, USA, Sept. 2001, pp. 6–10.

Copyright ©2001 IEEE. Reprinted, with permission, from the proceedings of PIMRC'01.

Performance Analysis of an Efficient Multipath Delay Estimation Approach in a CDMA Multiuser Environment

Elena-Simona Lohan, Ridha Hamila and Markku Renfors
Telecommunications Laboratory, Tampere Univ. of Technology
P.O.Box 553, FIN-33101, Tampere, Finland

Abstract—In this paper, we introduce an efficient and simple technique for estimating closely-spaced multipath delays in an asynchronous multiuser CDMA systems. The subchip resolution is achieved via a nonlinear quadratic operator called Teager-Kaiser operator, which exploits the structure of the cross-correlation function between the received signal and the reference code. Simulation results in the presence of multiple interfering users and Rayleigh fading multipath channels are presented. It is shown that the proposed technique is near far-resistant, and its performance in the presence of closely spaced multipaths is much better compared to the peak tracking with subtraction method. Moreover, it has the advantage of a very simple implementation, compared to other maximum likelihood approaches.

I. INTRODUCTION

Code Division Multiple Access (CDMA) communication systems have to cope with multipath propagation. Generally, the transmitted signal arrives at the receiver via multiple propagation paths at different delays which may add destructively, resulting in signal fading and consequently in receiver performance degradation. In CDMA applications, such as Third generation mobile communications or GPS receivers, it is important to achieve accurate delay estimation before despreading and data detection.

Most spread spectrum systems use spreading codes with non-ideal correlation properties. Moreover, non-ideal cross-correlation properties between the received signal and the despreading code replicas result in co-channel interference or multiuser-interference for radio communication systems, which is also called multi-transmitter interference for radio-navigation systems [1]. Generally, the performance of radio communication systems are heavily affected by the multipath and multiuser-interference. The maximum signal to noise ratio at the receiver is directly dependent on the amount shadowing, multipath, and co-

channel interference.

Usually, successive paths can be solved if they are spaced at more than one chip distance [2]. However, even if the path spacing is less than one chip interval some diversity gain can be achieved if we are capable to detect the paths and use them in the maximum ratio combining [3]. Optimal maximum likelihood methods can be employed for tracking simultaneously the path delays, amplitudes, and phases [1], [3] but they are usually too complex for practical purposes. Several subspace-based approaches have been proposed to deal with closely-spaced multipaths [4], [5]. Also, these algorithms are quite complex to implement and they are suitable only for systems employing short codes, i.e., when the user code is the same from one symbol to another. Another solution to solve closely-spaced paths is the peak tracking with pulse subtraction method [3], [6], [7]. The idea of this method is to approximate the output of the matched filter (or correlator) by a superposition of a set of reference correlation functions. Once we detect a multipath delay, its contribution is subtracted from the correlation function, and the successive delays are searched on the residual function. The pulse subtraction method does not require heavy computations and performs reasonably well if the paths are at more than half chip spacing [6], [7].

In this contribution, we first introduce a new approach for estimating closely-spaced multipaths in a Rake receiver based on a nonlinear quadratic operator called Teager-Kaiser operator. Then, we investigate the effect of multiuser interference on the performance of the proposed approach. The results are also compared with the peak tracking with subtraction technique, in the presence of multipath and multiuser interference.

II. MULTIPATH DELAY ESTIMATION BASED ON TEAGER-KAISER OPERATOR

In a downlink DS-CDMA scenario with K users in the system, the received signal can be written as [8]

$$r(t) = \sum_{k=1}^K \sqrt{P_k} \sum_{n=-\infty}^{\infty} b_{n,k} \sum_{l=1}^L \alpha_l^n e^{j\theta_l^n} s_k^n(t - \tau_l^n) + \eta(t), \quad (1)$$

where P_k is the power of user k , $b_{n,k}$ is the transmitted data symbol n of user k . α_l^n , θ_l^n , and τ_l^n are the amplitude,

This work was carried out in the project "Advanced Transceiver Architectures and Implementations for Wireless Communications" supported by the Academy of Finland. This work is also supported by Graduate School in Electronics, Telecommunications and Automation (GETA) and Tampere Graduate School in Information Science and Engineering (TISE).

phase and delay, respectively, of the l^{th} path during the symbol n . L is the number of channel paths, $s_k^n(\cdot)$ is the signature of user k during the symbol n , and $\eta(\cdot)$ is a complex additive white Gaussian noise.

The user signatures are expressed as follows

$$s_k^n(t) = \sum_{m=0}^{S_{F_k}-1} c_{m,k}^n p(t - mT_c - nT_{sym,k}) \quad (2)$$

where $c_{m,k}^n$ is the code value for m -th chip of user k during the symbol n , T_c is the chip interval, $p(\cdot)$ is the chip pulse shape, S_{F_k} is the spreading factor of user k , and $T_{sym,k}$ is the symbol interval of user k ($T_{sym,k} = S_{F_k}T_c$).

We assume that the desired user is the user 1. In conventional maximum likelihood approaches [1], delay estimation is based on the correlation between the received signal and the delayed replica of the desired user signature. The output of the correlator for user 1 during the symbol interval n is given by

$$y^n(\tau) = \frac{1}{T_{sym,1}} \int_{T_{sym,1}} r(t) s_1^n(t - \tau) + \tilde{\eta}(\tau). \quad (3)$$

Here, $\tilde{\eta}(\cdot)$ is the filtered noise (for convenience we dropped the subscript 1 from the correlator output function).

Assuming ideal cross- and auto- correlation code properties and rectangular pulse shape, the output of the correlator becomes

$$y^n(\tau) = \sqrt{P_1} b_{n,1} \sum_{i=1}^L \alpha_i^n e^{j\theta_i^n} \mathcal{R}(\tau_i^n - \tau) + \tilde{\eta}_1(\tau), \quad (4)$$

where $\mathcal{R}(\cdot)$ is the pulse shape autocorrelation function

$$\mathcal{R}(\tau) = \begin{cases} 1 - \frac{|\tau|}{T_c} & |\tau| \leq T_c \\ 0 & \text{otherwise.} \end{cases} \quad (5)$$

Here, $\tilde{\eta}_1(\cdot)$ is an additive noise process which incorporates the effects of additive noise, multiuser interference and inter-path and intersymbol interference (and which can be considered Gaussian by virtue of central limit theorem).

We notice that the output $y^n(\tau)$ of the correlator is a superposition of shifted triangular pulses, weighted by the channel tap complex coefficients and the data modulation within some additive noise. The data modulation can be removed in a coherent way if pilot data symbols are available, or non-coherently (by squaring or envelope detection) if no information is available about the data. In our simulations, we considered the case of non-data aided delay estimation. If the delays are searched directly on the envelope of the correlation function $y^n(\tau)$, the delay resolution is limited to half of the pulse width T_c [2], [3]. The multipaths closer than 1 chip distance are merging and they cannot be tracked directly from the envelope of the correlation function.

We may exploit the structure of the correlation function by applying the Teager-Kaiser (TK) operator to equation (4). The nonlinear quadratic TK operator was first introduced for measuring the real physical energy of a system [9]. It was found that this nonlinear operator exhibits several attractive features such as simplicity, efficiency and ability to track instantaneously-varying spatial modulation patterns [10]. Since its introduction, several applications have been derived for one-dimensional and two-dimensional signal processing [11], [12].

The continuous-time TK energy operator of a complex-valued signal $x(t)$ is defined as follows [11]

$$\Psi_c[x(t)] = \dot{x}(t)\dot{x}^*(t) - \frac{1}{2}[\ddot{x}(t)x^*(t) + x(t)\ddot{x}^*(t)]. \quad (6)$$

Similarly, the discrete-time Teager operator of a complex valued signal is given by [11]

$$\Psi_d[x(i)] = x(i-1)x^*(i-1) - \frac{1}{2}[x(i-2)x^*(i) + x(i)x^*(i-2)]. \quad (7)$$

Many useful properties of this nonlinear quadratic operator have been derived, and the analogy with the discrete-time domain has also been established [12], [13]. We notice first that applying the continuous-time TK operator to the pulse shape autocorrelation function (Eq. (5)) we obtain

$$\Psi_c[\mathcal{R}(t)] = \frac{\Pi(t, T_c)}{T_c^2} + \frac{\mathcal{R}(t)\delta(t)}{T_c}, \quad (8)$$

where $\Pi(t, T_c)$ stands for a rectangular function with unit amplitude and duration $2T_c$ centered at $t = 0$, defined by

$$\Pi(t, T_c) \triangleq \begin{cases} 1 & |t| \leq T_c \\ 0 & \text{otherwise,} \end{cases} \quad (9)$$

and $\delta(t)$ stands for the continuous-time Dirac function. Obviously, (8) shows that the TK operator applied to a triangular function provides a clear time-aligned peak location of the triangular pulse (at $t = 0$) in the presence of a certain 'noise' floor with magnitude $1/T_c^2$ [14].

By applying now the TK operator to equation (4), after some manipulations it follows

$$\begin{aligned} \Psi_c[y^n(\tau)] &= \sqrt{P_1} b_{n,1} \left\{ \left(\sum_{i=1}^L \alpha_i^n \frac{\Pi(\tau_i^n - \tau, T_c) \cos(\theta_i^n)}{T_c} \right)^2 \right. \\ &\quad + \left(\sum_{i=1}^L \alpha_i^n \frac{\Pi(\tau_i^n - \tau, T_c) \sin(\theta_i^n)}{T_c} \right)^2 \\ &\quad + \sum_{i=1}^L \sum_{i_1=1}^L \alpha_i^n \alpha_{i_1}^n \cos(\theta_{i_1}^n - \theta_i^n) \\ &\quad \left. \times \frac{\mathcal{R}(\tau_{i_1}^n - \tau) \delta(\tau_i^n - \tau)}{T_c} \right\} + \tilde{\eta}_2(\tau), \quad (10) \end{aligned}$$

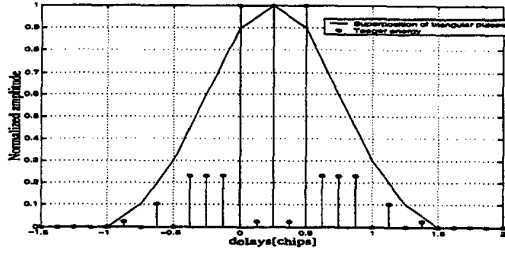


Fig. 1: Illustration of the TK principle for a 3-path static channel, $0.25T_c$ spacing between consecutive paths

where $\tilde{\eta}_2(\cdot)$ is the noise after the TK filtering. Notice that the above expression becomes very large if τ is equal to one of the true multipath delays τ_l^n . Therefore, the TK operator applied to the cross-correlation function (4) exhibits some peaks at the correct delay locations within certain 'noise' floor (due to the inter-path interference and the additive noise). Thus, the TK operator is capable of tracking very accurately the multipath delays τ_l^n independently of the delay spacing between the multipaths. In practice, the fading effect is compensated by non-coherent averaging over several symbols. The Teager energy applied to the correlation function, in the absence of noise and data modulation, is illustrated in Fig. 1 for a static channel with 3 taps spaced at 0, 0.25 and 0.5 chip delays.

The proposed TK approach is illustrated in Figure 2, for the non-data aided mode. By applying this nonlinear TK operator to the correlator output, one can easily estimate the multipath delays introduced by the channel. The multipath delays are simply estimated by selecting the time location of the highest (strongest) peaks of the TK operator output function. The number of the selected peaks depends on the considered number of multipath of the channel. Usually, there are less Rake fingers than multipaths in the channel, therefore the number of estimated peaks is usually equal to the number of Rake fingers. If the number of multipaths is less than the number of Rake fingers, a thresholding must be applied in order to estimate the correct number of paths.

III. SIMULATION RESULTS

A downlink scenario with rectangular pulse shaping and BPSK data modulation is considered in the simulations. The channel impulse response, generated randomly for each observation interval, is given by

$$h(t) = \sum_{i=1}^L \alpha_i e^{j\theta_i} \delta(t - \tau_i).$$

The delays are constant over N_{BA} symbols, N_{BA} being the block averaging length, i.e., the number of symbols used

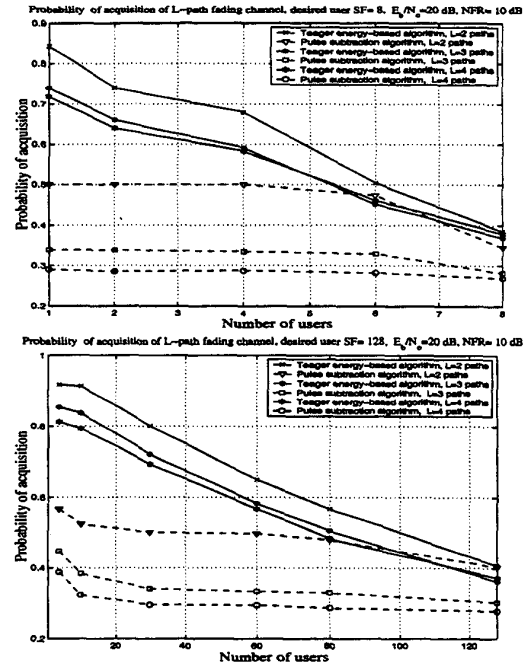


Fig. 3: Acquisition probability as a function of the number of users, $SF = 8$ and $SF = 128$, $D_{max} = 1/2T_c$.

in the non-coherent averaging of the TK operator applied to the correlation function (see Fig. 2). The correlation function was computed over one symbol interval which corresponds to a non-data aided approach, and the non-coherent averaging was used in order to diminish the effect of fading ($N_{BA} = 5$). At each N_{BA} symbols, a set of L delays are generated according to the uniform distribution $\mathcal{U}(\epsilon_l, \epsilon_{l+1})$, $l = 1, \dots, L$, where $\epsilon_l = N_s + (l-1)N_s D_{max}/2$, N_s being the number of samples per chip ($N_s = 8$) and D_{max} being the maximum separation between two consecutive path delays. The delays are rounded to the nearest integer, such that only integer multiples of the sampling interval are allowed. The amplitudes α_l are chosen according to the Rayleigh distribution (with equal average tap powers for all the L paths), and the phases θ_l are uniformly distributed over $[0, 2\pi]$.

The users are separated by orthogonal Walsh codes and have the same scrambling code (a segment of a Gold code of length $2^{18} - 1$). It is assumed that all the users have the same spreading factor. The near-far ratio is defined by [4]

$$NFR = 10 \log_{10} \frac{P_k}{P_1},$$

where P_k is the power of the interfering user k (all interfering users have the same power), and P_1 is the power

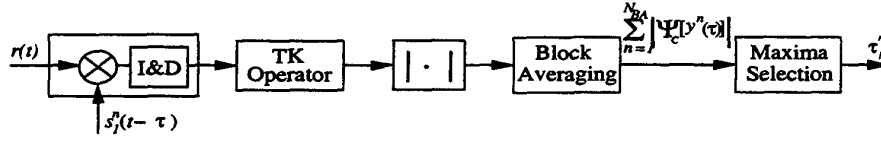


Fig. 2: TK approach for multipath delay estimation

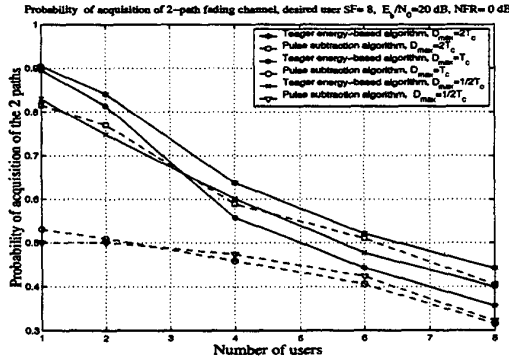


Fig. 4: Impact of the maximum separation between consecutive paths.

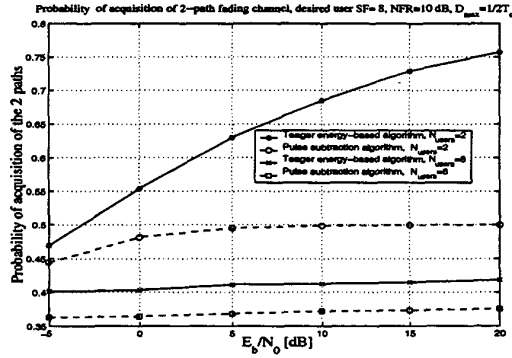


Fig. 5: Acquisition probability as a function of the E_b/N_0 .

of the desired user. We use an averaging over 600 delay estimates for the simulation results. The probability of acquisition is defined as the probability that all the L paths are estimated correctly within ± 1 sample error.

Figure 3 shows the deterioration of the probability of acquisition of the channel multipaths as a function of the number of users in the system. The number of users in a fully loaded system is directly related to number of available codes, and hence to the spreading factor. Two spreading factors are employed ($SF = 8$ and $SF = 128$), and three fading channels with 2 to 4 paths of equal average amplitudes are considered. We assume that the estimated number of paths is equal to the true number of paths.

The maximum separation D_{max} between successive paths is half chip. For this scenario of closely-spaced paths, we notice that the TK-based algorithm systematically outperforms the pulse subtraction algorithm with respect to the different number of users and multipaths in the system. The gain in the acquisition probability of TK-based method over the pulse subtraction method goes from about 10% at fully loaded systems up to 40% for single-user systems. However, the deterioration of the acquisition probability at fully loaded systems is significant for TK-based operator even though it still outperforms the pulse subtraction technique. The behaviour of the pulse subtraction algorithm remains almost constant with the number of users. This is due to the fact the pulse sub-

traction method fails to estimate with high accuracy very closely-spaced multipaths.

Figure 4 shows the behaviour of the two algorithms when increasing the maximum separation between successive paths. The farther away the paths, the more efficient becomes the pulse subtraction method. However, for D_{max} up to 2 chips, TK-based method is still better than the pulse subtraction method. The impact of the additive Gaussian noise is shown in Figure 5. The E_b/N_0 is the received energy per bit of desired user taking into considerations all the paths energies. We notice that for fully loaded systems, the multiple access interference (MAI) is more significant than the additive noise. Therefore, the acquisition probability is low, but almost constant with respect to E_b/N_0 . For only few users in the system, the MAI interference is small and the TK-based operator becomes very sensitive to the additive Gaussian noise. For example, at $E_b/N_0 = -5$ dB, we acquire correctly both paths 47% of the time when TK operator is used (compared with 75% for $E_b/N_0 = 20$ dB).

The near-far resistance is studied for two cases, as shown in Figure 6, for fully and un-fully loaded systems. The interfering users have all the same power, varying from 0 dB to 40 dB higher than the desired user power. It is clear that there is almost no impact of the near far ratio NFR on the acquisition probability (the slight variations are due to the fact that different realizations of noise and channel parameters are employed for each curve and only 600

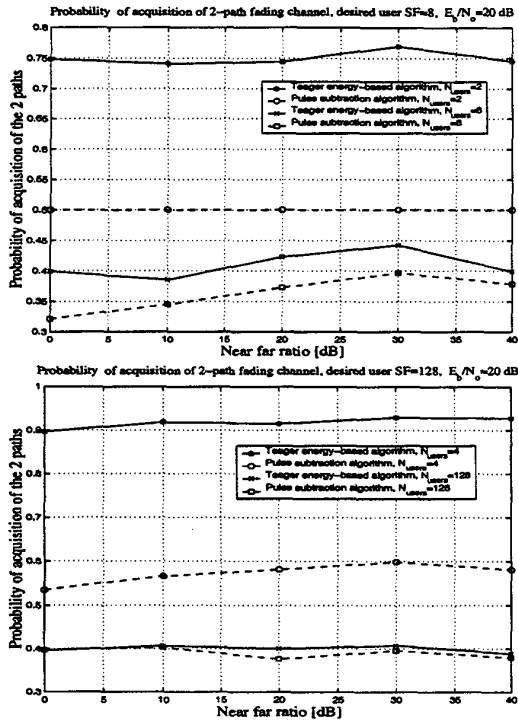


Fig. 6: Acquisition probability as a function of the near far ratio NFR, $SF = 8$ and $SF = 128$, $D_{max} = 1/2T_c$.

delay estimates are used in the statistics). Both Teager energy-based algorithm and pulse subtraction algorithm are near far resistant, but the Teager energy-based algorithm clearly outperforms the pulse subtraction method, especially in the presence of only few users.

IV. CONCLUSIONS

An algorithm for solving closely-spaced multipaths in the presence of multiuser and multipath interference has been presented and its performance has been assessed via simulations. This algorithm applies a non-linear Teager-Kaiser operator to the correlation function between the received signal and the code replica at the receiver. Also, it can be used both in a data-aided and non-data aided mode. The proposed approach requires very low computational complexity in addition to its simple implementation. The ability of solving closely-spaced paths comes from the exploitation of the properties of the cross-correlation function, in the presence of overlapped multipaths components.

It has been shown that the TK-based algorithm is near-far resistant and outperforms the peak tracking with pulse subtraction algorithm for all cases of closely-spaced mul-

tipaths, even though it is sensitive to additive Gaussian noise for a small number of users in the system. This algorithm has been applied to systems employing rectangular pulse shaping. In general, for each shape of the reference correlation function or pulse shaping filter used, there may exist a linear or nonlinear operator capable of estimating easily the closely-spaced multipath delays. It remains as a challenging topic for future work to derive other linear or nonlinear operator capable of tracking multipath delays using different pulse shaping filters, e.g., the root raised cosine pulse shaping.

REFERENCES

- [1] R. Van Nee, *Multipath and multi-transmitter interference in spread-spectrum communication and navigation system*, Delft University Press, 1995.
- [2] J. Proakis, *Digital Communications*, McGraw-Hill, 1989.
- [3] G.E. Bottomley, E. Sourour, and R.E. Ramesh, "Optimizing the performance of limited complexity Rake receivers," in *Proc. of the IEEE VTC*, vol. 2, 1998, pp. 968-972.
- [4] T. Östman, S. Parkvall, and B. Ottersten, "Improved MUSIC algorithm for estimation of time delays in asynchronous DS-CDMA systems," in *Proc. of the Asilomar Conference of Signals, Systems and Computers*, vol. 1, 1998, pp. 838-842.
- [5] Z. Kostić, G. Pavlović, "Resolving sub-chip spaced multipath components in CDMA communication systems," in *Proc. of the IEEE VTC*, vol. 1, 1993, pp. 469-472.
- [6] R. Hamila, S. Lohan, and M. Renfors, "Multipath delay estimation in GPS receivers," in *Proc. of the Nordic Signal Processing Symposium*, Kolmården, Sweden, 2000, pp. 417-420.
- [7] S. Lohan, M. Renfors, "Feedforward approach for estimating the multipath delays in CDMA systems," in *Proc. of the Nordic Signal Processing Symposium*, Kolmården, Sweden, 2000, pp. 125-128.
- [8] G.E. Bottomley, T. Ottosson, Y.P. Wang, "A generalized RAKE receiver for interference suppression," *IEEE Journal on Sel. Areas in Comm.*, vol. 18, pp. 1536-1545, Aug. 2000.
- [9] J. F. Kaiser, "On a simple algorithm to calculate the 'energy' of a signal," in *Proc. of the IEEE ICASSP'90*, Albuquerque, New Mexico, 1990, pp. 381-384.
- [10] P. Maragos, J.F. Kaiser, and T.F. Quatieri, "On amplitude and frequency demodulation using energy operators," *IEEE Trans. Sign. Proc.*, vol. 41, pp. 1532-1550, April 1993.
- [11] R. Hamila, J. Astola, F. Alaya Cheikh, M. Gabbouj, and M. Renfors, "Teager energy and the ambiguity function," *IEEE Trans. Sign. Proc.*, vol. 47(1), pp. 260-262, Jan. 1999.
- [12] R. Hamila, "Teager energy operator; Theory and Applications," *Licentiate Thesis*, Dec. 1998.
- [13] J.F. Kaiser, "Some Useful Properties of Teager's Energy Operators," in *Proc. of the IEEE ICASSP'93*, vol. III, 1993, pp. 149-152.
- [14] R. Hamila, M. Renfors, "Nonlinear operator for multipath channel estimation in GPS receivers," in *Proc. of the IEEE International Conference On Electronics, Circuits & Systems*, Jounieh, Lebanon, 2000, pp. 352-356.

Tampereen teknillinen korkeakoulu. Julkaisuja

309. Jussila, Tapio, Time-Resolved Optical and Electrical Phenomena of Bacteriorhodopsin and Its Derivatives on Polyelectrolyte Thin Films. 2000. 118 s.
310. Larjo, Jussi, Laser Diagnostics of Chemical Vapor Deposition. 2000. 121 s.
311. Kellomäki, Minna, Bioabsorbable and Bioactive Polymers and Composites for Tissue Engineering Applications. 2000. 246 s.
312. Mattila, Jouni, On Energy-efficient Motion Control of Hydraulic Manipulators. 2000. 88 s.
313. Toivola, Juha, Application of Statistical Methods to Modal Parameter Estimation. 2000. 181 s.
314. Jerábek, Filip, Analysis of Single Flank Test Results Providing Flank Topography Errors of Spiral Bevel Gears. 2000. 262 s.
315. Korhonen, Susanna, Ozone-based Treatments of Process Waters and Effluents in the Pulp and Paper Industry. 2000. 117 s.
316. Lipping, Tarmo, Processing EEG during Anaesthesia and Cardiac Surgery with Non-linear order Statistics based Methods. 2001. 102 s.
317. Hariharan, Ramalingam, Robust Signal Parameterisation Techniques for Speech Recognition. 2001. 162 s.
318. Männistö, Minna, Microbiology and *In Situ* Bioremediation Potential of Boreal Chlorophenol Contaminated Groundwater. 2001. 168 s.
319. Syrjärinne, Jari, Studies of Modern Techniques for Personal Positioning. 2001. 180 s.
320. Kuusilinna, Kimmo, Studies and Implementations of Bus-based Interconnections. 2001. 201 s.
321. Gold, David, The Indigenous Fisherman Divers of Thailand: Determining the hazards associated with indigenous diving practices and developing interventions to reduce the risk of diving-related injury and disease. 2001. 312 s.
322. Vekara, Timo, A Circuit Approach for the Time Domain Simulation of the Brake Magnet Actuator. 2001. 145 s.
323. Happonen, Harri, Framework for Integrating Knowledge and Process Dimensions of a Product Development System - a Theoretical and Empirical Study in the Field of Modern Process Automation. 2001. 188 s.
324. Pajunen, Sami, On Computational Methods in Large-deflection Elasto-plastic Structural Analysis. 2001. 114 s.
325. Aumala Olli, Dithering in Analogue-to-Digital Conversion. 2001. 81 s.
326. Kiss, Imre, On Speech Recognition in Mobile Communications. 2001. 165 s.
327. Mäkinen, Esa, Control of a Water Hydraulic Servo System. 2001. 94 s.
328. Lapinleimu, Ilkka, Ideal Factory - Theory of Factory Planning, Produceability and Ideality. 2001. 195 s.
329. Korpisaari, Petri, Studies on Data Fusion Techniques for Multitarget Tracking. 2001. 180 s.
330. Palm, Petteri, The Development and Reliability of Flip Chip Technology in Electronic Module Manufacturing. 2001. 111 s.
331. Huttunen-Saarivirta, Elina, Microstructural and Electrochemical Characterisation of Chemical Tin Coatings on Copper. 2001. 134 s.
332. Määttänen, Jarmo, Anisotropic Adhesive Interconnection: An Alternative for Solder Joints in High Density Electrical Contacts. 2001. 98 s.
333. Majuri, Hannu, Hyödynarviointi vesistöjen kunnostushankkeissa. 2001. 252 s.
334. Giurcăneanu, Ciprian Doru, On Lossless Signal Compression. 2001. 184 s.
335. Saarenrinne, Pentti, Turbulent Kinetic Energy Dissipation Rate Estimation from LDV and PIV Measurements. 2001. 90 s.
336. Naaranoja, Marja, Capabilities of Utilisation of Information Systems in Facilities Management. 2001. 171 s.
337. Lordache, Răzvan, Contributions to Robust Transmission of VQ Data over Finite Memory Channels and to VQ Image Coding. 2001. 160 s.
338. Lappalainen Ville, Low Bit Rate Video Coding on General-Purpose Processor. 2001. 204 s.
339. Vuorinen, Jyrki, Resonant Ultrasound Spectroscopy and Differential Scanning Calorimetry Studies of Materials for Property Specific Applications. 114 s. 2001.
340. Mattila, Ville-Veikko, Perceptual Analysis of Speech Quality in Mobile Communications. 2001. 282 s.
341. Santos, Marcelino, The Architectural Object as Aesthetic Object: Alvar Aalto's House of Culture. 2001. 238 s.
342. Linne, Marja-Leena, Computational Model for Granule Neuron Excitability. 2001. 151 s.
343. Mäkilouko, Marko, Leading Multinational Project Teams: Formal, Country Specific Perspective. 2001. 227 s.
344. Repo, Sami, On-line Voltage Stability Assessment of Power System - An Approach of Black-box Modelling. 2001. 175 s.
345. Nikkilä, Pekka, Mobilehydrauliikan puhtaustaso ja sen simulointi. 2001. 119 s.
346. Katara, Mika, Aspects of Continuous Behaviour – Design of Real-Time Reactive Systems in DisCo. 2001. 120 s.
347. Kivinen, Juha-Matti, A Variable Parameter Facility for Dynamic Testing of Polymer Covered Paper Machine Rolls. 2001. 105 s.
348. Hirsimäki, Mika, Structure Sensitivity and Energy Dependence of Activated and Non-activated surface Processes on Palladium Model Catalysts. 2001. 149 s.
349. Tico, Marius, On Design and Implementation of Fingerprint-Based Biometric Systems. 2001. 147 s.

350. Valkama, Mikko, *Advanced I/Q Signal Processing for Wideband Receivers: Models and Algorithms*. 2001. 120 s.
351. Lehto, Kirsi-Maarit, *Photochemical and Biological Degradation of Polycyclic Aromatic Hydrocarbons (PAHs)*. 2001. 167 s.
352. Shakespeare, John, *Identification and Control of Cross-machine Profiles in Paper Machines*. 2001. 180 s.
353. Lahnajärvi, Jani, *Structure Learning with Constructive Neural Networks*. 2001. 266 s.
354. Sahrakorpi, Seppo, *Studies in Electronic Band Structures, Momentum Matrix Elements and Their Significance in Angle-Resolved Photoemission*. 2001. 133 s.
355. Salonen, Pekka, *Development of Planar Antennas for Mobile and Access-Point Devices*. 2001. 120 s.
356. Osara, Karri, *Characterization of Abrasion, Impact-Abrasion and Impact Wear of Selected Materials*. 2001. 206 s.
357. Laasonen, Mauri, *Computer-Based Generation of Wall Elements Between Measured Spaces of Buildings*. 2001. 167 s.
358. Wang, Ye, *Selected Advances in Audio Compression and Compressed Domain Processing*. 2001. 140 s.
359. Lahtinen, Mika, *Aqueous Polyurethane Dispersions: Preparation, Characterisation and Properties*. 2002. 137 s.
360. Vippola, Minnamari, *Microstructural Study of Aluminum Phosphate Sealed Plasma Sprayed Alumina and Chromia Coatings*. 2002. 128 s.
361. Soini, Sari, *Microbial Ecology and Control in Water Hydraulic Systems*. 2002. 161 s.
362. Lampinen, Harri, *Studies and Implementations of Low-Voltage High-Speed Mixed Analog-Digital CMOS Integrated Circuits*. 2002. 178 s.
363. Nikander, Ari, *Novel Methods for Earth Fault Management in Isolated or Compensated Medium Voltage Electricity Distribution Networks*. 2002. 201 s.
364. Stenberg, Tuula, R.F. *Sputtered Artificial Passive Films - Preparation and Characterization* 2002. 103 s.
365. Tommiska, Markku, *Framework for Integrated Evolution; A Practical Socio-Technical Approach in Large-Scale Process Industry*. 2002. 155 s.
366. Saarela, Olli, *Multivariate Autoregressive Analysis in Locating the Origin of Fluctuation in Continuous Industrial Processes*. 2002. 137 s.
367. Gao, Nan, *Studies of Age-Hardenable Dilute Cu-Cr-P Alloys: Compositional Design, Characterization and Comparison with Other Copper Alloys*. 2002. 138 s.
368. Sun, Bin, *Customer-Oriented Nesting Optimization for Sheet Metal Manufacturing*. 2002. 162 s.
369. Päivinen, Minna, *The Assessment of Ergonomics and Usability of Consumer Products - Four Case Studies on Hand Tools*. 2002. 142 s.
370. Hyvönen, Mika, *Improving the Characteristics of the Pressure Intensifier with Integrated Control Valve*. 2002. 108 s.
371. Burian, Adrian, *Signal and Image Restoration Using the Median Cost Function or Phase Retrieval*. 2002. 168 s.
372. Adeleke, Jimoh, *Numerical Modelling and of Thermal Conditions in Casting Processes*. 2002. 171 s.
373. Yli-Kaakinen, Juha, *Optimization of Digital Filters for Practical Implementations*. 2002. 268 s.
374. Suhonen, Sami, *Aging Induced Effects on Noble Metal Oxides on Exhaust Catalysts Studied by Photoelectron Spectroscopy* 2002. 158 s.
375. Hamila, Ridha, *Synchronization and Multipath Delay Estimation Algorithms for Digital Receivers*. 2002. 140 s.

Tampereen teknillinen korkeakoulu
PL 527
33101 Tampere

Tampere University of Technology
P. O. B. 527
FIN-33101 Tampere Finland

ISBN 952-15-0838-8
ISSN 0356-4940

TTKK JULKAISUJA 375 RIDHA HAMILA